Demonstrating the Non-Abelian Nature of Majoranas

Master's Thesis

Written by *Svend Krøjer Møller*

10th August 2020

Supervised by
Karsten Flensberg

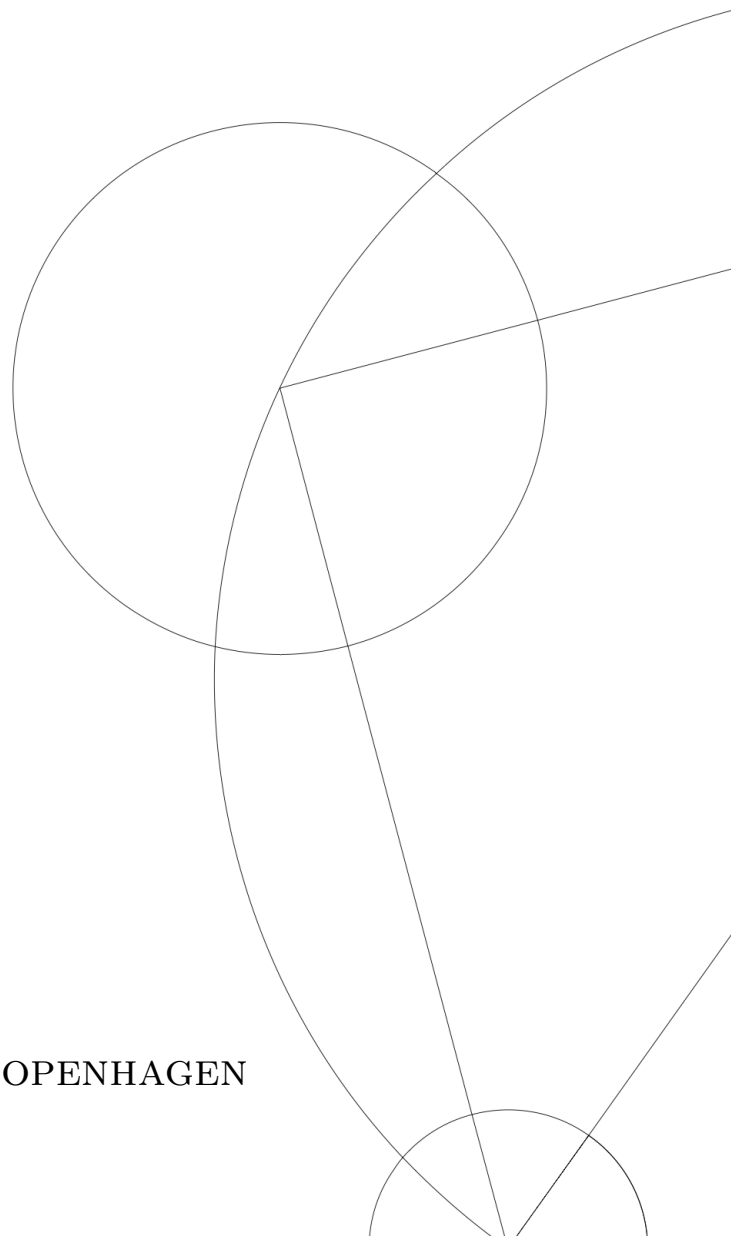

University of Copenhagen

Abstract

This thesis proposes an efficient protocol based on [1] to demonstrate the non-Abelian nature of Majorana bound states through charge-transfer processes using a quantum dot. We take into account systematical errors in the parameters of the Hamiltonian. Importantly, these errors split the ground state degeneracy and introduces relative dynamical phases between even and odd parity sectors. By winding the superconducting phase, we are able to effectively cancel the dynamical phases of subsequent charge-transfer processes, mitigating this main source of error. Further, we study the dynamics of the charge-transfer process through adiabatic perturbation theory [2]. Our findings show promising improvements compared to controlling the dot level energy linearly, suppressing transitions and dynamical phases at a substantially shorter time scale. We also discover a subtle correction to the adiabatic condition predicted by adiabatic perturbation theory due to its expansion parameter being dimensionful. We resolve this issue in our particular example by formulating the relevant dimensionless expansion parameter and discuss its implications. We support all of the above results numerically. Finally, in two smaller projects, we study multi-qubit gates in similar charge-transfer systems and manipulations of Majorana bound states in tunnel coupling-space.

Acknowledgements

I would like to thank my advisor Karsten Flensberg for introducing me to the topic of Majorana physics and for his great interest and thorough helpfulness in the project. Additionally, I have greatly appreciated Rubén Seoane Souto joining the project, always providing encouraging and illuminating comments. I also thank Alex Whiticar and Felix Passmann for introducing me to their experimental research and Michael Kastoryano for interesting discussions. Finally, a special thanks to Kim Splittorff for his guidance in all aspects of academia throughout my education.

Contents

Chapter 1

Introduction

In this thesis, we give a theoretical study of the manipulation of Majorana bound states in 1D systems with the aim of demonstrating their non-Abelian exchange statistics. In what follows, we give a non-technical overview to introduce concepts which are used throughout and motivate the present work. Then, in Sec. 2, we supplement with the mathematical details by reviewing selected parts of the foundational literature on Majorana bound states and thus sets the scene for the main body of the thesis. Here, in Sec. 3, we introduce and refine a protocol suggested by Flensberg [1] which utilizes quantum dots to manipulate Majorana bound states through adiabatic charge-transfer processes. In Sec. 4, we continue by studying the charge-transfer process with adiabatic perturbation theory before testing the predictions numerically in Sec. 5. In these two chapters, we aim to describe the optimal control of the quantum dot in a charge-transfer process and protocols which are robust against errors in the system parameters. After this main narrative, two smaller projects are discussed. In Sec. 6, we describe a charge-transfer device capable of performing rotations of more than two Majoranas and examine how the complexity of the device increases with the number of Majoranas undergoing the rotation. In Sec. 7, we instead consider how manipulation of Majoranas can be performed by changing tunnel couplings adiabatically and propose a protocol which can demonstrate the non-Abelian exchange statistics with this idea. Finally, in Sec. 8 we conclude on the thesis and discuss what future work remains in the effort to demonstrate the non-Abelian nature of Majorana bound states.

1.1 What we talk about when we talk about Majoranas

The condensed matter analogue of the Majorana fermion from particle physics is different in a few fundamental ways. Majorana fermions was originally hypothesized in 1937 by Ettore Majorana as a class of elementary particles which are their own antiparticles [3]. The aim of this description was to circumvent the need for introducing antiparticles to neutral elementary particles such as the neutrino. Whether the neutrino is a Majorana fermion remains an open question in particle physics and it is unknown if Nature exploits this mathematical possibility of self-conjugate elementary particles [4]. Two important aspects that distinguish the condensed matter version of Majorana's fermions, are that they are quasiparticle excitations which are not fermionic but rather constitutes half a fermion degree of freedom [5]. For this reason, the terms Majorana zero-modes or Majorana bound states are used instead. Though often used synonymously, we will make an effort to distinguish these terms to

avoid ambiguity. In the present thesis, we will also simply use *Majoranas* for short. What remains of Majorana's original idea is that also the Majoranas in condensed matter systems are their own antiparticles. Several interesting results follow from this property: Being a self-conjugate quasiparticle, the Majorana must be an equal superposition of an electron and a hole. In a particle-hole symmetric system, the electron has excitation energy E while the hole has energy $-E$ compared to the Fermi level, so to stay invariant after a transformation that interchanges electrons and holes, the energy must be zero [6]. This reasoning also explains the name Majorana zero-mode. It is, however, possible to couple Majorana zero-modes and split their energy such that they lose their zero-mode status. Consequently, we relax the use of "Majoranas" to not necessarily imply zero energy.

On a mathematical level, it is always possible to decompose fermionic creation and annihilation operators into two Majorana operators. Typically, this procedure is a simple change of basis without any physical implication as pairs of Majorana operators descending from the same fermion couple strongly due to their inherent proximity. For this reason, individual Majorana operators do not usually represent distinguishable physical modes. Interestingly, for certain Hamiltonians, single Majorana operators decouple entirely and thus become exact zero-modes [7]. The Majorana zero-modes are in these cases exponentially localized at the boundaries of the phase that support them. As boundaries or defects are typically separated, the Majorana zero-modes are as a result isolated. It is the bound and physically distinguishable states of these unpaired Majorana operators we talk about when we talk about Majoranas. It is also this property of Majoranas that has given them the moniker Majorana bound states. We use "Majoranas" to refer to the bound states as they resemble physical objects more so than the Majorana zero-modes. If the Majorana bound states are weakly coupled, their energy will be only slightly split making them near zero-modes. In this case it is still meaningful to talk about the Majorana bound states despite them not being exact zero-modes. Additionally, if several Majorana bound states are coupled the system may still retain Majorana zero-modes. These do in general not coalesce with the Majorana bound state but are spread over all of the states in the system resulting in a slight distinction between Majorana bound state and Majorana zero-mode. As the Majorana operators constitute half a fermion, the notion of occupancy of a Majorana bound state or zero-mode is meaningless. To speak of occupancy, we need an additional Majorana zero-mode to form a fermionic state. It is this non-local, zero energy fermion formed by two Majorana zero-modes that is an actual Dirac fermion and may rightfully be called the *Majorana fermion of a condensed matter system*. The properties of this non-local fermion and its constituent Majoranas are of immense interest in the context of topological quantum computing as we will briefly discuss in the next section.

1.2 Topology and prospects in quantum computing

Since the Majoranas each constitute half a fermion, there is always an even number of Majoranas in the systems harboring them. This fact of nature is related to the properties of being located at defects and having zero energy by the overarching concept of topological phases of matter [8, 10]. The emergence of Majoranas is related to both the systems spatial topology and the topology of its underlying phase of matter. We exemplify how the geometry of a system determines the number of Majoranas by considering a 1D wire. For such a system, the Majoranas are located at the two endpoints of the wire. The property of having two physical endpoints holds regardless of the exact geometry of the wire which we can imagine bending and twisting while maintaining the ends and thus the Majoranas. Contrary, bonding the two ends to form a loop or cutting the wire in half to make

two wire segments are topologically distinct from having a single wire and the number of Majoranas change accordingly. For the loop, the two Majoranas fuse and disappear as individual states while the cutting procedure makes two new Majoranas at the two new endpoints created. In this manner, the number of Majoranas can be understood as a topological invariant which is robust against the particular shape of the wire and where pairs of Majoranas can be created or removed only by changing the entire topology of the system. We also note that the cutting or bonding procedure always changes the number of Majoranas by two in agreement with the statement that Majoranas are created and destroyed in pairs. Universally, edge states appear in topological systems and this is embodied in the bulk-boundary correspondence relating the topology of the bulk (i.e. the phase of matter) to the existence of states living at the boundaries (which depends on the spatial topology as described). Following this correspondence, it is only certain topological phases which host Majorana. We can understand this notion of a phase exhibiting topological properties through the following example. In the very simplest case we can imagine the two energy bands of a non-degenerate, twolevel Hamiltonian. If the parameters of the Hamiltonian are continuously varied while maintaining the gap between the two bands, then the Hamiltonians determined by the given path in parameter space are topologically equivalent and resulting phase is unchanged. Alternatively, if a path in parameter space makes the two bands cross, such that the gap closes and reopens, at a given value of the parameters, then a topological phase transition occurs that distinguishes the phases before and after the crossing. The closing and reopening of the gap is a general defining characteristic of a topological phase transition [8]. We understand the nomenclature of topological in this context as the phase being dependent only on whether a crossing of the bands has occurred and not the intricate details of the exact shape of the energy bands and how those might depend on the smooth variation of parameters. Mathematically, a topological invariant changes at the described phase transition and indexes the particular phases. This is in contrast to the thermodynamic phase transition understood through spontaneous symmetry breaking and the free energy in Landau theory. In a topological phase transition, no symmetry is broken and the symmetries are rather used to classify the possible topological phases. In this classification, Majoranas can only exist in topological phases with particlehole symmetry which in turn protects and pins their energy to zero. [6, 8].

A pair of Majoranas constitute a fermionic level and a pair of fermions constitute a boson. Examples of the latter are Cooper pairs undergoing Bose-Einstein condensation in the superconducting state or simply a spin triplet having spin 1. Beside spin and Pauli exclusion, bosons and fermions also have distinct exchange statistics being respectively symmetric $(+1)$ and antisymmetric (-1) under exchange. Then, the natural question is; how do Majoranas behave under exchange being "half a fermion"? In short, Majoranas are anyons and the anyonic wave function can take on any phase under exchange rather than just -1 or -1. Specifically, Majoranas are non-Abelian anyons meaning that the phase gained under exchange can be matrix-valued [9]. This implies that the levels are degenerate and exchanging Majoranas produce a rotation within the degenerate manifold. The non-Abelian phase acquired does not depend on the dynamics of the exchange and can consequently be understood in terms of the geometric phase. The non-Abelian exchange statistics is an exotic feature of Majoranas which lays the foundation of topological quantum computing [11]. Interpreting the states in the degenerate level as a qubit, the exchange, or braiding, of Majoranas manipulates the states and thus acts as a quantum gate on the qubit. These qubit gates are topologically protected meaning their operation is exact and robust against local noise. The reason hereof is that the outcome of topological quantum gates only depend on which Majoranas have been braided and not how. Unfortunately, the

set of topologically protected quantum gates is not universal and needs to be supplemented by a non-protected single-qubit and two-qubit gate to accomplish universal quantum computing. In addition, a quantum computer based only on the set of topologically protected gates can be simulated efficiently on a probabilistic classical computer even though it encaptures phenomenas such as entanglement and superposition which are inherently quantum mechanical [12]. Experimentally, it is challenging to physically move the Majoranas to perform a real-space braiding. Instead, promising possibilities are braidings in a parameter-space where adiabatic control of a parameter in the Hamiltonian effectively corresponds to a real-space braiding. Although tantalizing, we do not attempt to describe the longterm ambition of universal topological quantum computing in this thesis. Instead, we focus on the demonstration of the non-Abelian nature of Majoranas which is expected to be a feasible experimental achievement on a substantially shorter time scale. It provides unmistakable confirmation of the presence of Majoranas in experiment. This is in itself an important result which exhibits the tremendous experimental advancements and enables further studies of the rich and exotic physics of Majoranas. To demonstrate their non-Abelian nature, the Majoranas must be manipulated in largely the same way as quantum computer would. For this reason, much of the language used in quantum computing will also be used here and parallels will be drawn to qubits, gates, etc. when relevant.

1.3 Where to find Majoranas

Being half an electron and half a hole, it is natural to search for Majoranas as quasiparticles in superconducting systems where the excitations are Bogoliubov quasiparticles which have both electron and hole components. In conventional s-wave superconductors, the Bogoliubov excitations are in general not an equal superposition of electrons and holes and the electron and hole parts have opposite spin due to Cooper pairs consisting of time reversed electron states [5]. For this reason, additional pieces are needed to engineer a topological superconductive state that hosts Majoranas. It turns out that strong spin-orbit coupling and an applied magnetic field are essential ingredients in this recipe as they gap out a spin degree of freedom while still supporting s-wave superconductivity through momentum dependent spin orientation [13, 14, 15]. In this sense, understanding the properties of Majoranas have paved the way to the discovery of new topological systems exhibiting superconductivity. The first experimental signatures of Majoranas was measured in 2012 where a somewhat robust zero energy bound state was observed in a proximitized nanowire [16]. Here, an InSb nanowire was used due to its strong spin-orbit coupling. The InSb wire is by itself a semiconductor but it was proximitized by bringing it into contact with a superconducting electrode (NbTiN). Since then, much research has accumulated evidence in favor of the midgap states being Majoranas, however, their non-Abelian exchange statistics remain to be demonstrated. Doing this will enable us to distinguish whether the zero energy states are fermionic subgap states or true Majoranas [17]. This thesis attempts to provide relevant protocols which may be realized in experiment to distinguish if the midgap states are non-Abelian and thus Majoranas.

Chapter 2

Models of Majorana bound states

This chapter gives a brief review of the Kitaev chain [7] and Oreg et al. [14]. These papers, along with Lutchyn et al. [15], are essential for understanding the appearance of Majorana bound states in 1D systems. In addition, we discuss braiding of Majoranas following Ivanov [18]. We begin by giving an overview our Majorana nomenclature:

Majorana summary

- *Majorana operators* - Operators γ_i that obey the Clifford algebra $\{\gamma_i, \gamma_j\} = 2\delta_{ij}$ and fulfills $\gamma = \gamma^\dagger$ and $\gamma^2 = 1$. Any two Majorana operators can be combined to form fermionic annihilation and creation operators $c^\dagger = \frac{1}{2}(\gamma_1 - i\gamma_2)$ and $c = \frac{1}{2}(\gamma_1 + i\gamma_2)$. Since it takes two Majorana operators to form a fermionic operator, they always come in pairs. In this sense, they constitute half a fermionic degree of freedom.

- *Majorana bound states* - Exponentially localized states represented by Majorana operators. The bound states are located at interfaces between topologically distinct phases and their appearance is topologically protected. In a 1D system they are found at the endpoints and consequently they are spatially separated. The Majorana bound states are non-Abelian anyons and do not obey fermionic exchange statistics. Their exchange instead multiplies a matrix-valued phase to the wave function. For short, we refer to the Majorana bound states and their underlying Majorana operators as "Majoranas".

- *Majorana zero-modes* - Topologically protected zero energy modes that are represented by Majorana operators which commute with the Hamiltonian $[H, \gamma] = 0$. Uncoupled Majorana bound states are also Majorana zero-modes. Generally, coupling Majorana bound states result in splitting the energy and potentially spreading the remaining zero-modes over the bound states.

- *Majorana fermions (in CM)* - The non-local fermionic states formed by two Majorana zero-modes. Due to the non-local nature of this Dirac fermion, it is protected against local noise. This fact makes the Majorana fermions sought after in the context of quantum computing as they constitute noise-protected qubits. The anyonic properties of the underlying Majorana zero-modes also permits protected quantum gates to manipulate the qubits, however, these are not sufficient for universal quantum computing.

2.1 The Kitaev chain

The Kitaev chain is the simplest 1D model which support Majorana bound states at its edges [7]. Being simple is its virtue as the appearance of Majoranas is a topological property that does not depend on the intrinsic details of the system [8]. In other words, also more physically realistic models will harbor Majoranas as long as they are in the same (Altland-Zirnbauer) symmetry class and their properties essentially correspond to the much simpler Kitaev chain.

The Kitaev chain is a tight binding model of a spin-polarized superconductor,

$$H = -\mu \sum_{j=1}^{L} (c_j^\dagger c_j - \frac{1}{2}) - t \sum_{j=1}^{L} (c_j^\dagger c_{j+1} + c_{j+1}^\dagger c_j) + \Delta \sum_{j=1}^{L} (c_j c_{j+1} + c_{j+1}^\dagger c_j^\dagger), \tag{2.1}$$

with chemical potential μ, hopping amplitude t and superconducting pairing Δ. The first sum represents the on-site energy, the second sum is the nearest neighbor hopping and the third is the superconducting pairing term. If the superconducting phase ϕ is non-zero, the fermionic operators can be transformed by letting $c_j \to c_j e^{-i\phi/2}$ to gauge away this phase. The fermionic creation and annihilation operators $c_j^\dagger$ and c_j can be decomposed in terms of their real and imaginary parts

$$c_j^\dagger = \frac{1}{2}(\gamma_{2j-1} - i\gamma_{2j}), \qquad c_j = \frac{1}{2}(\gamma_{2j-1} + i\gamma_{2j}), \tag{2.2}$$

where γ_i are Majorana operators obeying

$$\gamma_i^2 = 1, \qquad \gamma_i^\dagger = \gamma_i, \qquad \{\gamma_i, \gamma_j\} = 2\delta_{ij}. \tag{2.3}$$

In terms of the Majorana operators, two distinct phases can be observed. The topological trivial phase, depicted in Fig. 2.1a, occurs when the pairing between Majorana operators originating from the same site c_j is dominating. The topologically non-trivial phase, depicted in Fig. 2.1b, appears in the case where the pairing between Majorana operators of adjacent sites is dominating. In this phase, an isolated zero energy Majorana bound state is found at each end of the chain. To see this at the level of the Hamiltonian, consider the case $t = \Delta > 0,\ \mu = 0$, and rewrite eq. (2.1) in terms of the Majorana operators

$$H = it \sum_j \gamma_{2j}\gamma_{2j+1}. \tag{2.4}$$

The Majorana operators γ_1, γ_{2L} do not appear in the Hamiltonian and they can be combined in a non-local fermionic annihilation operator $d = (\gamma_1 + i\gamma_{2L})/2$. The energy of occupying $d^\dagger \tilde{d} = 1/2(1 + i\gamma_1\gamma_{2L})$ is zero due to γ_1, γ_{2L} commuting with the Hamiltonian and as a consequence the ground state is doubly degenerate. The degenerate ground states can be distinguished by the Hermitian operator $i\gamma_1\gamma_{2L}$ as

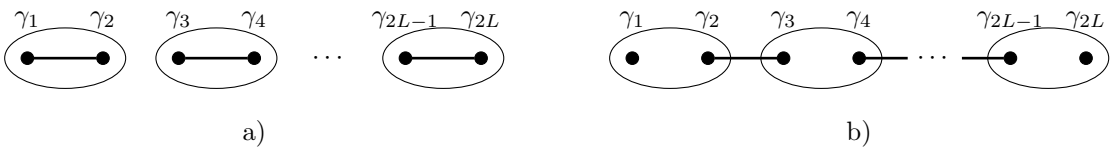

Figure 2.1: a) Pairing of Majorana operators originating from the same site c_j yields the topological trivial phase. b) The topological non-trivial phase occurs when Majorana operators of adjacent c_j's pair up. In this case there are two isolated zero energy Majorana bound states located on each end of the chain.

they have eigenvalues ± 1 for being unoccupied and occupied respectively. It is this degenerate ground state that is sought after in the context of quantum computation since the non-local nature of this qubit offers protection from local noise.

The topological qualities of the system are explicit if we go to a continuum model with periodic boundary conditions and consider the Fourier transform of eq. 2.1. According to the bulk-boundary correspondence, we do not expect Majorana bound states since there are no edges in this model. Nonetheless, the model will help us understand the topological phase and it becomes clear that it does not dependent on the exact tuning of parameters $t, \Delta > 0, \mu$ as in the example of Fig. 2.1b. We use the Fourier transformed fermionic operators,

$$c_j = \frac{1}{\sqrt{L}} \sum_k c(k) e^{ikj}, \qquad c_j^\dagger = \frac{1}{\sqrt{L}} \sum_k c^\dagger(k) e^{-ikj}. \tag{2.5}$$

By also using $1/L \sum_j e^{i(q-q')j} = \delta_{q,q'}$ we get

$$H - \frac{\mu L}{2} = \sum_k c^\dagger(k)(-\mu - 2t\cos(k))c(k) + \sum_k i\Delta \sin(k)(c(k)c(-k) + c^\dagger(k)c^\dagger(-k)), \tag{2.6}$$

or equivalently, in the Bogoliubov-de-Gennes formalism,

$$H - \frac{\mu L}{2} = \frac{1}{2} \sum_k C^\dagger(k) \mathcal{H}_{\mathrm{BdG}}(k) C(k), \qquad \mathcal{H}_{\mathrm{BdG}}(k) = -\Delta \sin(k)\tau_y - (\mu + 2t\cos(k))\tau_z, \tag{2.7}$$

where $C^\dagger = (c^\dagger(k), c(-k))$ and τ_i are the Pauli matrices acting on the electron/hole-space. We are interested in the energies of the Bogoliubov-de-Gennes Hamiltonian as the topological phases are separated by a gap closing/reopening dependent on the parameters μ, t, Δ. In general, the energies of a two-band model $\mathcal{H} = h_0 \mathbb{1} + \mathbf{h} \cdot \tau$ are given by

$$E_\pm = h^0 \pm |\mathbf{h}|, \tag{2.8}$$

which can be seen by squaring $\mathcal{H} - h_0 \mathbb{1}$. Evidently, a gap closing/reopening occurs if and only if $|\mathbf{h}| = 0$. In the case of the Kitaev chain, this happens for $h_y = -\Delta \sin(k) = 0$ and $h_z = -(\mu + 2t\cos(k)) = 0$

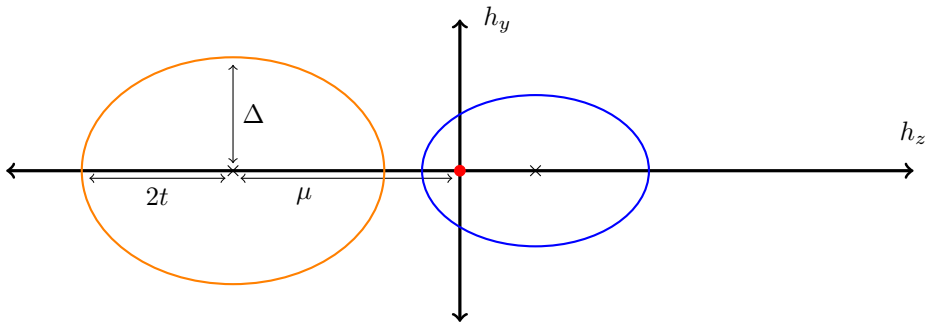

Figure 2.2: Two ellipses representing two topologically distinct Hamiltonians with different sets of parameters (μ, t, Δ). The orange ellipse corresponds to a topologically trivial phase which can immediately be recognized as the red origin lies outside the ellipse. Likewise, the blue ellipse encloses the origin and corresponds to the non-trivial phase. We can imagine lowering μ such that the rightmost point of the ellipse comes in contact with the origin. At this point, the gap closes and a topological phase transition occurs. If we continue lowering μ, the orange ellipse will eventually enclose the origin as the blue ellipse does.

having the solution $k = \pi,\ \mu = 2t$ for positive $\mu,\ t$. We have already identified the phase $2t > \mu$ as the topologically non-trivial phase supporting Majorana bound states. This topological transition can also be understood geometrically in the (h_z, h_y)-diagram of Fig. 2.2. Here, an ellipse centered at $h_z = -\mu$ is traced out when k runs from 0 to 2π. The topological index that changes at the transition is the winding of the origin. For $|\mu| > |2t|$ the origin is not enclosed by the ellipse which is counted as zero winding and the phase is topologically trivial. Contrary, for $|2t| > |\mu|$ the ellipse winds around the origin once as k runs from 0 to 2π corresponding to the topologically non-trivial state.

In general, the Majorana bound states are not localized to γ_1 or γ_{2L} as is the case in Fig. 2.1b. Instead, they are represented by a linear combination of all the Majorana operators γ_i but with exponentially decaying coefficients such that the Majorana bound states remain localized and have zero energy. This also implies that the overlap of the two Majorana bound states is exponentially suppressed by the ratio of the length of the chain to the typical localization length of the bound states. This is needed for the corresponding Majorana operators to anticommute. In what follows, we will see this exponential localization of Majorana bound states when we review a model predicting Majoranas in a physically realizable nanowire system.

2.2 Realizing Majorana bound states in nanowires

The first proposed physically realizable 1D model that have a topological non-trivial phase with Majorana bound states are found in Oreg et al. [14] and Lutchyn et al. [15]. They propose that Majoranas may be found in nanowires similar to the Kitaev chain rather than in surface vortices on topological insulators as in the earlier Fu-Kane model [13]. We will follow the approach of [14]. The first experimental signatures of Majoranas was observed just two years after the proposal of this model.

In view of the Kitaev chain, it appears that a system hosting Majorana bound states must be spinless. This is in contrast to conventional (s-wave) superconductivity where electrons of opposite spin (and momentum) combine in Cooper pairs. Perhaps surprisingly, it turns out that Majorana bound states can indeed appear in spinful s-wave systems. The system, however, must be helical; the property of having correlation between spin and momentum. Such a helical system has features of both being spinful and spinless, in the sense that both spin up and spin down electrons are present but there is no spin degree of freedom as the spin is tied to the momentum. In the following, we study such a helical system and see how it can host s-wave pairing while also being effectively spinless for the Majorana bound states to appear.

Take the Hamiltonian

$$H = \frac{1}{2}\int \mathrm{d}y\ \Psi^\dagger(y)\mathcal{H}(y)\Psi(y), \tag{2.9}$$

where $\Psi^\dagger = (\psi_\uparrow^\dagger, \psi_\downarrow^\dagger, \psi_\downarrow, -\psi_\uparrow)$ is in Nambu representation and $\psi_{\uparrow/\downarrow}(y)$ annihilates spin-up/down electrons at position y. In this basis, we consider a Bogoliubov-de-Gennes Hamiltonian given by

$$\mathcal{H}(y) = \left[\frac{p^2}{2m} - \mu(y)\right]\tau_z + up\sigma_z\tau_z + B(y)\sigma_x + \Delta(y)\tau_x, \tag{2.10}$$

where σ_i, τ_i are Pauli matrices acting on the spin and particle-hole space respectively. The Hamiltonian describes a quantum wire in the y-direction with controllable chemical potential $\mu(y)$. The wire is assumed to have strong spin-orbit coupling u throughout its length and proximity-induced

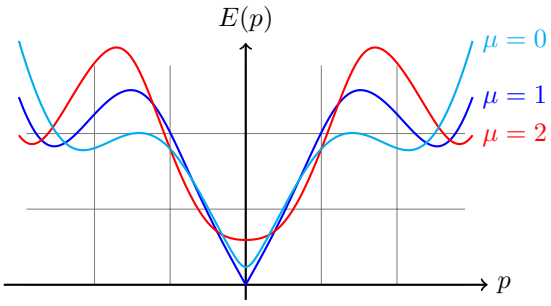

Figure 2.3: Excitation spectrum for different values of μ. The energy scale is set by $mu^2/2$ and the momentum scale is set by mu. With these scales $B = 5$ and $\Delta = 4$ has been chosen in the figure. For $\mu = 0$ we are in the B-dominated phase (cyan). Increasing μ to $\mu = 1$ results in a gap closing at $p = 0$, signaling a topological phase transition (blue). Further increasing μ reopens the gap again (red).

superconductivity of strength $\Delta(y)$. In addition, an external magnetic field $B(y)$ is pointing in the x-direction which is perpendicular to the wire and the spin-orbit coupling.

As discussed, the Majorana bound states require that there is no spin degree of freedom in the system. By applying a large magnetic field over the wire, the spin direction of the electrons parallel to the B-field is singled out due to Zeeman splitting, and the wire is in this regard effectively spinless. In spin bases perpendicular to the B-field, the electrons continue to have both up and down spin components. The strong spin-orbit coupling will correlate the momentum and the spin, in a basis perpendicular to the B-field, such that positive momentum corresponds predominantly to spin up and negative momentum corresponds predominantly to spin down. The system is now helical. The spin up electrons can then pair with spin down electrons as they have opposite momentum due to the spin-orbit coupling. This pairing results in conventional s-wave superconductivity. At the edges of this effectively spinless superconducting phase, we expect the Majorana bound states to be found, as is the case for the Kitaev chain. In order to investigate the possible phases, we take the parameters μ, Δ, B to be constant and calculate the spectrum. Squaring $\mathcal{H}$ gives

$$\mathcal{H}^2 - \xi^2 - (up)^2 - B^2 - \Delta^2 = 2\xi up\sigma_z + 2\xi B\sigma_x\tau_z + 2B\Delta\sigma_x\tau_x, \tag{2.11}$$

where $\xi = p^2/2m - \mu$. Squaring again uncovers the eigenenergies as the resulting matrix is proportional to the identity

$$\begin{aligned} (\mathcal{H}^2 - \xi^2 - (up)^2 - B^2 - \Delta^2)^2 &= (2\xi up)^2 + (2\xi B)^2 + (2B\Delta)^2 \\ \Rightarrow \quad E_\pm^2 &= \xi^2 + (up)^2 + B^2 + \Delta^2 \pm 2\sqrt{(\xi up)^2 + (\xi B)^2 + (B\Delta)^2}. \end{aligned} \tag{2.12}$$

At $p = 0$ the spectrum is gapped with the lowest energy solution E_0 being

$$E_0 = |B - \sqrt{\mu^2 + \Delta^2}|. \tag{2.13}$$

This gap can be either B-dominated $B^2 > \mu^2 + \Delta^2$ or pairing dominated $B^2 < \mu^2 + \Delta^2$ corresponding to two different topological phases. Thus changing any one of μ, Δ, B along the wire may result in a the gap closing and reopening and consequently facilitating an interface between topologically distinct phases, see Fig. 2.3. Here, an abrupt change of μ at $y = 0$ will be considered. Imagine a wire with left ($y < 0$) segment in the pairing dominated phase and right ($y > 0$) segment in the B-dominated

phase. The magnetic field is larger than the superconductive pairing $B > \Delta$ throughout the wire. In the right segment $\mu = 0$ is assumed, and in the left segment a large μ results in a pairing dominated phase $\mu^2 > B^2 - \Delta^2$.

The Majorana bound states are expected to be exponentially localized at the interface so we use the ansätze $\psi^{(l)} \propto \exp\big(k^{(l)}y\big)$ and $\psi^{(r)} \propto \exp\big(-k^{(r)}y\big)$ for the left and right segments respectively with $\mathrm{Re}(k^{(r)}), \mathrm{Re}(k^{(l)}) > 0$. Since we are interested in the behavior of the gap closing at $p = 0$, we linearize the Hamiltonian in p. By using the ansatz for the right segment, we get the Hamiltonian for $y > 0$,

$$\mathcal{H}^{(r)} = ik^{(r)}u\sigma_z\tau_z + B\sigma_x + \Delta\tau_x. \tag{2.14}$$

By squaring twice and looking for zero energy solutions with $\mathrm{Re}(k^{(r)}) > 0$ gives the result

$$k_{\pm}^{(r)}u = B \pm \Delta. \tag{2.15}$$

Rotating $\mathcal{H}^{(r)}$ by $U^\dagger = 1/2(1 - i\sigma_y)(1 - i\tau_y)$ sends $\sigma_x, \tau_x \to \sigma_z, \tau_z$ and $\sigma_z, \tau_z \to -\sigma_x, -\tau_x$ and results in

$$U\mathcal{H}^{(r)}U^\dagger = ik^{(r)}u\sigma_x\tau_x + B\sigma_z + \Delta\tau_z = \begin{pmatrix} B+\Delta & 0 & 0 & i(B\pm\Delta) \\ 0 & -B+\Delta & i(B\pm\Delta) & 0 \\ 0 & i(B\pm\Delta) & B-\Delta & 0 \\ i(B\pm\Delta) & 0 & 0 & -B-\Delta \end{pmatrix}. \tag{2.16}$$

This matrix can be seen to have one zero energy eigenstate for both the $+$ and the $-$ solution; $\phi_+'^{(r)} = 1/\sqrt{2}e^{i\pi/4}(-i, 0, 0, 1)^T$, $\phi_-'^{(r)} = 1/\sqrt{2}e^{i\pi/4}(0, -1, i, 0)^T$. Transforming back using $\phi = U^\dagger\phi'$ gives

$$\phi_+^{(r)} = \frac{1}{2}(1, -i, -i, 1)^T, \qquad \phi_-^{(r)} = \frac{1}{2}(1, -i, i, -1)^T \tag{2.17}$$

Now that we have found the eigenstates for the right segment, we can turn to the left segment. Using the ansatz, the Hamiltonian in this case becomes

$$\mathcal{H}^{(l)} = -ik^{(l)}u\sigma_z\tau_z - \mu\tau_z + B\sigma_x + \Delta\tau_x. \tag{2.18}$$

Squaring twice and looking for the zero energy solutions gives a quadratic equation for $(k^{(l)}u)^2$

$$\begin{aligned} 0 &= (k^{(l)}u)^4 - 2(B^2 + \Delta^2 - \mu^2)(k^{(l)}u)^2 + (\mu^2 + \Delta^2 - B^2)^2 \\ \Rightarrow \quad k_{\pm}^{(l)}u &= \Delta \pm \sqrt{B^2 - \mu^2}. \end{aligned} \tag{2.19}$$

There is no benefit of rotating $\mathcal{H}_l$ by $U^\dagger$ because of the μ-term. Instead, write out $\mathcal{H}_l$ in as a sum of the Δ-term and the B-term

$$\begin{aligned} \mathcal{H}_l = \Delta &\begin{pmatrix} -i & 0 & 1 & 0 \\ 0 & i & 0 & 1 \\ 1 & 0 & i & 0 \\ 0 & 1 & 0 & -i \end{pmatrix} \\ + B &\begin{pmatrix} -\mu/B \mp i\sqrt{1-\mu^2/B^2} & 1 & 0 & 0 \\ 1 & -\mu/B \pm i\sqrt{1-\mu^2/B^2} & 0 & 0 \\ 0 & 0 & \mu/B \pm i\sqrt{1-\mu^2/B^2} & 1 \\ 0 & 0 & 1 & \mu/B \mp i\sqrt{1-\mu^2/B^2} \end{pmatrix}. \end{aligned} \tag{2.20}$$

It is straightforward to see that the first term has zero energy eigenvectors $\phi_1^{(\Delta)} = (1, 0, i, 0)^T$, $\phi_2^{(\Delta)} = (0, 1, 0, -i)^T$, meaning that the zero energy eigenvectors of $\mathcal{H}_l$ must be a linear combination of the

form $\phi_{\pm}^{(l)} = \lambda_1\phi_1^{(\Delta)} + \lambda_2\phi_2^{(\Delta)}$. The second term of the above equation is block diagonal and if $(1, \alpha_{\pm})^T$ is a zero energy eigenvector of the upper left block, then $(-\alpha_{\mp}, 1)^T$ is a zero energy eigenvector of the lower right block. It is easy to find that $\alpha_{\pm} = \mu/B \pm i\sqrt{1-\mu^2/B^2}$ gives the desired zero energy solution and that $\phi_{\pm}^{(B)} = 1/2(1, \alpha_{\pm}, i, -i\alpha_{\mp}^{-1})^T$ is a zero energy eigenvector for the B-matrix. Compare it with the solution $\phi_{\pm}^{(l)}$ found for the Δ-matrix

$$\frac{1}{2}\begin{pmatrix} 1 \\ \alpha_{\pm} \\ i \\ -i\alpha_{\mp}^{-1} \end{pmatrix} = \lambda_1 \begin{pmatrix} 1 \\ 0 \\ i \\ 0 \end{pmatrix} + \lambda_2 \begin{pmatrix} 0 \\ 1 \\ 0 \\ -i \end{pmatrix}. \tag{2.21}$$

The two solutions are commensurable for $\lambda_1 = 1/2,\ \lambda_2 = \alpha_{\pm}/2$ if $\alpha_{\mp}^{-1} = \alpha_{\pm}$, which is indeed the case

$$\alpha_{\mp}^{-1} = \frac{1}{\mu/B \mp i\sqrt{1-\mu^2/B^2}} = \frac{\mu/B \pm i\sqrt{1-\mu^2/B^2}}{(\mu/B \mp i\sqrt{1-\mu^2/B^2})(\mu/B \pm i\sqrt{1-\mu^2/B^2})} = \alpha_{\pm}, \tag{2.22}$$

as the last denominator is one. In conclusion, the zero energy solutions for the left segment is

$$\phi_{\pm}^{(l)} = 1/2(1, \alpha_{\pm}, i, -i\alpha_{\pm})^T, \qquad \alpha_{\pm} = \mu/B \pm i\sqrt{1-\mu^2/B^2}. \tag{2.23}$$

We need to match the wave functions for the left and right segments at $y = 0$ such that the Majorana bound state wave function is continuous while also $\int \mathrm{d}y\ \Psi^\dagger(y)\phi(y) = \int \mathrm{d}y\ (\Psi^\dagger(y)\phi(y))^\dagger$ is a Majorana operator. Wave function matching $L_+\phi_+^{(l)} + L_-\phi_-^{(l)} = R_+\phi_+^{(r)} + R_-\phi_-^{(r)}$ gives the following equations for the complex coefficients $L_{\pm}, R_{\pm}$

$$L_+ + L_- = R_+ + R_-, \tag{2.24}$$

$$L_+\alpha_+ + L_-\alpha_- = -i(R_+ + R_-), \tag{2.25}$$

$$i(L_+ + L_-) = i(R_- - R_+), \tag{2.26}$$

$$-i(L_+\alpha_+ + L_-\alpha_-) = R_+ - R_-. \tag{2.27}$$

The first and third equation gives $R_+ = 0$ and $L_+ + L_- = R_-$ while the second and fourth equation is identical for $R_+ = 0$. Demanding that $\Psi^\dagger(y)\exp\Big(-k_-^{(r)}y\Big)R_-\phi_-^{(r)}$ is Hermitian gives $R_-^* = R_-$ and we choose $R_- = 1$. We can now solve for $L_{\pm}$ in the equations $L_+ + L_- = 1$ and $L_+\alpha_+ + L_-\alpha_- = -i$ which give

$$L_{\pm} = \pm\frac{\alpha_{\mp} + i}{\alpha_+ - \alpha_-}. \tag{2.28}$$

Finally, the wave function of the Majorana bound state can be written (up to a real normalisation factor)

$$\phi(y) = \begin{cases} L_+\exp\Big(k_+^{(l)}y\Big)\phi_+^{(l)} + L_-\exp\Big(k_-^{(l)}y\Big)\phi_-^{(l)} & y < 0 \\ \exp\Big(-k_-^{(r)}y\Big)\phi_-^{(r)} & y > 0 \end{cases}. \tag{2.29}$$

The solution is constructed such that $\Psi^\dagger(y)\phi(y) = (\Psi^\dagger(y)\phi(y))^\dagger$ holds for each $y > 0$. It is straightforward, but tedious, to check that the this is also the case for $y < 0$.

In experiment, one of the critical errors influencing the Majoranas is quasiparticle poisoning. It is an error changing the parity of the system and its origin may come from inside the system or the outside environment. An electron from the environment may enter the nanowire and thus changes the occupancy of the Majorana fermion. This can be combated by introducing a large charging energy to the nanowire, preventing electrons from settling in the Majorana system. Quasiparticle poisoning

from within the system is also possible with two different mechanisms. One is the excitation of an electron with its subsequent relaxation in the Majorana state. Alternatively, trivial subgap states may also exchange occupancy with the Majoranas. Both of these possibilities can be prevented by inducing a large superconducting gap. We do not take these errors into account in the present work but instead refer the reader to [19]. We continue by studying the Majoranas as non-Abelian anyons and their braiding.

2.3 Braiding Majoranas and their anyonic properties

We continue by discussing the real-space braiding of Majoranas and show their non-Abelian exchange statistics. Following Ivanov [18], we begin by considering Majoranas in a 2D system, rather than in 1D, as this is conceptually simpler. The results from the 2D case also applies to networks of 1D wires where Majoranas can be interchanged in much the same manner.

Majoranas can be found on the surface of certain topological insulators with proximity induced superconductivity [13]. Here, they reside in the centers of vortices which winds the superconducting phase by 2π. The exact circumstances of the appearance of Majoranas is for the present discussion not relevant as the treatment is entirely general. We use that the vortices harboring the Majoranas winds the superconducting phase and how the Majoranas respond to this winding. Recall that the fermionic operators can gauge away the superconducting phase by letting $\tilde{c} = e^{-i\phi/2}c$. When the superconducting phase transforms as $\phi \to \phi + 2\pi$, the fermionic operators acquire a sign,

$$\tilde{c} = ce^{-i\phi/2} \to -ce^{-i\phi/2} = -\tilde{c}, \tag{2.30}$$

and likewise for the creation operator. The same also applies to Majoranas as they are linear combinations of the fermionic operators,

$$\begin{gathered} \gamma \to -\gamma, \\ \text{for } \phi \to \phi + 2\pi. \end{gathered} \tag{2.31}$$

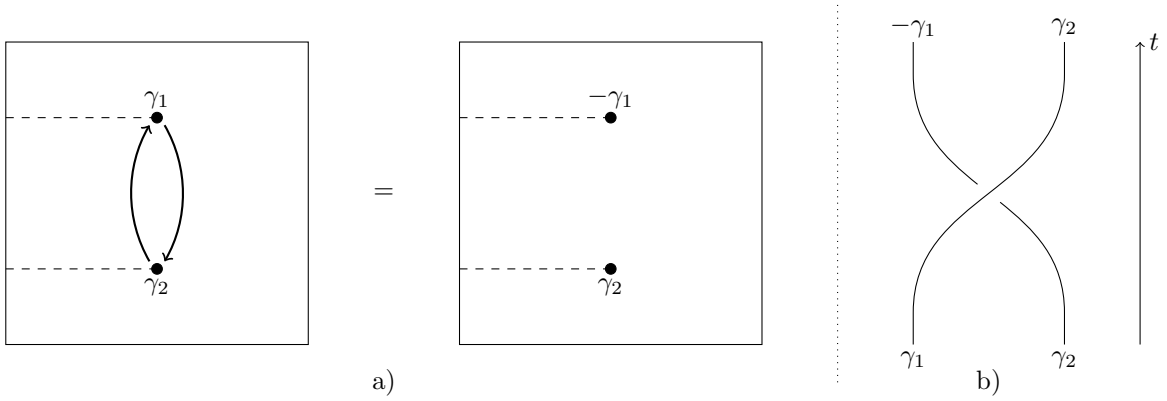

Figure 2.4: a) Exchanging two Majoranas results in exactly one crossing of the branch cuts indicated by dashed lines. In this example γ_2 crosses the branch cut and its phase jumps by π as it takes the place of γ_1. We have a choice when choosing the branch cuts. Had we drawn the cuts to the left rather than to the right, γ_2 would change sign instead of γ_1 and this is simply a choice of convention. b) The corresponding braid of world lines in a braid diagram with the time along the second axis.

In other words, the phase of the Majoranas experience a winding of π when the superconducting phase winds 2π. Due to this winding, we need to insert branch cuts to keep the superconducting phase single-valued. When a Majorana crosses such a branch cut it changes sign as its phase jumps by π. In Fig. 2.4a, we illustrate that upon exchange of two Majoranas one will cross a branch cut and its sign will flip. The corresponding braid is shown in Fig. 2.4b. The associated operator when interchanging, or braiding, two Majoranas γ_i and γ_{i+1} thus is

$$T_i = \begin{cases} \gamma_i & \to \gamma_{i+1}, \\ \gamma_{i+1} & \to -\gamma_i, \end{cases} \tag{2.32}$$

leaving other possible Majoranas invariant. Note that performing this operation twice flips the sign of both Majoranas and thus also flips the sign of the associated fermion. This is in agreement with the exchange statistics of spin-1/2 particles. At this point we can imagine having $2n$ Majoranas which we may try to braid as in Fig. 2.4b. We perform operations on adjacent pairs of Majoranas by braiding them. These operations form a group called the braid group B_{2n} with group elements T_i, $i = 1, 2, \ldots, 2n-1$. The defining relation of the braid group is shown in Fig. 2.5,

$$T_i T_{i+1} T_i = T_{i+1} T_i T_{i+1}. \tag{2.33}$$

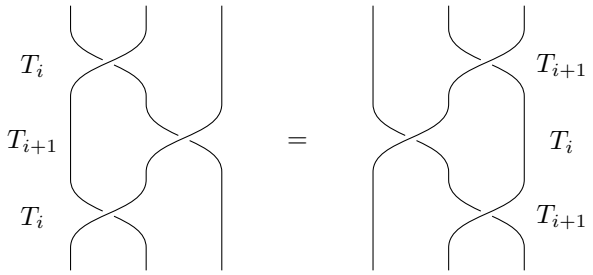

Figure 2.5: Braid diagram of the defining relation of the braid group.

The braid group has different representations and each representation corresponds to different classes of particles. The one-dimensional representation is the simplest and includes the exchange statistics of fermions, bosons and Abelian anyons [10]. The Majoranas, being non-Abelian, obey higher-dimensional representations and we can write the group elements using the Majorana operators,

$$B_i = \frac{1}{\sqrt{2}}(1 + \gamma_i \gamma_{i+1}), \tag{2.34}$$

adhering to the same defining relation $B_i B_{i+1} B_i = B_{i+1} B_i B_{i+1}$ while being non-commutative $[B_i, B_{i+1}] = \gamma_i \gamma_{i+2}$. These are unitary operators transforming Majoranas as in eq. (2.32). This is an idealized mathematical description of the exchange of Majoranas. Physically, errors occur if the Majoranas overlap significantly or if their exchange is not performed adiabatically. The latter may result in exciting the states such that they leave the degenerate manifold. We postpone the discussion of such errors and continue in the idealized case and consider how the degenerate ground states change under braiding. A fermionic state formed by γ_1 and γ_2 has annihilation operator $d_1 = \frac{1}{2}(\gamma_1)$ and number operator $d_1^\dagger d_1 = 1/2(1 + i\gamma_1\gamma_2)$. We represent it the unoccupied state by $|0\rangle_{\mathrm{M12}}$ and the occupied state by $|1\rangle_{\mathrm{M12}} = d_1^\dagger |0\rangle_{\mathrm{M12}}$. These states are eigenvectors of $i\gamma_1\gamma_2$ with eigenvalues ∓ 1 respectively. Braiding γ_1 and γ_2 amounts to a simple phase shift,

$$B_1 |0\rangle_{\mathrm{M12}} = \frac{1}{\sqrt{2}}(1 + \gamma_1\gamma_2) |0\rangle_{\mathrm{M12}} = \frac{1}{\sqrt{2}}(1 + i) |0\rangle_{\mathrm{M12}}. \tag{2.35}$$

No physical change is imparted upon the state as the phase can not be measured. For this reason we need more than two Majoranas be able to demonstrate their non-Abelian exchange statistics. Include now an additional pair of Majoranas γ_3, γ_4 with occupation states $|0\rangle_{\mathrm{M34}}$ and $|1\rangle_{\mathrm{M34}} = d_2^\dagger |0\rangle_{\mathrm{M34}}$. Braiding γ_2 and γ_3 now changes the occupancy of the states. Take for example the $|0\rangle_{\mathrm{M12}} |0\rangle_{\mathrm{M34}}$ state,

$$B_{23} |0\rangle_{\mathrm{M12}} |0\rangle_{\mathrm{M34}} = \frac{1}{\sqrt{2}}(1 + i(d_1^\dagger - d_1)(d_2^\dagger + d_2)) |0\rangle_{\mathrm{M12}} |0\rangle_{\mathrm{M34}} = \frac{1}{\sqrt{2}} |0\rangle_{\mathrm{M12}} |0\rangle_{\mathrm{M34}} + \frac{i}{\sqrt{2}} |1\rangle_{\mathrm{M12}} |1\rangle_{\mathrm{M34}}\,, \tag{2.36}$$

which can be statistically distinguished from $|0\rangle_{\mathrm{M12}} |0\rangle_{\mathrm{M34}}$ by occupancy measurements. Applying B_{23} again gives

$$B_{23}^2 |0\rangle_{\mathrm{M12}} |0\rangle_{\mathrm{M34}} = |1\rangle_{\mathrm{M12}} |1\rangle_{\mathrm{M34}}\,, \tag{2.37}$$

up to a phase. This is in accordance with the superconducting system conserving parity due to particle-hole symmetry. Physically, this is the case since the Majorana fermions are occupied with electrons from a broken Cooper pair. In general, any sequence of braid operations can be applied to the Majorana system where each topologically distinct braid corresponds to a distinct unitary acting on the state. Interpreting the two states in this system as a qubit, $|0\rangle = |0\rangle_{\mathrm{M12}} |0\rangle_{\mathrm{M34}}$ and $|1\rangle = |1\rangle_{\mathrm{M12}} |1\rangle_{\mathrm{M34}}$, we can understand the double-braid as a NOT-gate which can be represented by σ_x. This quantum gate is topologically protected in the sense that it depends only on the exchange of Majoranas and not the detailed circumstances of path that they have undergone. In this way, it is protected from perturbations to the path provided that the Majoranas do not overlap. Further, the gate is exact as the outcome does not depend on tuning any systems parameters. The quantum gates that can be constructed with a similar braiding procedure are the single-qubit Clifford gates consisting of the Pauli matrices and their squareroots [9]. They do not constitute an universal set of quantum gates but do support intrinsically quantum mechanical aspects such as superposition of the qubit. The Clifford gates can be supplemented by a non-protected two-qubit gate to reach a set of universal of quantum gates. Additionally, an interesting result, the Gottesman-Knill theorem [12], states that a quantum computer based on the Clifford gates can be efficiently simulated by a probabilistic classical computer despite its inherently quantum mechanical structure.

We learn that it is essential for a protocol demonstrating the non-Abelian exchange statistics of Majoranas to measure the occupancy in one basis and perform the braiding in another. At least four Majoranas are needed for this purpose but only the braiding between two of these is necessary. In addition, performing the braid a number of times gives different occupation of the final state. In 1D these types of real-space braidings can also be performed if the geometry of the wires are suitable [20]. Of course, in a single wire the Majoranas can not be moved past each other if we naively try to braid them in this manner. Instead, we can imagine a T-shaped junction where one Majorana is moved from the left endpoint to the bottom of the middle leg. Then, the Majorana at the right end can be moved through to the left and the Majorana deposited at the bottom of the middle leg can be moved to the right endpoint completing the exchange. The Majoranas are envisioned to be moved by adjusting the boundary between topological phases by controlling a large number of gate electrodes. This is impractical in experiments. For this reason, proposals that try to implement a braiding protocol for Majoranas typically aim to braid in a different space than real-space [9]. Braiding in a parameter-space can result in the same unitary operators acting on the Majoranas without moving them. Another advantage is that these operations are not restricted to the Clifford gates and may even constitute a universal set of gates. The downside is that the operations are no longer protected

by topology as they depend on the parameters. However, the operations continue to be a geometric rather than a dynamical phenomena which upholds some of the error-protection. It is difficult to say which implementation of a possible future topological quantum computer is optimal. On a shorter time horizon, it is believed that the parameter-space braiding is more suitable for demonstration of the non-Abelian exchange statistics of Majoranas. In the remainder of this thesis we consider two kinds of parameter-space braiding ideas. Primarily, we focus on the charge-transfer process where charge is transferred from a quantum dot to a Majorana system by adiabatically adjusting the level energy of the dot. Towards the end, we also discuss a protocol based on braiding in a tunnel coupling-space. Here, braiding-like operations can be performed by adiabatically varying the tunnel couplings between a number of Majoranas and single quantum dot. We begin this narrative by reviewing a conceptually simple charge-transfer protocol in the next chapter.

Chapter 3

Detecting Majorana bound states through charge-transfer

In the last decade, much experimental effort has been directed towards realizing and measuring the existence of Majorana bound states [16, 17]. With these experiments, many signatures of Majoranas has been observed. A conclusive fingerprint of the states being true Majoranas would be to demonstrate their non-Abelian exchange statistics. In this chapter, we review a proposal by Flensberg [1] where the non-Abelian nature of Majoranas is tested through adiabatic charge-transfer processes. This protocol relies on finely tuning and controlling the system parameters to avoid splitting the ground state degeneracy and introduce relative dynamical phases between the even and odd parity sectors. Following our review of [1], we take into consideration the effect of errors in the tuning of the Hamiltonian parameters. By understanding the errors well, we can propose an efficient protocol which is experimentally simpler and to some extend alleviates systematical errors in the parameters. In the two subsequent chapters, we consider errors due to the charge-transfer process not being entirely adiabatic and test the proposed protocol numerically.

3.1 Reviewing a charge-transfer protocol

Following Flensberg [1], we begin by studying a simple system consisting of a spin-polarized quantum dot (with fermionic annihilation operator c_1) coupled to a Majorana bound state (with Majorana operator γ_1), see Fig. 3.1. We assume that the dot is spin-polarized due to the strong Zeeman field required to facilitate the topological phase, leaving a single dot level. There is a second Majorana bound state γ_2 which together with γ_1 forms a basis for a fermionic annihilation operator $d_1 = 1/2(\gamma_1 + i\gamma_2)$. The coupling between the dot and Majorana bound state is v_1 and the dot level energy

Figure 3.1: Illustration of the setup which the Hamiltonian of eq. (3.1) describes. The quantum dot D1 (green) is coupled to the Majorana bound state M1 (red) with strength v_1. The Majorana bound states are located at the ends of the topological superconductor (blue).

ε is controllable. The effective Hamiltonian describing the system is

$$H_1 = \varepsilon c_1^\dagger c_1 + (v_1^* c_1^\dagger - v_1 c_1)\gamma_1. \tag{3.1}$$

The underlying idea is conceptually simple; since the Hamiltonian preserves parity, we can adiabatically change the occupation of the dot by tuning ε and thereby change the parity of the Majorana bound states. The even and odd parity states of the system are $\{|0\rangle_{\mathrm{D1}}|0\rangle_{\mathrm{M12}},\ |1\rangle_{\mathrm{D1}}|1\rangle_{\mathrm{M12}}\}$ and $\{|0\rangle_{\mathrm{D1}}|1\rangle_{\mathrm{M12}},\ |1\rangle_{\mathrm{D1}}|0\rangle_{\mathrm{M12}}\}$ with subscript D1 and M12 denoting the dot and Majorana system respectively. The Hamiltonian is in this basis given by

$$H_1^\rho = \begin{pmatrix} 0 & v_1 \\ v_1^* & \varepsilon \end{pmatrix}, \tag{3.2}$$

for both even $\rho = -$ and odd $\rho = +$ parity. The ground state energy then is

$$E_1^\rho = \varepsilon/2 - \sqrt{(\varepsilon/2)^2 + |v_1|^2}, \tag{3.3}$$

which is doubly degenerate. Consider the system to be in a ground state for $\varepsilon/|v_1| \to \infty$, i.e. the dot is unoccupied,

$$|i\rangle = |0\rangle_{\mathrm{D}}(\alpha|0\rangle_{\mathrm{M12}} + \beta|1\rangle_{\mathrm{M12}}). \tag{3.4}$$

During a process where $\varepsilon/|v_1|$ is changed adiabatically from ∞ to $-\infty$, the dot is filled and the state of the system is

$$|p\rangle = a(\varepsilon)|0\rangle_{\mathrm{D}}(\alpha|0\rangle_{\mathrm{M12}} + \beta|1\rangle_{\mathrm{M12}}) + b(\varepsilon)|1\rangle_{\mathrm{D}}(\alpha|1\rangle_{\mathrm{M12}} + \beta|0\rangle_{\mathrm{M12}}), \tag{3.5}$$

which is a snapshot ground state $v_1 a(\varepsilon) = E_1^\rho b(\varepsilon)$. A key point is that the Majorana system is degenerate throughout the process such that there is no relative dynamical phase obtained between the two parity states. As the Hamiltonian is identical for the even and odd parity sectors, also the relative geometric phase is zero. At the end of the process, the dot has been emptied ($b = 1$), yielding the final state,

$$|f\rangle = |0\rangle_{\mathrm{D}}(\alpha|1\rangle_{\mathrm{M12}} + \beta|0\rangle_{\mathrm{M12}}). \tag{3.6}$$

The total operation on the Majorana system after the process is

$$|i\rangle_{\mathrm{M12}} = \alpha|0\rangle_{\mathrm{M12}} + \beta|1\rangle_{\mathrm{M12}} \to |f\rangle_{\mathrm{M12}} = \alpha|1\rangle_{\mathrm{M12}} + \beta|0\rangle_{\mathrm{M12}}, \tag{3.7}$$

corresponding to

$$|f\rangle_{\mathrm{M12}} = \gamma_1|i\rangle_{\mathrm{M12}}. \tag{3.8}$$

The physical process of filling or emptying the dot thus results in the operator γ_1 acting on the Majorana state. Interpreting the two states of the Majorana system as a qubit, the bit is flipped corresponding to a NOT-gate. Errors can occur in the quantum dot, changing its occupancy to the coupling to the environment. Contrary to the parity errors in the Majorana system, parity errors on the dot are easy to detect. By measuring the charge on the dot, we can deduce if any errors have occurred or whether the dot is in its desired state.

We will now turn to an extended setup and see how a device with increased complexity translates to the complexity of the operations on the Majorana system. Consider also coupling the dot to the second Majorana bound state γ_2 with strength v_2, see Fig. 3.2. This introduces an additional

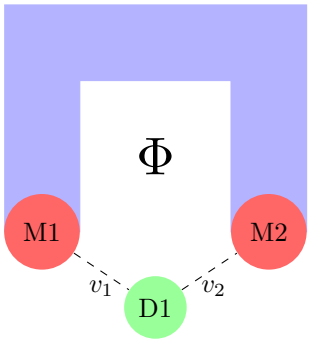

Figure 3.2: Illustration of two Majorana bound states (red) coupled to a quantum dot (green). The phase between v_1 and v_2 can be controlled by a magnetic flux Φ. This setup enables all 2-Majorana rotations $\exp(\Delta\theta\gamma_1\gamma_2)$ to be performed on the Majorana system.

coupling term to the Hamiltonian of eq. (3.1) of the form $(v_2^* c_1^\dagger - v_2 c_1)\gamma_2$ which results in the following Hamiltonian matrix,

$$H_{12}^\rho = \begin{pmatrix} 0 & v^\rho \\ (v^\rho)^* & \varepsilon \end{pmatrix}, \tag{3.9}$$

where $v^\rho = v_1 + \rho\, i\, v_2$ for the even and odd cases which breaks the degeneracy of the ground state. We will study this Hamiltonian and the associated charge-transfer process in detail throughout the thesis. We choose a gauge which parameterizes the couplings through the real coefficients v, θ, ϕ,

$$v_1 = v\cos(\theta)e^{i\phi/2}, \qquad v_2 = v\sin(\theta). \tag{3.10}$$

The magnetic flux Φ through the horseshoe-shaped superconductor in Fig. 3.2 controls the phase difference $\phi = \Phi/(h/(2e))$. To find the eigenenergies, we write the Hamiltonian matrix in terms of the Pauli matrices,

$$H_{12}^\rho = \frac{\varepsilon}{2}\mathbb{1} + \mathrm{Re}[v^\rho]\sigma_x - \mathrm{Im}[v^\rho]\sigma_y - \frac{\varepsilon}{2}\sigma_z \tag{3.11}$$

The energy of the even and odd ground states are (see eq. (2.8)),

$$E_\pm^\rho = \varepsilon/2 \pm \sqrt{(\varepsilon/2)^2 + |v^\rho|^2} = \varepsilon/2 \pm \sqrt{(\varepsilon/2)^2 + v^2(1 + \rho\sin(2\theta)\sin(\phi/2))}, \tag{3.12}$$

where all parameters are taken to be controllable. Imagine tuning the phase difference to $\phi = 2\pi n$ with n integer (corresponding to the fraction v_1/v_2 being real) such that the degeneracy between the even and odd sectors is recovered. The degeneracy of the ground state is important as it ensures that no relative dynamical phase is gained between the even and odd sectors. The role of the geometric phase will be covered in Sec. 3.2. Using that v_1/v_2 is real while rewriting the Hamiltonian in terms of $\tilde{c}_1 = c_1\exp(i\phi/2)$ yields

$$H_{12} = \varepsilon\tilde{c}_1^\dagger\tilde{c}_1 + v(\tilde{c}_1^\dagger - \tilde{c}_1)\gamma_{12}, \tag{3.13}$$

with

$$\gamma_{12} = \cos(\theta)\gamma_1 + \sin(\theta)\gamma_2, \tag{3.14}$$

being a new Majorana operator. The Hamiltonian is now on the same form as eq. (3.1) so the previous treatment also applies here. Emptying or filling the dot adiabatically corresponds to applying the operator γ_{12} on the Majorana system. This operation is far more capable than the bit flip produced

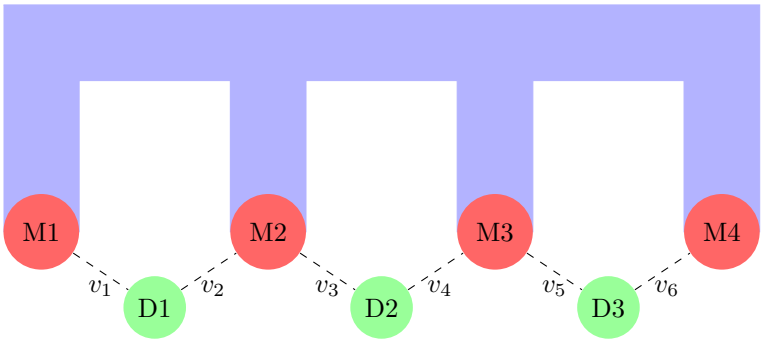

Figure 3.3: Illustration of a setup where all unitary operations can be performed on the qubit consisting of the four Majorana Bound states (red) by adiabatically emptying and filling the quantum dots (green). This device can also be used to show that the operations are non-Abelian verifying that the sub gap states are in fact Majorana.

by γ_1 due to θ being controllable. By applying γ_{12} twice with different, but still real, ratios $|v_1|/|v_2|$, the resulting operator takes the form

$$\gamma_{12}\gamma'_{12} = (\cos(\theta)\gamma_1 + \sin(\theta)\gamma_2)(\cos(\theta')\gamma_1 + \sin(\theta')\gamma_2) = \cos(\Delta\theta) + \sin(\Delta\theta)\gamma_1\gamma_2 = \exp(\Delta\theta\gamma_1\gamma_2),$$

where $\Delta\theta = \theta' - \theta$. The possible operations which can be made on the Majorana system are thus all 2-Majorana rotationsexp$(\Delta\theta\gamma_1\gamma_2)$. By tuning $\Delta\theta = \pi/4$ we perform the braiding operation on the Majoranas,

$$\exp\Big(\frac{\pi}{4}\gamma_1\gamma_2\Big) = \frac{1}{\sqrt{2}}(1 + \gamma_1\gamma_2). \tag{3.15}$$

This operation is not topologically exact as it depends on the tuning of θ and ϕ. It is, however, possible to produce a much richer set of operation on the Majorana system for this reason. The Majorana operators can be represented by Pauli matrices acting on the two-level Majorana system $\{|0\rangle_{\mathrm{M12}}, |1\rangle_{\mathrm{M12}}\}$ by

$$\gamma_1 = \sigma_x, \quad \gamma_2 = \sigma_y, \quad \gamma_1\gamma_2 = i\sigma_z. \tag{3.16}$$

Thus, the 2-Majorana rotation $\exp(\Delta\theta\gamma_1\gamma_2) = \exp(i\Delta\theta\sigma_z)$ corresponds to a rotation with angle θ around the z-axis on the Bloch sphere of the Majorana system. The entire Bloch sphere can be covered if the system is slightly extended such that also rotations around the x-axis can be performed. Having introduced two additional Majorana bound states γ_3 and γ_4 (with annihilation operator d_2), a qubit may now be defined through four Majorana bound states in the subspace of even parity $\{|00\rangle, |11\rangle\}$ where $|11\rangle = d_1^\dagger d_2^\dagger |00\rangle = d_1^\dagger d_2^\dagger |0\rangle_{\mathrm{M12}} |0\rangle_{\mathrm{M34}}$. Additionally, another quantum dot D2 (with annihilation operator c_2) couples to γ_2 and γ_3 with couplings v_3, v_4 respectively, see Fig. 3.3. By emptying and filling D2 in the same manner as D1, a rotation on the Bloch sphere about the x-axis can now be performed as $\gamma_2\gamma_3 = i\sigma_x$ when acting on a state $|\alpha\rangle$ in the even subspace

$$\gamma_2\gamma_3 |\alpha\rangle = i(d_1^\dagger - d_1)(d_2^\dagger + d_2) |\alpha\rangle = i(d_1^\dagger d_2^\dagger + d_2 d_1) |\alpha\rangle = i\sigma_x |\alpha\rangle . \tag{3.17}$$

In conclusion, by manipulating D1 and D2 as described, corresponds to rotations around the x- and z-axes. Combining these two kinds of operations covers the entire Bloch sphere and thus all unitary operations can be performed on the Majorana qubit system. We can use these unitaries to demonstrate the non-Abelian nature of Majoranas. In [1] such a protocol is proposed. First, pairs of Majoranas are initiated in the state $|0\rangle$. This can be achieved by splitting the even and odd ground state energies

by adjusting ϕ and let the system relax to the overall ground state. Measuring the charge on the dot and tuning its energy $|\varepsilon| >> v$ confirms that the Majoranas has reached their desired initial state. We will not go into details about the charge-measurement procedure here but instead refer the reader to Munk et al. [21] for a thorough treatment or Sec. 7.2 for a brief introduction. Relevant to the present discussion is that we assume that the charge-measurement is projective to a subspace with definite parity. In addition, we take the charge-measurement to be weak such that it is the time-averaged charge within each parity subspace that is measured. In this way, the occupancy of a pair of Majoranas can be deduced by measuring the charge of the dot. Continuing with the protocol, we use non-commuting operators defined by

$$F_i = \frac{1}{\sqrt{2}}(\gamma_i + \gamma_{i+1}), \tag{3.18}$$

which corresponds to the ideal situation $\theta = \pi/4$, or equivalently $|v_i| = |v_{i+1}|$. Applying the operators F_1, F_2, F_3 on an initial state $|00\rangle$ in different order displays the non-Abelian nature of the Majorana bound states,

$$F_1F_2F_2F_3\,|00\rangle = |11\rangle\,, \tag{3.19}$$

$$F_2F_1F_3F_2\,|00\rangle = |00\rangle\,. \tag{3.20}$$

The above equalities hold up to a phase. An occupation-measurement of the Majorana system can then distinguish between the order of the two sequences. If the zero energy states are not Majorana bound states, but rather trivial sub gap states, then the emptying and filling of the dot would result in Abelian operations on the zero energy states. The above protocol depends on the fine tuning of the system parameters ϕ, θ and the adiabatic control of ε. In experiment, such a protocol would require to perform the initialization-operation-measurement-cycle repeatedly to be able to confidently distinguish the order of operations statistically. In the remainder of this chapter, we study the effects of systematical errors in ϕ, θ before considering the adiabatic control of the dot level energy in 4.1. We assume throughout that the system parameters can be tuned precisely but not accurately. For this reason, we consider only the systematical errors and not the statistical errors. Understanding these errors enable us to propose a more refined protocol which mitigates the effect of the errors.

3.2 The effect of systematic errors in the coupling parameters

A statistical error in θ has straightforward implications as it merely results in shifting the weights given to γ_1 and γ_2 in $\cos(\theta)\gamma_1 + \sin(\theta)\gamma_2$, moving it a way from the ideal situation $\theta = \pi/4$. Errors in ϕ are on the other hand more involved. If we have not tuned the system to $\phi = 2\pi n$, the different parity states are not degenerate and a relative dynamical phase is gained between the even and odd sectors whose effect we study later in this section. The errors in ϕ also influences the relative geometric phase and we study this effect first. To understand implications of $\phi \neq 2\pi n$, we will view the operation on the Majorana system as giving different phases to the even and odd states. By rewriting in terms of the fermionic operators,

$$\cos(\theta)\gamma_1 + \sin(\theta)\gamma_2 = e^{i\theta}d_1^\dagger + e^{-i\theta}d_1. \tag{3.21}$$

We can understand $d_1^\dagger$ and d_1 as acting on the even or odd parity sector if we also consider the operation on the dot. To exemplify, let the initial state in our consideration be

$$|i\rangle = |0\rangle_{\mathrm{D1}}\,(\alpha\,|0\rangle_{\mathrm{M12}} + \beta\,|1\rangle_{\mathrm{M12}}), \tag{3.22}$$

Filling the dot adiabatically corresponds to using the operator $c_1^\dagger$, and due to parity conservation, we must act with $d_1^\dagger$ on $|0\rangle_{\mathrm{M12}}$ and d_1 on $|1\rangle_{\mathrm{M12}}$. In this manner, $d_1^\dagger$ is assigned to the even sector acting on $|0\rangle_{\mathrm{D1}}|0\rangle_{\mathrm{M12}}$. Likewise, d_1 is assigned to the odd sector. Thus, the total operator acting on the initial state is,

$$|f\rangle = P_\uparrow |i\rangle, \qquad P_\uparrow = c_1^\dagger(d_1^\dagger + d_1), \tag{3.23}$$

giving the final state $|f\rangle = |1\rangle_{\mathrm{D1}}(\alpha|1\rangle_{\mathrm{M12}} + \beta|0\rangle_{\mathrm{M12}})$. The index $\uparrow/\downarrow$ denotes filling and emptying the dot respectively. In addition, we will use $U_\uparrow(\phi,\theta)$ to denote the part of $P_\uparrow$ that acts on the Majorana system. In this case, we have $U_\uparrow^0(\phi = 2\pi n, \theta = 0) = d_1^\dagger + d_1$. Note that if we had started in $|1\rangle_{\mathrm{D1}}$ and emptied the dot by applying c_1, we would instead assign $d_1^\dagger$ to the odd sector and vice versa. In this case, the operator acting on $|i\rangle$ would be $P_\downarrow = c_1(d_1^\dagger + d_1)$ with the Majorana part $U_\downarrow^0(\phi,\theta) = U_\uparrow^0(\phi,\theta)$. This is the same story leading up to eq. (3.8) where the even and odd Hamiltonians are identical and no relative geometric phase is gained. In the case of one dot coupled to two Majoranas as in Fig. 3.2, the even and odd state acquires different geometric phases amounting to a relative geometric phase $\theta_\uparrow^G$ when filling the dot. The relative geometric phase may depend on θ, ϕ so we need to assign the phase $\theta_\uparrow^G(\phi,\theta)/2$ to the even state and $-\theta_\uparrow^G(\phi,\theta)/2$ to the the odd state. As an operator, we attach these phases to the relevant fermionic operators, $d_1^\dagger$ for the even part and d_1 for the odd,

$$M_\uparrow^G(\phi,\theta) = e^{i\theta_\uparrow^G/2} d_1^\dagger + e^{-i\theta_\uparrow^G/2} d_1, \tag{3.24}$$

taking into account $\phi \neq 2\pi n$. Compare this operator to eq. (3.21). When emptying the dot, the geometric phases are reversed. The even state acquires $-\theta_\uparrow^G(\phi,\theta)/2$ and the odd state acquires $\theta_\uparrow^G(\phi,\theta)/2$. This is canceled by the fact that d_1 now is assigned to the even sector and vice versa. For this reason, the operator acting on the Majorana system is identical when filling and emptying the dot $U_\downarrow^G(\phi,\theta) = U_\uparrow^G(\phi,\theta)$, despite the geometric phase changing sign. We continue by computing the geometric phases for the even and odd ground states to determine the general operator $M(\phi,\theta)$. The snapshot eigenstates of the Hamiltonian in eq. (3.9) is,

$$\left|\Psi_\pm^\rho(t)\right\rangle = \frac{1}{\sqrt{(E_\pm^\rho(t))^2 + |v^\rho|^2}} \begin{pmatrix} v^\rho \\ E_\pm^\rho(t) \end{pmatrix}. \tag{3.25}$$

We have chosen a different gauge for each parity such that the snapshot eigenstates are on the form $(e^{ia}\cos b(t), \sin b(t))^T$. In an adiabatic process taking time T, we remain in the snapshot eigenstates and acquire a geometric phase given by,

$$\theta^G = i\int_0^T \mathrm{d}t \,\langle\Psi(t)|\,\frac{\mathrm{d}}{\mathrm{d}t}\,|\Psi(t)\rangle\,. \tag{3.26}$$

By straightforward calculations we get,

$$\theta^G = i\int_0^T \mathrm{d}t (e^{-ia}\cos b(t), \sin b(t)) \begin{pmatrix} -e^{ia}\dot{b}(t)\sin b(t) \\ \dot{b}(t)\cos b(t) \end{pmatrix} = 0, \tag{3.27}$$

which vanishes. When emptying or filling the dot, no geometric phase is gained for a given parity using this gauge. However, the gauge choice is different for each parity and this amounts to a relative geometric phase between the even and the odd ground states. Taking the example of filling the dot, the ground states at $t = 0$ are subject to $\varepsilon/|v^\rho| \to \infty$ and as a result $E_-^\rho(0) \to 0$, giving,

$$\left|\Psi_-^\rho(0)\right\rangle \to \begin{pmatrix} v^\rho/|v^\rho| \\ 0 \end{pmatrix}. \tag{3.28}$$

The relative phase $\theta^G(t=0)$ between these two states is found through

$$\tan\big(\theta^G(0)\big) = \frac{\mathrm{Im}[\langle\Psi_-^+(0)|\Psi_-^-(0)\rangle]}{\mathrm{Re}[\langle\Psi_-^+(0)|\Psi_-^-(0)\rangle]} = -\tan(2\theta)\cos(\phi/2). \tag{3.29}$$

Similarly, after the process, at $t=T$, the energy is $E_-^\rho(T)/|v^\rho| \to -\infty$ and the ground states are $|\Psi_-^\rho(T)\rangle = (0,1)^T$. Consequently, at time $t=T$ the relative phase between the even and odd snapshot ground states is zero,

$$\theta^G(T) = 0. \tag{3.30}$$

The accumulated relative geometric phase between the even and the odd ground states when filling the dot thus is

$$\theta_\uparrow^G(\phi,\theta) = \theta^G(T) - \theta^G(0) = \arctan[\tan(2\theta)\cos(\phi/2)]. \tag{3.31}$$

If we instead empty the dot, the geometric phase is reversed, $\theta_\downarrow^G(\phi,\theta) = -\theta^G(T) + \theta^G(0) = -\theta_\uparrow^G$. As discussed, the resulting operation performed on the Majorana system is the same in either case,

$$U_\uparrow^G(\phi,\theta) = e^{i\theta_\uparrow^G/2} d_1^\dagger + e^{-i\theta_\uparrow^G/2} d_1 = \cos\big(\theta_\uparrow^G/2\big)\gamma_1 + \sin\big(\theta_\uparrow^G/2\big)\gamma_2, \tag{3.32}$$

which simplifies to the known result $\cos(\theta)\gamma_1 + \sin(\theta)\gamma_2$ for $\phi = 0$.

Understanding the operation on the Majorana system by evolving the even and odd sectors with different phases is very useful. It has enabled us to compute the effect of systematic errors in ϕ. This would not have been possible with the picture used in [1] where the Majorana operator γ_{12} only in the ideal situation $\phi = 2\pi n$ factors out, see eq. (3.13). In the remainder of this section, we exploit that we can treat the the dynamical phase on equal footing with the geometric phase. We use this to determine the effect of the relative dynamical phase induced by the degeneracy split between the even and odd parity sectors when $\phi \neq 2\pi n$. We begin again with the example where the dot is filled adiabatically in a time T and introduce the dimensionless time-parameter $s = t/T$. The relative dynamical phase between the even and odd ground states is in this case

$$\theta_\uparrow^D(\phi,\theta) = -T\int_0^1 \mathrm{d}s\ (E_-^-(s) - E_-^+(s)), \tag{3.33}$$

which is a dynamical quantity dependent on the time it takes to perform the operation. Since $\theta_\uparrow^D$ increases with T and the adiabatic condition assumes that T is large, it is important to minimize the dynamical phase in other ways. It is also useful to introduce the dimensionless dot level energy $x = \varepsilon/(2v)$. In Sec. 4.1, we argue that it is optimal to control the dot level energy during the charge-transfer process according to

$$\dot{x}(s) = \pm\Omega_\eta (x(s)^2 + 1)^{\eta/2}, \tag{3.34}$$

since it is a power of the energy gap between ground state and excited state. Here, the dot denotes a derivative with respect to the dimensionless time s. The real constant Ω_η is determined through the initial condition of the differential equation and the sign $(+/-)$ corresponds to emptying/filling and η is a real parameter. In Sec. 4.2, we compute Ω_η, see eq. (4.44). This ansatz is relevant as it enables us to replace the integral over time with an integral over the dimensionless dot level energy. Expanding the relative dynamical phase to leading order in $\sin(2\theta)\sin(\phi/2) \ll 1$ and rewriting in terms of $x, \dot{x}$, we find

$$\theta^D_\uparrow(\phi,\theta) = -\sin(2\theta)\sin(\phi/2)Tv\int_{-\infty}^{\infty}\mathrm{d}x\ \frac{1}{\dot{x}\sqrt{x^2+1}} = -\sin(2\theta)\sin(\phi/2)\frac{Tv}{\Omega_\eta}\frac{\sqrt{\pi}\Gamma(\eta/2)}{\Gamma((\eta+1)/2)}, \tag{3.35}$$

for $\eta > 0$.

If $\eta \leq 0$, the integral diverges and this puts a bound our choice of reasonable η. Contrary to the geometric phase, the dynamical phase does not pick up a relative sign when emptying the dot since the above integrand is even and so $\theta^D_\uparrow = \theta^D_\downarrow = \theta^D$. This introduces a distinction in the operations on the Majorana system depending on whether the dot has been filled or emptied. When filling the dot, we attach the phases $\theta^D/2$ and $-\theta^D/2$ to $d_1^\dagger$ and d_1 respectively in addition to the geometric phases. This gives the total operator acting on the Majorana state during a process where the dot is filled,

$$U_\uparrow(\phi,\theta) = e^{i(\theta^G_\uparrow+\theta^D)/2}d_1^\dagger + e^{-i(\theta^G_\uparrow+\theta^D)/2}d_1 = \cos\big((\theta^G_\uparrow+\theta^D)/2\big)\gamma_1 + \sin\big((\theta^G_\uparrow+\theta^D)/2\big)\gamma_2. \tag{3.36}$$

When the dot is emptied, the phases $\theta^D/2$ and $-\theta^D/2$ is instead attached to d_1 and $d_1^\dagger$ respectively,

$$U_\downarrow(\phi,\theta) = e^{i(\theta^G_\uparrow-\theta^D)/2}d_1^\dagger + e^{-i(\theta^G_\uparrow-\theta^D)/2}d_1 = \cos\big((\theta^G_\uparrow-\theta^D)/2\big)\gamma_1 + \sin\big((\theta^G_\uparrow-\theta^D)/2\big)\gamma_2. \tag{3.37}$$

The dynamical phase results in $U_\uparrow(\phi,\theta) \neq U_\downarrow(\phi,\theta)$ breaking the symmetry between the operators when filling and emptying the dot. With these operators, we can reverse the effect of the geometric phases but the dynamical phases accumulate. Interestingly, both the geometric and dynamical phases changes signs when $\phi \to \phi + 2\pi$. For the geometric phase,

$$\begin{aligned}\theta^G_\uparrow(\phi+2\pi,\theta) &= \arctan[\tan(2\theta)\cos(\phi/2+\pi)] = -\arctan[\tan(2\theta)\cos(\phi/2)]\\ &= -\theta^G_\uparrow(\phi,\theta),\end{aligned} \tag{3.38}$$

and for the dynamical phase,

$$\begin{aligned}\theta^D(\phi+2\pi,\theta) &= -\sin(2\theta)\sin(\phi/2+\pi)\frac{Tv}{\Omega_\alpha}\frac{\sqrt{\pi}\Gamma(\alpha/2)}{\Gamma((\alpha+1)/2)} = \sin(2\theta)\sin(\phi/2)\frac{Tv}{\Omega_\alpha}\frac{\sqrt{\pi}\Gamma(\alpha/2)}{\Gamma((\alpha+1)/2)}\\ &= -\theta^D(\phi,\theta),\end{aligned} \tag{3.39}$$

since they both depend sinusoidally on $\phi/2$. In experiment, ϕ can be wound by 2π using the magnetic flux through the device. The change in magnetic field that accomplishes this winding depends on the geometry of the device and must be determined experimentally for the given sample. Performing this extra step is worthwhile as it enables a protocol where the dynamical phases can be canceled due to this sign flip. Therefore, we have now four fundamental operators. We produce a summary of the four fundamental operators and the associated relative phases gained between the even and odd ground states,

$$U_\uparrow(\phi) \longleftrightarrow \theta^G_\uparrow + \theta^D, \tag{3.40}$$

$$U_\downarrow(\phi) \longleftrightarrow -\theta^G_\uparrow + \theta^D, \tag{3.41}$$

$$U_\uparrow(\phi+2\pi) \longleftrightarrow -\theta^G_\uparrow - \theta^D, \tag{3.42}$$

$$U_\downarrow(\phi+2\pi) \longleftrightarrow \theta^G_\uparrow - \theta^D. \tag{3.43}$$

The explicit dependence on ϕ, θ has been suppressed unless where relevant. This overview also presents a quick method for determining the resulting operator acting on a pair of Majoranas from several

charge-transfer processes. By keeping track of the signs of the geometric and dynamical phases, we can simply add up the contributions from each process and assign the resulting phase to the even and odd states. We will use this method and the four fundamental operators in the next section to construct a protocol that efficiently demonstrate the non-Abelian exchange statistics of the Majoranas. By having all four combinations of $(\pm\theta^G_\uparrow \pm \theta^D)$ we can propose a protocol where the dynamical phase of subsequent operations will be canceled.

3.3 Introducing an efficient protocol

In the protocol suggested in [1], errors was not included. In this section, we propose a protocol which relies on fewer operations and tries to cancel the main source of error; the relative dynamical phase between the even and odd parity sectors. In the previous section, we have learned that there are contributions from both the geometric phase and the dynamical phase. It is the geometric phase that produces the non-Abelian effects associated with the Majoranas. The dynamical phase results in trivial effects reducing the visibility of the non-Abelian effects. For this reason, we should ideally design a protocol where the dynamical phase appears minimally. In Sec. 2.3, we have seen that Majorana non-Abelian statistics can be demonstrated by performing operations on the M23 Majoranas if we measure in the M12/M34-basis. Consequently, it is useful to change the basis to the M23/M14-basis when understanding the result of the operations on M23. We will call the M23/M14-basis the operation-basis as opposed to the measurement-basis of M12/M34. The fermionic annihilation operators in the operation-basis are

$$\tilde{d}_1 = \frac{1}{2}(\gamma_2 + i\gamma_3), \quad \tilde{d}_2 = \frac{1}{2}(\gamma_1 + i\gamma_4). \tag{3.44}$$

We define the occupancy states in the operation-basis as

$$\left|\widetilde{000}\right\rangle = |0\rangle_{\mathrm{D2}} \left|\tilde{0}\right\rangle_{\mathrm{M23}} \left|\tilde{0}\right\rangle_{\mathrm{M14}}, \tag{3.45}$$

$$\left|\widetilde{111}\right\rangle = c_2^\dagger \tilde{d}_1^\dagger \tilde{d}_2^\dagger \left|\widetilde{000}\right\rangle. \tag{3.46}$$

Note that no changes are made to the basis of the dot. The creation and annihilation operators in the operation-basis are related to the measurement-basis $d_1 = \frac{1}{2}(\gamma_1 + i\gamma_2)$, $d_2 = \frac{1}{2}(\gamma_3 + i\gamma_4)$ through

$$d_1 = \frac{1}{2}(\tilde{d}_2 + \tilde{d}_2^\dagger) + \frac{i}{2}(\tilde{d}_1 + \tilde{d}_1^\dagger), \tag{3.47}$$

$$d_2 = \frac{1}{2}(\tilde{d}_2 - \tilde{d}_2^\dagger) - \frac{i}{2}(\tilde{d}_1 - \tilde{d}_1^\dagger). \tag{3.48}$$

We can relate the states in the measurement-basis to the states in the operation-basis. One way of deducing their relation is to use $d_1 |00\rangle = 0$ and $d_2 |00\rangle = 0$ and use the ansatz $|00\rangle = a \left|\widetilde{00}\right\rangle + b \left|\widetilde{01}\right\rangle + c \left|\widetilde{10}\right\rangle + d \left|\widetilde{11}\right\rangle$, omitting the state of the dot. We find for the Majorana states,

$$d_1 |00\rangle = \frac{1}{2}(\tilde{d}_2 + \tilde{d}_2^\dagger + i\tilde{d}_1 + i\tilde{d}_1^\dagger)\left(a \left|\widetilde{00}\right\rangle + b \left|\widetilde{01}\right\rangle + c \left|\widetilde{10}\right\rangle + d \left|\widetilde{11}\right\rangle\right) \tag{3.49}$$

$$= \frac{1}{2}\left((b+ic) \left|\widetilde{00}\right\rangle + (ib-c) \left|\widetilde{11}\right\rangle + (a+id) \left|\widetilde{01}\right\rangle + (ia-d) \left|\widetilde{10}\right\rangle\right) = 0, \tag{3.50}$$

$$d_2 |00\rangle = \frac{1}{2}(\tilde{d}_2 - \tilde{d}_2^\dagger - i\tilde{d}_1 + i\tilde{d}_1^\dagger)\left(a \left|\widetilde{00}\right\rangle + b \left|\widetilde{01}\right\rangle + c \left|\widetilde{10}\right\rangle + d \left|\widetilde{11}\right\rangle\right) \tag{3.51}$$

$$= \frac{1}{2}\left((b+ic) \left|\widetilde{00}\right\rangle + (c+ib) \left|\widetilde{11}\right\rangle + (-a-id) \left|\widetilde{01}\right\rangle + (ia-d) \left|\widetilde{10}\right\rangle\right) = 0, \tag{3.52}$$

and thus $b+ic=b-ic=0$ implying $b=c=0$ and $a+id=0$ giving $a=1/\sqrt{2}$ and $d=i/\sqrt{2}$. Using $d_1^\dagger$ and $d_2^\dagger$ expressed in the operation-basis we can build the rest of the states,

$$|00\rangle = \frac{1}{\sqrt{2}}\left(\left|\widetilde{00}\right\rangle + i\left|\widetilde{11}\right\rangle\right), \tag{3.53}$$

$$|01\rangle = \frac{1}{\sqrt{2}}\left(\left|\widetilde{01}\right\rangle + i\left|\widetilde{10}\right\rangle\right), \tag{3.54}$$

$$|10\rangle = \frac{1}{\sqrt{2}}\left(\left|\widetilde{01}\right\rangle - i\left|\widetilde{10}\right\rangle\right), \tag{3.55}$$

$$|11\rangle = \frac{1}{\sqrt{2}}\left(\left|\widetilde{00}\right\rangle - i\left|\widetilde{11}\right\rangle\right). \tag{3.56}$$

In the protocol in eqs. (3.19) and (3.20), we can experimentally distinguish between the states $|00\rangle$ and $|11\rangle$. In the operation-basis, we see that $|00\rangle$ and $|11\rangle$ corresponds to different relative phases between $\left|\widetilde{00}\right\rangle$ and $\left|\widetilde{11}\right\rangle$. It is exactly the relative phase between $\left|\widetilde{00}\right\rangle$ and $\left|\widetilde{11}\right\rangle$ we affect in the charge-transfer process with M23. To see this, we assume to initialize in the state

$$|000\rangle = \frac{1}{\sqrt{2}}\left(\left|0\widetilde{00}\right\rangle + i\left|0\widetilde{11}\right\rangle\right). \tag{3.57}$$

Here, $\left|0\widetilde{00}\right\rangle$ is considered even as the joint parity of D2 and M23 is even. Accordingly, it evolves with the Hamiltonian describing even parity and acquires the phase we associate with the even sector during the charge-transfer process. Likewise, $\left|0\widetilde{11}\right\rangle$ is subject to the time-evolution of the odd Hamiltonian. Algebraically, filling the dot results in

$$|000\rangle \to c_2^\dagger\left(e^{i(\theta_\uparrow^G+\theta^D)/2}\tilde{d}_1^\dagger + e^{-i(\theta_\uparrow^G+\theta^D)/2}\tilde{d}_1\right)\frac{1}{\sqrt{2}}\left(\left|0\widetilde{00}\right\rangle + i\left|0\widetilde{11}\right\rangle\right) \tag{3.58}$$

$$\to \frac{1}{\sqrt{2}}\left(e^{i(\theta_\uparrow^G+\theta^D)/2}\left|1\widetilde{10}\right\rangle + ie^{-i(\theta_\uparrow^G+\theta^D)/2}\left|1\widetilde{01}\right\rangle\right), \tag{3.59}$$

which introduces the relative phase $\theta_\uparrow^G+\theta^D$ between the even and odd states. We may now use the summary in eqs. (3.40)-(3.43) to formulate a good protocol where the order of operations can be clearly distinguished by occupation measurements. We begin by focusing on the geometric phase as this is the effect we are interested in. We notice that we can add and subtract the geometric phase from subsequent operations by using $U_\uparrow$ and $U_\downarrow$,

$$U_\downarrow(\phi,\theta)U_\uparrow(\phi,\theta) \longleftrightarrow (-\theta_\uparrow^G+\theta^D)+(\theta_\uparrow^G+\theta^D) = 2\theta_D, \tag{3.60}$$

$$U_\uparrow(\phi,\theta)U_\uparrow(\phi,\theta) \longleftrightarrow (\theta_\uparrow^G+\theta^D)+(\theta_\uparrow^G+\theta^D) = 2\theta_\uparrow^G+2\theta_D. \tag{3.61}$$

We should also keep in mind the physical restriction of not being able to fill the dot twice in a row but must alternate between filling and emptying. This disqualifies the second of the above equations but it can be salvaged by inserting an operator such as $\gamma_2 = U_{\uparrow/\downarrow}(\phi,\theta=0) = \tilde{d}_1^\dagger + \tilde{d}_1$ where the dot can be emptied. The upside of using γ_2 in the protocol is that it does not depend on tuning ϕ or θ. Using γ_2 gives the physically relevant protocol,

$$\gamma_2 U_\downarrow(\phi,\theta)U_\uparrow(\phi,\theta) \longleftrightarrow (-\theta_\uparrow^G+\theta^D)+(\theta_\uparrow^G+\theta^D) = 2\theta_D, \tag{3.62}$$

$$U_\uparrow(\phi,\theta)\gamma_2 U_\uparrow(\phi,\theta) \longleftrightarrow (\theta_\uparrow^G+\theta^D)+(\theta_\uparrow^G+\theta^D) = 2\theta_\uparrow^G+2\theta_D. \tag{3.63}$$

It is clear that U and γ_2 does not commute. The difference is most pronounced when $2\theta_\uparrow^G=\pi$ which in the ideal case $\phi=2\pi n$ corresponds to $\theta=\pi/4$. Acting with these operators on the initial Majorana state in measurement-basis gives

$$\gamma_2 U_\downarrow(\phi,\theta)U_\uparrow(\phi,\theta)\,|00\rangle = \cos\big(\theta^D\big)\,|01\rangle - i\sin\big(\theta^D\big)\,|10\rangle\,, \tag{3.64}$$

$$U_\uparrow(\phi,\theta)\gamma_2 U_\uparrow(\phi,\theta)\,|00\rangle = \cos\big(\theta^G_\uparrow+\theta^D\big)\,|01\rangle - i\sin\big(\theta^G_\uparrow+\theta^D\big)\,|10\rangle\,. \tag{3.65}$$

In the ideal situation $\theta^G_\uparrow = \pi/2,\ \theta^D = 0$, we would measure $|01\rangle$ for the first order of operations and $|10\rangle$ for the second order, distinguishing between the two sequences of operations. Even when the parameters $\phi,\ \theta$ are only slightly deviating from the ideal case, the dynamical phase might still be significant since it depends on the time scale of the process in addition to the parameters in the Hamiltonian. This restricts the range of the parameters where the final states of the two orders can be distinguished statistically by repeating the protocol. By also using the ϕ-flipped operators $U_{\uparrow/\downarrow}(\phi+2\pi,\theta)$ it is possible to have the dynamical phases of subsequent operations canceling. Here, we exploit that the ϕ-flip, $\phi\to\phi+2\pi$, changes the sign of the dynamical phase. Consider in this case the corresponding relative phase,

$$\gamma_2 U_\downarrow(\phi+2\pi,\theta)U_\uparrow(\phi,\theta) \longleftrightarrow -(-\theta^G_\uparrow+\theta^D)+(\theta^G_\uparrow+\theta^D) = 2\theta_G, \tag{3.66}$$

$$U_\uparrow(\phi+2\pi,\theta)\gamma_2 U_\uparrow(\phi,\theta) \longleftrightarrow -(\theta^G_\uparrow+\theta^D)+(\theta^G_\uparrow+\theta^D) = 0, \tag{3.67}$$

where the last of the U-operators have been ϕ-flipped, canceling the dynamical phases and leaving only the geometric phases. In the measurement-basis, the outcome of the operations in eqs. (3.66) and (3.67) are

$$\gamma_2 U_\downarrow(\phi+2\pi,\theta)U_\uparrow(\phi,\theta)\,|00\rangle = \cos\big(\theta^G_\uparrow\big)\,|01\rangle - i\sin\big(\theta^G_\uparrow\big)\,|10\rangle\,, \tag{3.68}$$

$$U_\uparrow(\phi+2\pi,\theta)\gamma_2 U_\uparrow(\phi,\theta)\,|00\rangle = |01\rangle\,. \tag{3.69}$$

The benefit of performing the ϕ-flip is evident. By canceling the dynamical phase, the second order of operations gives the result $|01\rangle$ regardless of the parameters. In the ideal case $\theta^G_\uparrow = \pi/2$, the outcome of the two sequences is different. Close to the ideal case, the two sequences can be distinguished statistically, however, the outcome is identical for $\theta^G_\uparrow = n\pi$ so experiments should be tuned away from this point.

We have proposed two similar protocols in eqs. (3.64-3.65) and (3.66-3.67) which can exhibit the non-Abelian nature of Majoranas. Compared to the protocol in [1], our protocol has a few advantages. The protocols need only to perform operations on the M23 Majorana pair instead of all three pairs. The number of operations is three rather than four with one being the parameter independent γ_2-operation. Noticeably, the second protocol described in eqs. (3.66-3.67) includes an additional initial step. By determining the change in magnetic flux that results in a winding of the coupling phase ϕ by 2π, the second protocol can cancel the contribution from the dynamical phase. This trick broadens the range of parameters for which the protocol can confidently show the non-Abelian nature of the Majoranas as we show numerically in Sec. 5. If ϕ is not wound by 2π exactly, but rather is offset by a small amount $\delta\phi$ to $\phi+2\pi+\delta\phi$, the ϕ-flip-trick suppresses the dynamical phase to a value of the order $\delta\phi$ which is still a significant improvement if $\delta\phi \ll 1$. At this point, we have addressed two of the four parameters in the Hamiltonian. Having covered the coupling parameters ϕ,θ we are left with the dot level energy ε and coupling strength v. So far we have simply assumed that the control of ε is completely adiabatic and not taken into account the errors that may arise when emptying or filling the in finite time. The relevance is two-fold; errors due to non-adiabaticity may result in exciting the system out of the ground state manifold which corrupts the protocol. On the other hand, we need also

to minimize the dynamical phase. As a consequence, the time scale of the emptying/filling-process should be long enough to suppress the excitations but still sufficiently short to minimize the dynamical phase. In this context, the coupling strength v plays a subtle but important role. In the next chapter, we review the framework of adiabatic perturbation theory due to Rigolin et al. [2] and use it to asses the corrections due to non-adiabatic errors. Following in Sec. 4, we test our predictions from adiabatic perturbation against a numerical simulation.

Chapter 4

Adiabatic perturbation theory

In the charge-transfer operation described in Sec. 3.1, several assumptions are made which might require to fine tune the device. We have discussed the possible issues of tuning the tunnel couplings between Majoranas and the dot in the previous chapter. In this chapter, we analyze the issues due to a non-adiabatic dot level evolution. We imagine the dot level energy to be controlled slowly in experiment to secure that the system evolves adiabatically and remains in the ground state manifold. The gap between the ground state and the excited state depends heavily on the particular value of $\varepsilon(t)$ during the charge-transfer process. For this reason, the dot level energy can be changed faster when the gap is large but needs to change slower when the gap is smaller. This is important as we need also to keep in mind that the undesired dynamical phase grows with the time T it takes to complete the process. This competition between adiabaticity and minimization of the dynamical phase raises two questions: 1) What is the optimal time scale of the charge-transfer process and 2) how should the dot level energy be controlled as a function of time? To answer these questions, we will first develop adiabatic perturbation theory following Rigolin et al. [2]. This is a perturbation theory in the small quantity $1/T$ which we will then apply to the charge-transfer process to calculate the first order corrections in $1/T$. This treatment will give rise to some slightly subtle details about the perturbation theory not being expanded in a dimensionless parameter rendering the results erroneous. In the last section of this chapter, we try to amend these issues by formulating the relevant dimensionless expansion parameter for the charge-transfer process.

4.1 Deriving adiabatic perturbation theory

We begin the derivation of adiabatic perturbation theory by studying a non-degenerate n-level quantum system before specializing to the two-level case. Let us consider a generic time-dependent Hamiltonian $H(t)$ evolving states $|\Psi(t)\rangle$ according to the Schrödinger equation,

$$i\frac{1}{T}\frac{\mathrm{d}}{\mathrm{d}s}|\Psi(s)\rangle = H(s)|\Psi(s)\rangle\,, \tag{4.1}$$

where $s = t/T$ and T is the characteristic time scale of the Hamiltonian. The instantaneous eigenenergies are assumed non-degenerate and are given by

$$H(s)|n(s)\rangle = H(s)E_n(s), \tag{4.2}$$

where $|n(s)\rangle$ are the snapshot eigenstates in this chapter. The adiabatic theorem states that if a the system starts out in a state $|n(s=0)\rangle$, then the system remains in that snapshot eigenstate $|n(s)\rangle$

throughout the time evolution, given that the characteristic time scale of the Hamiltonian T is much larger than the energy separation between E_n and the rest of the spectrum, i.e. $T \gg |E_i - E_n|^{-1}$. The aim is now to develop an adiabatic perturbation theory in the small quantity $1/T$ from which the first order corrections to the adiabatic approximation can be derived. A further benefit of adiabatic perturbation theory is that it states the condition for the adiabatic theorem precisely and rigorously.

The main difficulty is to find an ansatz for the state $|\Psi(s)\rangle$ which factors out the highly oscillatory dynamical phases $e^{-iT\omega_n(s)}$ and secondly, the geometrical phases $e^{i\gamma_n(s)}$. In terms of the rescaled time s, the dynamical and geometric phases are given by

$$\omega_n(s) = \int_0^s \mathrm{d}s' \; E_n(s'), \tag{4.3}$$

$$\gamma_n(s) = i\int_0^s \mathrm{d}s' \; \langle n(s')|\dot{n}(s')\rangle \,, \tag{4.4}$$

where the dot denotes $\frac{\mathrm{d}}{\mathrm{d}s}$. An appropriate ansatz is given in [2],

$$|\Psi(s)\rangle = \sum_{p=0}^{\infty} \frac{1}{T^p} \sum_{n,m=0} e^{-iT\omega_m(s)} e^{i\gamma_m} b_{nm}^{(p)}(s)\, |n(s)\rangle \,, \tag{4.5}$$

where $b_{nm}^{(p)}(s)$ are complex valued time dependent coefficients. With this ansatz, the number of coefficients has been expanded from the original N degrees of freedom in the Schrödinger equation to N^2 coefficients for each order in the perturbation theory p. We will later use this redundancy to enforce restrictions on the coefficients. The object of the adiabatic perturbation theory is to find expressions for these coefficients. The $p = 0$ term in eq. (4.5) descirbes the adiabatic evolution, whice gives a constraint to the zeroth order coefficients. Demanding that the system evolves according to the snapshot eigenstates implies

$$b_{nm}^{(0)}(s) = 0 \qquad \text{for } n \neq m. \tag{4.6}$$

A further implication is that the initial state is described by the adiabatic theorem, meaning

$$\sum_{m=0} b_{nm}^{(p)}(0) = 0 \qquad \text{for } p \geq 1. \tag{4.7}$$

By inserting the ansatz into the Schrödinger equation of eq. (4.1) and left multiplying with $\langle k(s)|$ while using orthonormality of the snapshot eigenstates, we get

$$\sum_{m=0}\sum_{p=0}^{\infty} \frac{1}{T^p} e^{-iT\omega_m(s)} e^{i\gamma_m} \left(iT\Delta_{km}(s) b_{km}^{(p)}(s) + \dot{b}_{km}^{(p)}(s) - M_{mm}(s) b_{km}^{(p)}(s) + \sum_{n=0} M_{kn}(s) b_{nm}^{(p)}(s) \right) = 0, \tag{4.8}$$

where $\Delta_{nm}(s) = E_n(s) - E_m(s)$ and $M_{nm}(s) = \langle n(s)|\dot{m}(s)\rangle$. The $\frac{1}{T^p} iT\Delta_{km}(s) b_{km}^{(p)}(s)$ term seems to be divergent for $1/T \to 0$, but due to the constraints of the zeroth order coefficients it remains finite. To see this, rewrite the term as

$$\sum_{p=0}^{\infty} \frac{1}{T^p} iT\Delta_{km}(s) b_{km}^{(p)}(s) = iT\Delta_{km}(s) b_{km}^{(0)}(s) + \sum_{p=0}^{\infty} \frac{i}{T^p} \Delta_{km}(s) b_{km}^{(p+1)}(s). \tag{4.9}$$

The apparent diverging term has been separated from the sum. Now it is clear that for $k = m$ it vanishes due to $\Delta_{kk}(s) = 0$ while for $k \neq m$ it vanishes due to the constraint from eq. (4.6). Substituting back in gives

$$\sum_{m=0}\sum_{p=0}^{\infty} \frac{1}{T^p} e^{-iT\omega_m(s)} e^{i\gamma_m} \left(i\Delta_{nm}(s) b_{nm}^{(p+1)}(s) + \dot{b}_{nm}^{(p)}(s) - M_{mm}(s) b_{nm}^{(p)}(s) + \sum_{k=0} M_{nk}(s) b_{km}^{(p)}(s) \right) = 0, \tag{4.10}$$

where n and k has been interchanged. We impose that the above condition is fulfilled order by order in $1/T$ and further demand the condition is satisfied also for each m. We have freedom to choose the latter as we have introduced additional degrees of freedom from the ansatz. The coefficients can be calculated recursively from the resulting equations

$$i\Delta_{nm}(s)b_{nm}^{(p+1)}(s) + \dot{b}_{nm}^{(p)}(s) + W_{nm}(s)b_{nm}^{(p)}(s) + \sum_{\substack{k=0\\k\neq n}} M_{nk}(s)b_{km}^{(p)}(s) = 0, \tag{4.11}$$

where $W_{nm}(s) = M_{nn}(s) - M_{mm}(s)$ has been introduced. This is a key result from [2]. The coefficients can now be calculated for $n \neq m$ as

$$b_{nm}^{(p+1)}(s) = \frac{i}{\Delta_{nm}(s)}\left(\dot{b}_{nm}^{(p)}(s) + W_{nm}(s)b_{nm}^{(p)}(s) + \sum_{\substack{k=0\\k\neq n}} M_{nk}(s)b_{km}^{(p)}(s)\right). \tag{4.12}$$

For the $n = m$ case, both $\Delta_{nm}(s)$ and $W_{nm}(s)$ vanishes and we must integrate eq. (4.11) for $p+1$. This yields

$$b_{nn}^{(p+1)}(s) = b_{nn}^{(p+1)}(0) - \sum_{\substack{k=0\\k\neq n}} \int_0^s \mathrm{d}s'\ M_{nk}(s')b_{kn}^{(p+1)}(s'). \tag{4.13}$$

Here, $b_{nn}^{(p+1)}(0)$ is related to all the other $(p+1)$-order coefficients through eq. (4.7) which is then determined by the equation for $n \neq m$. Inserting the equation for $b_{kn}^{(p+1)}(s')$ in the integrand gives

$$\begin{aligned} b_{nn}^{(p+1)}(s) = &- \sum_{\substack{k=0\\k\neq n}} b_{nk}^{(p+1)}(0) - i\sum_{\substack{k=0\\k\neq n}} \int_0^s \mathrm{d}s' \frac{M_{nk}(s')W_{kn}(s')}{\Delta_{kn}(s')} b_{kn}^{(p)}(s') \\ &- i\sum_{\substack{k=0\\k\neq n}} \int_0^s \mathrm{d}s' \left(\frac{M_{nk}(s')}{\Delta_{kn}(s')}\dot{b}_{kn}^{(p)}(s') + \sum_{\substack{m=0\\m\neq k}} \frac{M_{nk}(s')M_{km}(s')}{\Delta_{kn}(s')}) b_{mn}^{(p)}(s')\right). \end{aligned} \tag{4.14}$$

Using this equation alongside eq. (4.12) enables us to compute the time dependent coefficients to a given order in $1/T$ while only using the eigenenergies and eigenstates of the Hamiltonian.

At this point, we specialize to the relevant case of the two-Majorana charge-transfer system. The even and odd sectors can each be described as a two level system in a gauge with no geometric phase which implies $W_{nm}(s) = 0$. We further assume that the initial state is the ground state and calculate the first order correction in $1/T$. Starting in the ground state corresponds to the initial condition

$$\sum_{m=0}^{1} b_{nm}^{(0)}(0) = \delta_{n0}. \tag{4.15}$$

Using the initial condition and that the zeroth order coefficients are non-dynamical in eq. (4.12) (the $n \neq m$ case) gives

$$b_{01}^{(1)}(s) = 0, \tag{4.16}$$

$$b_{10}^{(1)}(s) = i\frac{M_{10}(s)}{\Delta_{10}(s)}. \tag{4.17}$$

Similarly, for the $n = m$ case in eq. (4.14) we get

$$b_{00}^{(1)}(s) = i\int_0^s \mathrm{d}s' \frac{|M_{10}(s')|^2}{\Delta_{10}(s')}, \tag{4.18}$$

$$b_{11}^{(1)}(s) = -i\frac{M_{10}(0)}{\Delta_{10}(0)}. \tag{4.19}$$

Here it has been used that $M_{nm} = -M_{mn}^*$ which can be seen by taking the derivative wrt. s of the orthonormality relation,

$$\langle n(s)|m(s)\rangle = \delta_{nm} \Longrightarrow M_{nm}(s) = -M_{mn}^*(s). \tag{4.20}$$

Having computed the first order coefficients we can now write down the time dependent state up to first order in adiabatic perturbation theory

$$\begin{aligned}|\Psi(s)\rangle = e^{-iT\omega_0(s)}&\left(1 + \frac{i}{T}\int_0^s \mathrm{d}s' \frac{|M_{10}(s')|^2}{\Delta_{10}(s')}\right)|0(s)\rangle \\ &+ \frac{i}{T}\left(e^{-iT\omega_0(s)}\frac{M_{10}(s)}{\Delta_{10}(s)} - e^{-iT\omega_1(s)}\frac{M_{10}(0)}{\Delta_{10}(0)}\right)|1(s)\rangle\,.\end{aligned} \tag{4.21}$$

Demanding that the first order contributions are small gives the exact condition for the application of the adiabatic theorem,

$$\frac{1}{T}\int_0^s \mathrm{d}s' \frac{|M_{10}(s')|^2}{\Delta_{10}(s')} \ll 1, \tag{4.22}$$

$$\frac{1}{T}\left|e^{-iT\omega_0(s)}\frac{M_{10}(s)}{\Delta_{10}(s)} - e^{-iT\omega_1(s)}\frac{M_{10}(0)}{\Delta_{10}(0)}\right| \ll 1. \tag{4.23}$$

These are the main points of [2]. In the system consisting of two Majoranas coupled to a dot, there are additional energy scales which need to be compared to the dimensionful expansion parameter $1/T$. Additionally, the way $\varepsilon(t)$ is controlled also introduces a dimensionless parameter relevant to the proper dimensionless expansion parameter. These aspects are not covered by the original work of [2] and give rise to some subtleties, challenging that eqs. (4.22) and (4.23) are the only relevant conditions in our case. We address this in Sec. 4.3 but begin with applying adiabatic perturbation theory as derived above to the two-Majorana charge-transfer system, to understand how it works.

4.2 Investigating adiabatic perturbation theory

In this section we apply adiabatic perturbation theory to the two-Majorana charge-transfer system depicted in Fig. 3.2. This is an exercise in doing adiabatic perturbation theory where we disregard the subtleties arising from the expansion parameter $1/T$ being a dimensionful quantity. For this reason, the following results should be applied with care. We use this section as a stepping stone leading up to the next section where we formulate adiabatic perturbation theory in dimensionless parameters. We consider the process where the dot is filled during a time T. We assume that the process is symmetric with the initial dot level energy being $\varepsilon(s = 0) = \varepsilon_0$ and the final level energy being $\varepsilon(s = 1) = -\varepsilon_0$. We take the dimensionless quantity $x_0 = \varepsilon_0/(2v) \gg 1$ to be large so a charge is transferred from the Majoranas to the dot. This is a large dimensionless parameter which may also influence the perturbation theory and we also postpone much of this discussion to the the next

section. We continue by reminding ourselves of the present situation. The instantaneous eigenenergy equations for the even ($\rho = -$) and odd ($\rho = +$) sectors in dimensionless quantities are

$$\frac{1}{v}H^\rho(s)\,|n^\rho(s)\rangle = X_n^\rho(s)\,|n^\rho(s)\rangle\,, \quad \frac{1}{v}H^\rho(s) = \begin{pmatrix} 0 & v^\rho/v \\ (v^\rho/v)^* & 2x(s) \end{pmatrix}, \tag{4.24}$$

with dimensionless eigenenergies

$$X_n^\rho(s) = x(s) \pm \sqrt{x(s)^2 + |v^\rho|^2/v^2}, \tag{4.25}$$

expressed in terms of the dimensionless dot level energy $x(s) = \varepsilon(s)/(2v)$ and $|v^\rho|^2/v^2 = 1 + \rho\sin(2\theta)\sin(\phi/2)$. The ground state energy is indexed by $n = 0$ corresponding to the $(-)$ solution while the excited state is indexed by $n = 1$ and uses $(+)$. The corresponding eigenstates are

$$|n^\rho(s)\rangle = \frac{1}{\sqrt{X_n^\rho(s)^2 + |v^\rho|^2/v^2}} \begin{pmatrix} v^\rho/v \\ X_n^\rho(s) \end{pmatrix}, \tag{4.26}$$

The energy difference between the ground states and excited states for each parity, $\Delta_{10}^\rho(s)$, and $M_{10}^\rho(s)$, which is dimensionless, are the building blocks for adiabatic perturbation theory and relevant for us to compute. The energy difference has not been made dimensionless as it needs to carry a dimension to counter the dimensionful expansion parameter. To leading order in $\sin(2\theta)\sin(\phi/2) \ll 1$, the energy difference is independent of ρ and we drop this superscript,

$$\Delta_{10}(s) = 2v\sqrt{x(s)^2 + 1}. \tag{4.27}$$

To calculate $M_{10}^\rho(s)$, we take the derivative with respect to s of the snapshot eigenstate, eq. (4.24), and left multiply with $\langle m^\rho(s)|$ to get

$$M_{nm}^\rho(s) = \frac{\langle n^\rho(s)|\,\frac{1}{v}\dot{H}^\rho(s)\,|m^\rho(s)\rangle}{\Delta_{mn}(s)/v}. \tag{4.28}$$

By direct computation,

$$\langle 1^\rho(s)|\,\frac{1}{v}\dot{H}^\rho(s)\,|0^\rho(s)\rangle = \frac{2\dot{x}(s)X_0^\rho(s)X_1^\rho(s)}{\sqrt{|v^\rho|^4/v^4 + |v^\rho|^2/v^2(X_0^\rho(s)^2 + X_1^\rho(s)^2) + X_0^\rho(s)^2X_1^\rho(s)^2}}. \tag{4.29}$$

Since $X_0^\rho(s)$ and $X_1^\rho(s)$ are the eigenvalues of $\frac{1}{v}H^\rho(s)$, the above equation can easily be simplified using

$$X_0^\rho(s)^2 + X_1^\rho(s)^2 = \mathrm{tr}\left[\frac{1}{v^2}H^\rho(s)^2\right] = \mathrm{tr}\begin{bmatrix} |v^\rho|^2/v^2 & 2x(s)v^\rho/v \\ 2x(s)(v^\rho/v)^* & |v^\rho|^2/v^2 + 4x(s)^2 \end{bmatrix} = 2|v^\rho|^2/v^2 + 4x(s)^2, \tag{4.30}$$

$$X_0^\rho(s)X_1^\rho(s) = \det\left[\frac{1}{v}H^\rho(s)\right] = \det\begin{bmatrix} 0 & v^\rho/v \\ (v^\rho/v)^* & 2x(s) \end{bmatrix} = -|v^\rho|^2/v^2. \tag{4.31}$$

Inserting these gives

$$\langle 1^\rho(s)|\,\frac{1}{v}\dot{H}^\rho(s)\,|0^\rho(s)\rangle = \frac{-2\dot{x}(s)|v^\rho|/v}{\sqrt{\mathrm{tr}\left[\frac{1}{v^2}H^\rho(s)^2\right] - 2\det\left[\frac{1}{v}H^\rho(s)\right]}} = \frac{-2\dot{x}(s)|v^\rho|/v}{\Delta_{10}(s)/v}, \tag{4.32}$$

where it has been used that $\Delta_{10}^\rho(s)/v = \sqrt{(X_1^\rho(s) - X_0^\rho(s))^2} = \sqrt{\mathrm{tr}\left[\frac{1}{v^2}H^\rho(s)^2\right] - 2\det\left[\frac{1}{v}H^\rho(s)\right]}$. For $M_{nm}^\rho(s)$, we finally get

$$M_{nm}^\rho(s) = \frac{-\dot{x}(s)|v^\rho|/v}{2(x(s)^2 + 1)}. \tag{4.33}$$

We are now ready to calculate the first order corrections in $1/T$. We begin by considering the ground state only and then we consider transitions. To this order in adiabatic perturbation theory, the even and odd ground states evolve according to eq. (4.21) in the process where the dot is filled,

$$|0^\rho(0)\rangle \longrightarrow e^{-iT\omega_0^\rho(s)}e^{iA^\rho(s)}\,|0^\rho(s)\rangle\,, \tag{4.34}$$

where it has been used that $1+x\approx e^x$ since

$$A^\rho(s)=\frac{1}{T}\int_0^s \mathrm{d}s'\frac{|M_{10}^\rho(s')|^2}{\Delta_{10}(s')}, \tag{4.35}$$

is assumed small, see eq. (4.22). Note that the correction phase $A^\rho(s)$ is not a new quantum phase but rather a correction to the existing dynamical and geometric phases arising since the evolution is not entirely adiabatic. Substituting the expressions for $\Delta_{10}(s)$ and $M_{10}^\rho(s)$ gives,

$$A^\rho(s=1)=\frac{|v^\rho|^2/v^2}{8Tv}\int_0^1 \mathrm{d}s\frac{\dot{x}(s)^2}{(x(s)^2+1)^{5/2}}=\frac{|v^\rho|^2/v^2}{8Tv}\int_0^1 \mathrm{d}s\;\mathcal{L}(x,\dot{x}). \tag{4.36}$$

Minimising this phase is a variational problem reminiscent of Lagrangian mechanics. Here, the correction phase acts as a kinetic action. Since the Lagrangian in this case does not depend explicitly on time, we can use the Beltrami identity,

$$C=\dot{x}\frac{\mathrm{d}\mathcal{L}}{\mathrm{d}\dot{x}}-\mathcal{L} \tag{4.37}$$

where C is a constant dependent on initial conditions. In classical mechanics, C would correspond to the energy in a conserved system, and since the Lagrangian only has a kinetic term, we have

$$\mathcal{L}(x,\dot{x})=C\longrightarrow \dot{x}(s)=\pm\sqrt{C}(x(s)^2+1)^{5/4}, \tag{4.38}$$

where filling the dot would correspond to the $(-)$ solution. It becomes relevant to study a slightly generalized version of this differential equation. In Sec. 3.2, we considered

$$\dot{x}(s)=\pm\Omega_\eta(x(s)^2+1)^{\eta/2}, \tag{4.39}$$

which would correspond to $\eta=5/2$ in the present case. It is worthy to note that the rate of change of the dot level energy is proportional to the energy gap to some power. This is a good ansatz as it captures the correspondence of going fast/slow when the gap is large/small. The solution to the η-dependent first order non-linear differential equation in eq. (4.39) is

$$K_\eta-\Omega_\eta s=x(s)F\left(\frac{1}{2},\frac{\eta}{2};\frac{3}{2};-x(s)^2\right), \tag{4.40}$$

with K_η being a constant of integration and $F(a,b;c;z)$ is the Gauss hypergeometric function defined by

$$F(a,b;c;z)=\frac{\Gamma(c)}{\Gamma(a)\Gamma(b)}\sum_{n=0}^{\infty}\frac{\Gamma(a+n)\Gamma(b+n)}{\Gamma(c+n)n!}z^n,\qquad \text{for } |z|<1. \tag{4.41}$$

Inserting the initial condition $x(s=0)=x_0=\varepsilon_0/(2v)$ determines K_η. Since $x_0\gg 1$, the right hand side is expanded in powers of $1/x_0$. To do this, the transformation formula for the hypergeometric function is used,

$$F(a,b;c;z)=\frac{\Gamma(c)\Gamma(b-a)}{\Gamma(b)\Gamma(c-a)}(-z)^{-a}F(a,a-c+1;a-b+1;1/z)+(a\leftrightarrow b),\qquad \text{for } |\arg(-z)|<\pi, \tag{4.42}$$

yielding,

$$K_\eta = \left(\frac{\Gamma(\frac{3}{2})\Gamma(\frac{\eta-1}{2})}{\Gamma(\frac{\eta}{2})} + \frac{\Gamma(\frac{3}{2})\Gamma(\frac{1-\eta}{2})}{\Gamma(\frac{1}{2})\Gamma(\frac{3-\eta}{2})} x_0^{1-\eta} \right) \left(1 + \mathcal{O}(x_0^{-2})\right) \approx \begin{cases} \frac{\sqrt{\pi}\Gamma(\frac{\eta-1}{2})}{2\Gamma(\frac{\eta}{2})}, & \text{for } \eta > 1, \\ \frac{x_0^{1-\eta}}{1-\eta}, & \text{for } \eta < 1. \end{cases} \tag{4.43}$$

Importantly, for $\eta < 1$, the leading contribution in x_0 is $K_\eta \sim x_0^{1-\eta}$ which is large. Eventually, this leads the condition $\eta > 1$ in order to avoid large non-adiabatic corrections. This is similar to the bound $\eta > 0$ which prevents the dynamical phase from also growing large with x_0, see eq. (3.35). The symmetry of the process implies $x(1/2) = 0$ and this determines the constant Ω_η through $\Omega_\eta = 2K_\eta$, giving,

$$\Omega_\eta \approx \begin{cases} \frac{\sqrt{\pi}\Gamma(\frac{\eta-1}{2})}{\Gamma(\frac{\eta}{2})}, & \text{for } \eta > 1, \\ 2\sinh^{-1}(x_0), & \text{for } \eta = 1, \\ \frac{2}{1-\eta} x_0^{1-\eta}, & \text{for } \eta < 1, \end{cases} \tag{4.44}$$

to leading order in $1/x_0$. The limiting case $\eta = 1$ has also been included where the solution to eq. (4.39) is simply $x(s) = \sinh\big(\Omega_{\eta=1}(\frac{1}{2} - s)\big)$. Here, $\Omega_{\eta=1}$ is logarithmically diverging with x_0. We may now continue with computing the correction phase. For general η, we can not use the Beltrami identity but can instead compute the integral by substituting $\mathrm{d}s = \mathrm{d}x/\dot{x}$. We find

$$A_\eta^\rho(1) = \frac{\Omega_\eta |v^\rho|^2/v^2}{8Tv} \int_{-x_0}^{x_0} \mathrm{d}x \frac{1}{(x^2+1)^{\frac{5-\eta}{2}}} \approx \frac{\sqrt{\pi}\Gamma(\frac{4-\eta}{2})}{8\Gamma(\frac{5-\eta}{2})} \frac{\Omega_\eta}{Tv} |v^\rho|^2/v^2, \tag{4.45}$$

for both filling and emptying and to leading order in $1/x_0$. Here, we have an upper bound $\eta < 4$ as the integral over x will otherwise diverge with $x_0 \to \infty$. In the present case, where $\eta = 5/2$, we find

$$A_{\eta=\frac{5}{2}}^\rho(1) = \frac{4\pi^3 |v^\rho|^2/v^2}{\Gamma(\frac{1}{4})^4 Tv}, \tag{4.46}$$

where $\frac{4\pi^3}{\Gamma(1/4)^4} = 0.717770\ldots$. Demanding that $A_{\eta=\frac{5}{2}}^\rho(1)$ must be small results in

$$Tv \gg 1, \tag{4.47}$$

which is what we would expect from the adiabatic theorem as v represents the smallest gap during the process. For general η we need to enforce

$$Tv \gg \Omega_\eta, \tag{4.48}$$

to keep $A_\eta^\rho(1) \ll 1$. If $\eta < 1$, then $\Omega_\eta \sim x_0^{1-\eta}$ which is large in our model, demanding the time scale to be even slower. This implies that besides relating T to a relevant energy scale, which in our case is v, we need also a dimensionless parameter which describes the way we are performing the adiabatic transport. In our situation, Ω_η is the relevant parameter describing our choice of adiabatic transport and it may be large due to its dependence on x_0 for $\eta < 1$. The parameter $x_0 = \varepsilon_0/(2v)$ is the ratio between the largest gap and the smallest gap in the process, and in this way, the adiabatic condition has knowledge of all relevant energy scales. Physically $\eta < 1$ corresponds to going relatively slower when the gap is large compared to when the gap is small. This is clearly an unsound course of action if adiabaticity is desired. Note that controlling the dot linearly $\dot{x} = \text{const.}$ corresponds to choosing $\eta = 0$ and that this is outside $\eta > 1$. In the next section, we show that the relevant expansion parameter for

the adiabatic perturbation theory in this setup is $\Omega_\eta/(Tv)$ and find the strictest upper bound on η. We continue this section by considering the second of the two conditions for adiabaticity, eq. (4.23). This equation describes the transition to the excited state. Since the process is symmetric we have $\frac{M^\rho_{10}(0)}{T\Delta_{10}(0)} = \frac{M^\rho_{10}(1)}{T\Delta_{10}(1)}$ and we consider the former,

$$\left|\frac{M^\rho_{10}(0)}{T\Delta_{10}(0)}\right| \ll 1, \tag{4.49}$$

$$\frac{x_0^{\eta-3}|\Omega_\eta||v^\rho|/v}{4Tv} \ll 1, \tag{4.50}$$

to leading order in $1/x_0$. For $\eta < 1$ the restriction is $Tv \gg x_0^{-2}$ which is less strict than $Tv \gg 1$. For $\eta > 1$ on the other hand, $Tv \gg x_0^{\eta-3}$, setting a stricter bound from above $1 < \eta \leq 3$ as the relevant range for η. Specifically, for the optimal value $\eta = 5/2$, we get

$$\left|\frac{M^\rho_{10}(0)}{T\Delta_{10}(0)}\right| = \frac{\sqrt{2\pi^3}|v^\rho|/v}{\Gamma(\frac{1}{4})^2 Tv\sqrt{x_0}} \tag{4.51}$$

For values of η within the bound, the transition amplitude is further suppressed by $1/\sqrt{x_0}$. Physically, it makes sense that a large gap prevents transitions to the excited state and hints to us that we can choose η such that the transition may be neglected. Mathematically, it is a result of the correction phase depending on the entire path through the integral whereas the transition amplitude only depends on the initial and final values. Choosing $\eta > 1$ corresponds to changing the dot level energy relatively quicker when the gap is larger as compared to when the gap is smaller and this leads to transitions. In this way, our analysis shows that the trade-off leading to the bound $1 < \eta < 3$ can again be understood as the balance between going fast/slow and having transitions/phases. In addition, we have learned that it is relevant to control the rate of change of the dot level energy proportional to the energy gap to some power as this captures the effect of going fast/slow when the gap is large/small. We have also found that the time scale of the process should be compared to the smallest gap and a parameter determined by how we perform the adiabatic transport. This parameter may depend on the ratio between the smallest and largest gap and can therefore be significant. Furthermore, it appears to be possible to suppress transitions focusing our attention to the correction phase. We are left in a situation where we wish to simultaneously minimize the relative dynamical phase, which is proportional to Tv/Ω_η, and the non-adiabatic corrections growing with $\Omega_\eta/(Tv)$. We may be able to resolve this issue by noting that the relative phases between the even and the odd states are further suppressed by $\sin(2\theta)\sin(\phi/2)$ and it may therefore be possible to choose $\Omega_\eta/(Tv) \sim 1$ given that transitions can be suppressed by $1/x_0$. In the next section, we explore the possibility of choosing $\Omega_\eta/(Tv) \sim 1$ while finally resolving the outstanding issues arising from expanding adiabatic perturbation theory in the dimensionful $1/T$.

4.3 The dimensionless adiabatic expansion parameter

The dimensionality of the expansion parameter $1/T$ leaves the coefficients $b^{(p)}_{nm}(s)$ dimensionful. Consequently, we can not trust that higher order coefficients are smaller than lower order coefficients. Naively, this can be solved by expanding in $1/Tv$ but the large, dimensionless gap-ratio x_0 may also play a significant role. In the previous section, we saw how x_0 could help suppress the transition amplitude but also implied the bound $1 < \eta < 3$. In this section, we take into account both the dimensionality captured by v and the contributions from Ω_η which represents our choice when controlling

the dot level energy. When doing so, we find a stricter adiabatic condition which was overlooked in [2] but is latent in adiabatic perturbation theory.

Since adiabatic perturbation theory is built out of three components, $\frac{\mathrm{d}}{\mathrm{d}s}$, $\Delta_{nm}(s)$, $M_{nm}(s)$ (assuming $W_{nm}(s) = 0$), it is relevant to understand how they behave for $x \to x_0$,

$$\frac{\mathrm{d}}{\mathrm{d}s} = \dot{x}\frac{\mathrm{d}}{\mathrm{d}x} \longrightarrow \Omega_\eta x_0^{\eta-1}, \tag{4.52}$$

$$\Delta_{nm}(s) = 2v\sqrt{x(s)^2+1} \longrightarrow v x_0, \tag{4.53}$$

$$M_{nm}(s) = \frac{-\dot{x}(s)}{2(x(s)^2+1)} \longrightarrow \Omega_\eta x_0^{\eta-2}. \tag{4.54}$$

To ensure that the perturbation theory is tractable, implying that the ordering in p is meaningful, we need to enforce

$$\frac{b_{nm}^{(p+1)}(s)}{T^{p+1}} \lesssim \frac{b_{nm}^{(p)}(s)}{T^p}. \tag{4.55}$$

We will use this condition along with eqs. (4.12) and (4.14) relating a $p+1$-order coefficient to coefficients one order lower. We begin with the $n = m$ case of eq. (4.14),

$$b_{nn}^{(p+1)}(s) = -\sum_{\substack{k=0\\k\neq n}} b_{nk}^{(p+1)}(0) - i\sum_{\substack{k=0\\k\neq n}}\int_0^s \mathrm{d}s' \left(\frac{M_{nk}(s')}{\Delta_{kn}(s')}\frac{\mathrm{d}}{\mathrm{d}s'}b_{kn}^{(p)}(s') + \sum_{\substack{m=0\\m\neq k}}\frac{M_{nk}(s')M_{km}(s')}{\Delta_{kn}(s')})b_{mn}^{(p)}(s')\right). \tag{4.56}$$

Applying the tractability condition of eq. (4.55) to the above equation results in two restrictions from the integrals,

$$\int_{-x_0}^{x}\mathrm{d}x'\frac{\Omega_\eta}{Tv}\frac{1}{(x^2+1)^{\frac{3-\eta}{2}}}\frac{\mathrm{d}}{\mathrm{d}x'}b_{kn}^{(p)}(x') \lesssim b_{nm}^{(p)}(x) \longrightarrow \begin{cases}\frac{\Omega_\eta}{Tv}x_0^{\eta-3} \lesssim 1 & \text{for } \eta > 3,\\ \frac{\Omega_\eta}{Tv} \lesssim 1 & \text{for } \eta < 3,\end{cases} \tag{4.57}$$

$$\int_{-x_0}^{x}\mathrm{d}x'\frac{\Omega_\eta}{Tv}\frac{1}{(x^2+1)^{\frac{5-\eta}{2}}}b_{mn}^{(p)}(x') \lesssim b_{nm}^{(p)}(x) \longrightarrow \begin{cases}\frac{\Omega_\eta}{Tv}x_0^{\eta-4} \lesssim 1 & \text{for } \eta > 4,\\ \frac{\Omega_\eta}{Tv} \lesssim 1 & \text{for } \eta < 4,\end{cases} \tag{4.58}$$

having rewritten in terms of x instead of s. For the integrals to be convergent for $x_0 \to \infty$, we must choose $\eta < 3$. If we do not make this choice, we have a stricter condition for adiabaticity $\Omega_\eta/(Tv) \lesssim x_0^{3-\eta}$. Note that the $\eta < 4$ condition from the second equation corresponds to the same bound found for the correction phase in the previous section. The stricter bound $\eta < 3$ appears since we are doing a more general treatment here, taking into account also the higher order terms. Furthermore, when choosing $\eta < 3$ we find the condition $\Omega_\eta/(Tv) \lesssim 1$ which we have already discussed: The largeness of $\Omega_\eta \sim x_0^{1-\eta}$ for $\eta < 1$ is undesirable as it requires $Tv \gg x_0^{1-\eta}$. For these reasons we have the bound $1 < \eta < 3$ but as we will see now, we must further restrict this range. Continuing with the $n \neq m$ case of eq. (4.12), we get

$$b_{nm}^{(p+1)}(s) = \frac{i}{\Delta_{nm}(s)}\left(\frac{\mathrm{d}}{\mathrm{d}s}b_{nm}^{(p)}(s) + M_{nm}(s)b_{mm}^{(p)}(s)\right), \tag{4.59}$$

Demanding that the perturbation theory is tractable (eq. (4.55)) then gives,

$$\frac{1}{T\Delta_{nm}(s)}\frac{\mathrm{d}}{\mathrm{d}s} \lesssim 1 \longrightarrow \frac{\Omega_\eta}{Tv}x_0^{\eta-2} \lesssim 1, \tag{4.60}$$

$$\frac{M_{nm}(s)}{T\Delta_{nm}(s)} \lesssim 1 \longrightarrow \frac{\Omega_\eta}{Tv}x_0^{\eta-3} \lesssim 1, \tag{4.61}$$

Here, we should bound $\eta \leq 2$ and this was not captured by the conditions (4.22) and (4.23). Note that the second of the above equations corresponds to the $\eta \leq 3$ bound from the previous section when calculating the transition amplitude. These equations also show that $\eta < 2$ suppresses the $n \neq m$ coefficients and thus the transitions to the excited states. We have now the final bound on η,

$$1 < \eta \leq 2. \tag{4.62}$$

This bound has some important consequences for the results in the previous section. Here, we found that $\eta = 5/2$ was an optimal choice for adiabaticity for the case where only first order corrections in $1/T$ were considered, eq. (4.36). Noting that this choice is outside the above bound, we can conclude that terms higher order in p can become more significant than the first order corrections, leaving the validity range of the adiabatic expansion. This issue can be cured by either choosing $Tv \gg x_0^{1/2}$ or simply by choosing η within the bound. To minimize the effect of the environment, it is desirable to have a short time scale T. For this reason, it is optimal to choose η within the bound in eq. (4.62). This treatment show that it is important to be conscious of what is regarded as the small adiabatic parameter. If $1/(Tv) \ll 1$ is chosen, then the bound $1 < \eta \leq 2$ follows. If instead $\Omega_\eta/(Tv) \ll 1$ is chosen, the lower bound is incorporated in the parameter and $\eta \leq 2$ remains. The upper bound can also be included in the parameter through $x_0^{\eta-2}\Omega_\eta/(Tv) \ll 1$ for $\eta > 2$. Regardless of which of the three possible adiabatic parameters is used, the conclusion is the same: We should choose $1 < \eta \leq 2$ to avoid needing to slow down the the time of the process due to x_0.

Ideally, we should minimize the relative dynamical phase while maintaining an adiabatic transport. These statements appears to be contradicting as it requires $\Omega_\eta/Tv \sim 1$, leaving the adiabatic regime. This may be possible as we are only interested in the relative phases which are suppressed by $\sin(2\theta)\sin(\phi/2)$ and since the transition amplitude can be suppressed by $1/x_0$. Despite leaving the adiabatic regime, we may still use the results from adiabatic perturbation theory to guide our choices. Controlling the dot level energy according to $\dot{x} = \pm\Omega_\eta(x^2+1)^{\eta/2}$ while adhering to $1 < \eta \leq 2$ is the main point we draw from adiabatic perturbation theory. Outside this bound we need to enforce $Tv \sim x_0^{1-\eta}$ or $Tv \sim x_0^{\eta-2}$ instead of the less restrictive $Tv \sim 1$. Adiabatic perturbation theory further predicts that the transition amplitude is suppressed by x_0 for $\eta < 2$. It can also be suppressed/enhanced by choosing $\Omega_\eta/(Tv) \lesseqgtr 1$ but this has a cost for the relative phase. In the next chapter, we test the predictions of adiabatic perturbation theory numerically.

Chapter 5

Simulating the protocols and the charge-transfer process

In this chapter, we test the predictions from the previous chapters numerically. We simulate the time-dependent Schrödinger equation by time evolving states iteratively. We begin by reviewing our implementation of this time evolution. Then, we simulate a single charge-transfer process to determine the optimal values of η and the time scale of the process T. Having decided how to perform the charge-transfer process, we simulate the two protocols of Sec. 3.3 and compare to the theoretical predictions.

5.1 Implementation of the time evolution

When simulating the charge-transfer process, we are going to consider the filling of the dot. The even and odd ground state (see eq. (4.26)) are evolved with the time-dependent Hamiltonian through,

$$|\Psi^\rho(s_N)\rangle = \exp[-iTH^\rho(s_N)\delta s_N]\dots\exp[-iTH^\rho(s_2)\delta s_2]\exp[-iTH^\rho(s_1)\delta s_1]\,|0^\rho(s_1)\rangle\,, \tag{5.1}$$

where the time evolution is divided into N time intervals, $U_i^\rho = \exp[-iTH^\rho(s_i)\delta s_i]$. The array of time intervals δs_i is determined through an array of evenly spaced energies $x_i = x(s_i) = \varepsilon(s_i)/(2v)$ from x_0 to $-x_0$ with spacing $\delta x = \frac{2x_0}{N}$,

$$\delta s_i = \frac{\delta x}{\dot{x}_i} = \frac{\delta x}{\Omega_\eta(x_i^2+1)^{\eta/2}}. \tag{5.2}$$

Here, we have used the ansatz in eq. (4.39). We recall that the Hamiltonian matrix is given by

$$H^\rho(s_i) = \begin{pmatrix} 0 & v^\rho \\ (v^\rho)^* & \varepsilon(s_i) \end{pmatrix} = vx_i\mathbb{1} + v\sqrt{x_i^2+|v^\rho/v|^2}\;(\hat{n}^\rho\cdot\sigma), \tag{5.3}$$

with $\hat{n}^\rho = (\mathrm{Re}\,v^\rho/v, -\mathrm{Im}\,v^\rho/v, -x_i)/\sqrt{x_i^2+|v^\rho/v|^2}$ a unit vector and σ the vector of Pauli matrices. The term proportional to the identity only gives a common phase and will be left out. The i'th time evolution operator now becomes

$$U_i^\rho = \exp\left[-i\frac{Tv}{\Omega_\eta}\frac{\sqrt{|v^\rho/v|^2+x_i^2}}{(x_i^2+1)^{\eta/2}}\delta x\;(\hat{n}^\rho\cdot\sigma)\right] = \cos\theta_i^\rho\mathbb{1} - i\sin\theta_i^\rho(\hat{n}^\rho\cdot\sigma), \tag{5.4}$$

having introduced

$$\theta_i^\rho = \frac{Tv}{\Omega_\eta} \frac{\sqrt{|v^\rho/v|^2 + x_i^2}}{(x_i^2+1)^{\eta/2}} \delta x. \tag{5.5}$$

It is a good approximation to divide the time evolution into N iterations when $\theta_i^\rho \ll 1$. Assuming $\Omega_\eta/(Tv) \sim 1$ implies $N \gg x_0^{2-\eta}$ and $N \gg x_0$ for $i = 1$ and $i = N/2$ respectively. As an example, if $x_0 = 100$ we could choose $N = 10^4$ for $\eta \geq 1$. It gets harder to simulate the charge-transfer process for smaller values of η. To get the same precision for $\eta = 0$, we need $N = 10^6$. The $\eta = 0$ case is interesting as it corresponds to controlling the dot level linearly. In the next section, proceed by discussing the results from the simulations of the charge-transfer process.

5.2 Simulating the charge-transfer process

The simulation of the charge-transfer process evolves the even and odd ground states (see eq. (4.26)) according to

$$|0^\rho(s_1)\rangle \to |\Psi^\rho(s_N)\rangle = \alpha^\rho e^{\rho i \theta_\uparrow^G/2 + \delta\theta_0^\rho} |0^\rho(s_N)\rangle + \beta^\rho e^{\delta\theta_1^\rho} |1^\rho(s_N)\rangle, \tag{5.6}$$

where $\theta_\uparrow^G$ is the zeroth order geometric phase of eq. (3.31), $\delta\theta_{0/1}^\rho$ are the phase of the even and odd ground/excited state and $|\beta^\rho|^2$ are the transition amplitudes to the even and odd excited states. We begin by investigating how x_0 influences the transition amplitude and compare it to the predictions of adiabatic perturbation theory. In Fig. 5.1, we have plotted the transition amplitude of the even sector $|\beta^-|^2$ as a function of η in the range $\eta = [1; 3]$. The plot contains 1000 equidistant samples of η in this range for each value $x_0 = 10,\ 30,\ 100$ with $N = 10^4$ iterations in the time evolution. We have chosen $\Omega_\eta/(Tv) = 1$, $\theta = \pi/4$ and $\phi = 2\pi/100$ in this example.

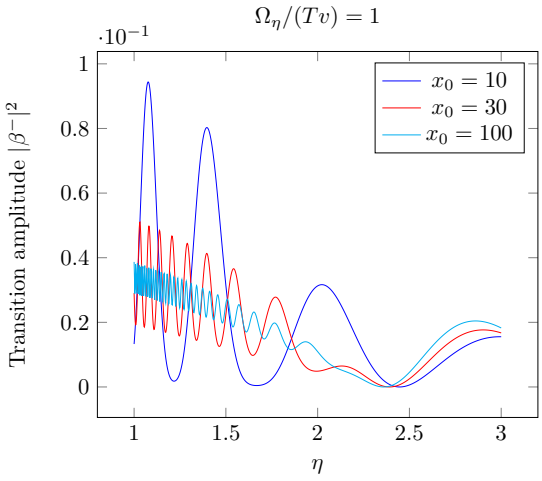

Figure 5.1: Plot of the even transition amplitude $|\beta^-|^2$ as a function of η for different values of x_0. A large x_0 suppresses the amplitude of oscillations for $\eta \leq 2$.

	$\lvert\beta^-\rvert^2$	$\delta\theta_0^- - \delta\theta_0^+$	T
$\eta = 0$	$3.7 \cdot 10^{-3}$	-0.66 rad	263 ns
$\eta = 2$	$2.9 \cdot 10^{-5}$	-0.12 rad	4.14 ns

Table 5.1: Comparison between transition amplitudes, relative phases between the even and odd ground state and the time scale of the charge-transfer process for $\eta = 0$ and $\eta = 2$ when $\Omega_\eta/(Tv) = 1/2$. Other relevant parameters in this example: $x_0 = 100$, $\theta = \pi/4$, $\phi = 2\pi/100$ and $N = 10^6$. The period of the process T has been calculated using $\varepsilon_0 = 0.2$ meV, the typical magnitude of the induced gap.

We see that increasing the value of x_0 suppresses the amplitude of the oscillations for $\eta < 2$. This is in qualitative agreement with the predictions from adiabatic perturbation theory. The finer details of these oscillations and their offset is not described well by adiabatic perturbation theory as we are on the boundary of the adiabatic regime $\Omega_\eta/(Tv) = 1$. Additionally, we see that the behavior of the

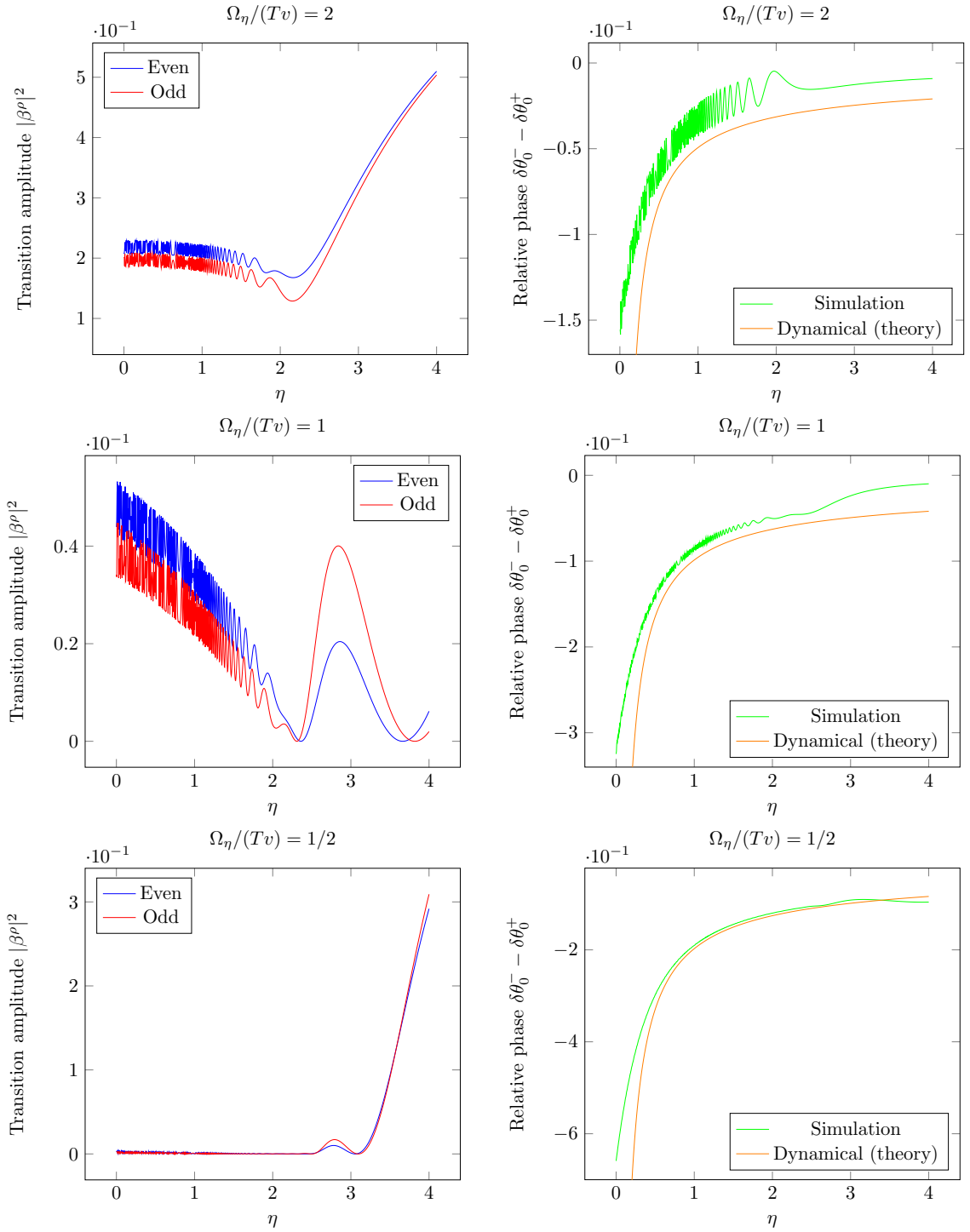

Figure 5.2: Plots of the dependence of the transition amplitude and relative phase on the parameter η for $\Omega_\eta/(Tv) = 2,\ 1,\ 1/2$. The transition amplitude $|\beta^\rho|^2$ is suppressed by $\Omega_\eta/(Tv) < 1$ while $\Omega_\eta/(Tv) > 1$ suppresses the relative phase $\delta\theta_0^- - \delta\theta_0^+$. Overall, there is qualitative agreement with the theoretical predictions of Sec. 4.3.

amplitude is markedly different for $\eta < 2$ compared to $\eta > 2$. This is in good agreement with the prediction that we are outside the validity range of adiabatic perturbation theory for $\eta > 2$ unless $\Omega_\eta/(Tv) \lesssim x_0^{2-\eta}$ is chosen. This behavior is also seen in the panels of Fig. 5.2, especially for the transition amplitudes. In this figure, we have plotted the even and odd transition amplitudes $|\beta^\rho|^2$ in the left column and the error to the zeroth order relative geometric phase between the even and the odd ground states $\delta\theta_0^- - \delta\theta_0^+$ in the right column. This error phase is the relative phase computed in the simulation where the zeroth order geometric phase of eq. (3.31) has been subtracted. In these plots, the range is $\eta = [0; 5]$ with 1000 samples and the adiabatic parameter is $\Omega_\eta/(Tv) = 2$, 1, 1/2 for the top, middle and bottom rows respectively. Additional parameters are $x_0 = 100$, $\theta = \pi/4$, $\phi = 2\pi/100$ and $N = 10^5$. Comparing the amplitude plots in the left column, we notice an important characteristic. The adiabatic parameter $\Omega_\eta/(Tv)$ can suppress the transition amplitude greatly for $\eta < 2$. Unlike x_0, which only suppresses the amplitude of oscillations, $\Omega_\eta/(Tv)$ suppresses the offset of the oscillations. This effect appears to be very sensitive to the adiabatic parameter as $\Omega_\eta/(Tv)$ only varies with a factor of four between the top and the bottom panels but the transition amplitude drops by several orders of magnitude. This is in qualitative agreement with adiabatic perturbation theory as exact dependence on $\Omega_\eta/(Tv)$ cannot be captured for $\Omega_\eta/(Tv) \sim 1$. When studying the error phase in the right column, we notice two aspects. The first is that the error phase follows the general trend of the zeroth order dynamical phase from eq. (3.35). This is especially clear in the lower right panel where the non-adiabatic corrections are suppressed by $\Omega_\eta/(Tv) < 1$ compared to the top right panel where $\Omega_\eta/(Tv) > 1$. The second aspect to notice is that the error phase's dependence on $\Omega_\eta/(Tv)$ is approximately linear due to the dynamical phase depending linearly on $\Omega_\eta/(Tv)$. For this reason, the error phase $\delta\theta_0^- - \delta_0^+$ does not depend as dramatically on $\Omega_\eta/(Tv)$ as the transition amplitudes. These facts combined with the ϕ-flip protocol (3.66-3.67), where the relative dynamical phases cancel, suggest that it is beneficial to take advantage of the large suppression of the transition amplitude for $\Omega_\eta/(Tv) < 1$. The trade-off for the error phase is comparatively small and the ϕ-flip protocol cancel much of the dynamical contribution. When considering the bottom panels of Fig. 5.2, we also advocate for using $\eta = 2$ as the relative phase is slightly smaller for higher η while the transition amplitude is suppressed in the entire range $1 < \eta \leq 2$. To demonstrate the benefits of these choices, we have produced an example in Tab. 5.1 which compares controlling the dot level energy linearly ($\eta = 0$) to controlling the rate of change of the level energy proportional to the gap ($\eta = 2$). These two cases corresponds to

$$x(s) = \begin{cases} 2x_0\left(\frac{1}{2} - s\right), & \text{for } \eta = 0, \\ \tan\!\big(2\,\mathrm{atan}(x_0)\left(\frac{1}{2} - s\right)\big), & \text{for } \eta = 2, \end{cases} \tag{5.7}$$

solving the differential equation in eq. (4.39). Since $\Omega_\eta/(Tv) = 1/2$ is chosen, the transition amplitude is suppressed in both cases yet the $\eta = 2$ case is smaller by two orders of magnitude. Also the error phase is smaller by a factor of 5 in favor of $\eta = 2$. Impressively, the $\eta = 2$ case performs better than $\eta = 0$ while the time scale is 60 times shorter. The time scale T has been calculated through $T = 2\Omega_\eta/v$ using eq. (4.44) and $\varepsilon_0 = 0.2$ meV. This value has been chosen as it corresponds to the induced gap in experiments. Using this and $x_0 = 100$, we additionally find $v = 1$ μeV for the coupling strength.

The simulations have confirmed the trade-off between transition amplitude and relative dynamical phase. In addition, we also witness the breakdown of adiabatic perturbation theory for $\eta > 2$ as predicted. Perhaps surprisingly, the transition amplitude appears to be strongly suppressed by

$\Omega_\eta/(Tv) < 1$ when $x_0 \gg 1$ while the relative phase follows the general trend of the zeroth order relative dynamical phase. These insights are useful when determining how to control the level energy in the charge-transfer. As demonstrated, we may suppress the transition amplitude with a comparatively small cost in the relative phase. Since the error phase found in the simulations follows the general trend of the relative dynamical phase, we can expect to be able to cancel the contributions using the ϕ-flip protocol. In the next section, we apply the set of parameters $\eta = 2$ and $\Omega_\eta/(Tv) = 1/2$ suggested by the simulation of the single charge-transfer process to simulations of the protocols in Sec. 3.3.

5.3 Simulating the protocols

We simulate the protocols as three consecutive charge-transfer processes of the D2/M23-system, see Fig. 3.3. The three processes all have the same time scale T given by the choice of parameters $\Omega_\eta/(Tv) = 1/2$, $x_0 = 100$ and $\eta = 2$. What distinguishes the three processes are the coupling parameters θ and ϕ. We model the change in the coupling parameters between the single charge-transfer processes to be instant with no effect on the states in accordance with the sudden approximation. We wish to investigate the range for which each protocol can confidently distinguish the two orders of operations statistically. For this reason, we will need to sample and compare many different values of (ϕ, θ). The even and odd ground states have a very slight dependence on these parameters which is suppressed by $1/x_0$. We took this dependence into account in the previous simulation but it is appropriate to neglect it here. We imagine that the initial states are prepared identically in the measurement-basis (M12/M34) and not in the operation-basis (M23/M14). This may give a very slight discrepancy but most important is that the preparation is consistent. This also applies to the simulation where we use the same initial states for all pairs (θ, ϕ) such that the final results are easy to compare. Algebraically, this simply corresponds to letting $x_0 \to \infty$ in eq. (4.26) for the initial states giving $|i\rangle = (1, 0)^T$ for both the even and odd sector in the D2/M23-basis. Due to the large suppression of the transition amplitude found in the previous section, we also neglect these effects. This setup makes the simulation relatively simple to perform. The three consecutive charge-transfer processes evolve the states according to Sec. 5.1. The result of the simulation is relevant to understand in both the operation-basis and in the measurement-basis,

$$\begin{pmatrix}1\\0\end{pmatrix} \longrightarrow e^{-i\rho\theta^S}\begin{pmatrix}0\\1\end{pmatrix} \text{ (D2/M23-basis)}, \tag{5.8}$$

$$|00\rangle \longrightarrow f\,|01\rangle + g\,|10\rangle \text{ (measurement-basis)}, \tag{5.9}$$

where $\theta^S(\phi, \theta)$ is half the relative phase introduced between the even and odd states in the operation-basis and $f(\phi, \theta), g(\phi, \theta)$ are the coefficients to $|01\rangle$ and $|10\rangle$. As shown in Sec. 3.3, the relative phase in the operation-basis is related to the amplitude in the measurement-basis. In this case, the correspondence is

$$|g|^2 = \sin^2(\theta^S). \tag{5.10}$$

We will also compare to the theoretical predictions from the protocols. We remind ourselves of the first protocol in eqs. (3.64-3.65),

$$\gamma_2 U_\downarrow(\phi, \theta) U_\uparrow(\phi, \theta) \longrightarrow |g|^2 = \sin\big(\theta^D\big)^2, \tag{5.11}$$

$$U_\uparrow(\phi, \theta)\gamma_2 U_\uparrow(\phi, \theta) \longrightarrow |g|^2 = \sin\big(\theta^G_\uparrow + \theta^D\big)^2, \tag{5.12}$$

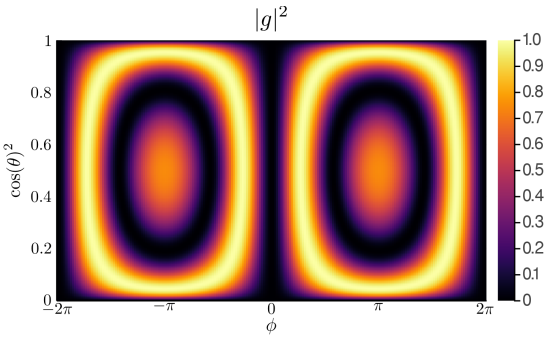

(a) Simulation of $\gamma_2 U_\downarrow(\phi,\theta)U_\uparrow(\phi,\theta)$.

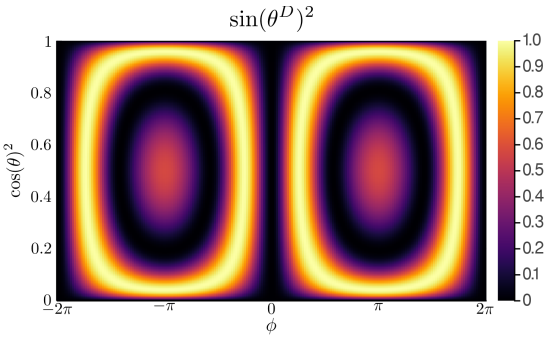

(b) Theory for $\gamma_2 U_\downarrow(\phi,\theta)U_\uparrow(\phi,\theta)$.

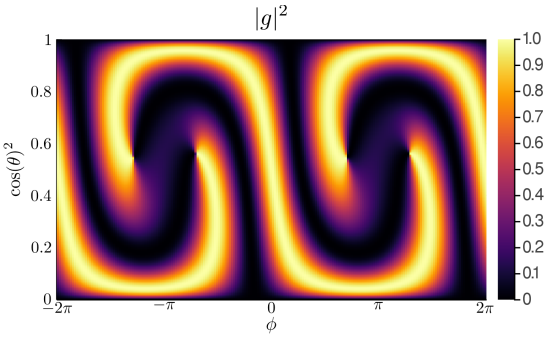

(c) Simulation of $U_\uparrow(\phi,\theta)\gamma_2 U_\uparrow(\phi,\theta)$.

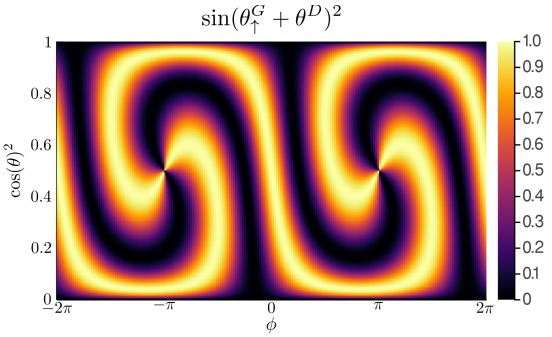

(d) Theory for $U_\uparrow(\phi,\theta)\gamma_2 U_\uparrow(\phi,\theta)$.

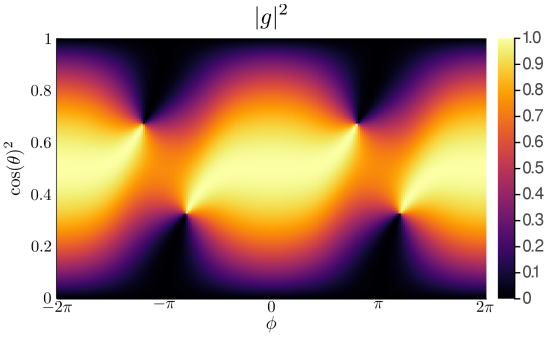

(e) Simulation of $\gamma_2 U_\downarrow(\phi+2\pi,\theta)U_\uparrow(\phi,\theta)$.

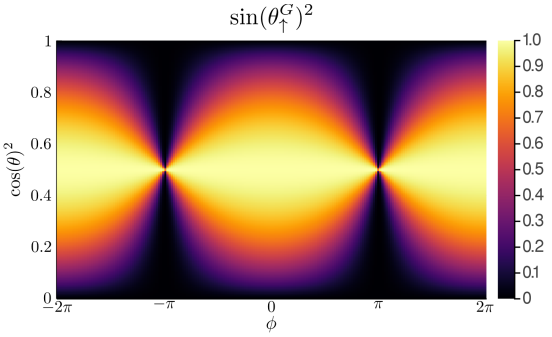

(f) Theory for $\gamma_2 U_\downarrow(\phi+2\pi,\theta)U_\uparrow(\phi,\theta)$.

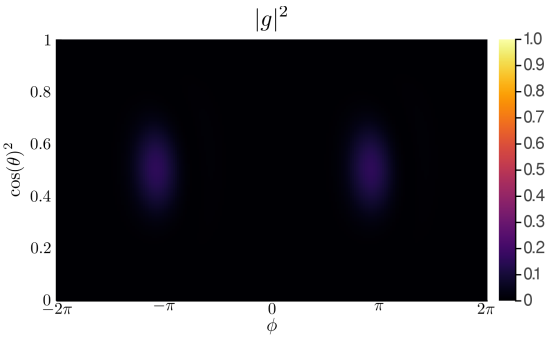

(g) Simulation of $U_\uparrow(\phi+2\pi,\theta)\gamma_2 U_\uparrow(\phi,\theta)$.

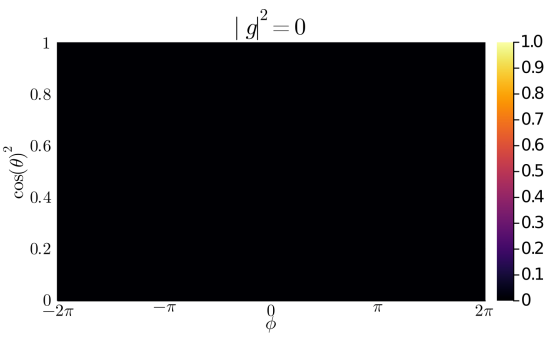

(h) Theory for $U_\uparrow(\phi+2\pi,\theta)\gamma_2 U_\uparrow(\phi,\theta)$.

Figure 5.3: The first/second protocol is presented in the top/bottom four panels. There is good agreement between the theoretical predictions (right column) and the numerical data (left column) outside the regions near $(\phi = \pm\pi, \theta = \pi/4)$. The ideal region near $(\phi = 0, \theta = \pi/4)$ is larger in the bottom four panels compared to the top panels due to the cancellation of the dynamical phases.

and of the second protocol, which utilizes the ϕ-flip,

$$\gamma_2 U_\downarrow(\phi + 2\pi, \theta) U_\uparrow(\phi, \theta) \longrightarrow |g|^2 = \sin\left(\theta_\uparrow^G\right)^2, \tag{5.13}$$

$$U_\uparrow(\phi, \theta)\gamma_2 U_\uparrow(\phi, \theta) \longrightarrow |g|^2 = 0, \tag{5.14}$$

with $\theta_\uparrow^G(\phi, \theta)$ and θ^D given by eqs. (3.31) and (3.35). Note that we have assumed that the value of (ϕ, θ) does not change between subsequent operations and that γ_2 corresponds to $\theta = 0$. In Fig. 5.3, we have produced color maps of the amplitude $|g|^2$ for the first and second protocol from the simulation and the theoretical prediction. On the first axes, we have $\phi = [-2\pi; 2\pi]$ while $\cos(\theta)^2 = [0; 1]$ is on the second axes. The color map consists of 200×200 evenly distributed pairs $(\phi, \cos(\theta)^2)$ with $N = 3000$ iterations for each single charge-transfer process. We observe good agreement between simulation (left column) and theory (right column) for both order of operations and for both protocols. The only discrepancies are in the regions around $(\phi = \pm\pi, \theta = \pi/4)$. This is to be expected as we have assumed $\sin(2\theta)\sin(\phi/2) \ll 1$ in the theoretical prediction. The amplitude $|g|^2$ represents the probability of measuring the state $|10\rangle$ after a given order of operations. Experimentally, this probability can be found statistically by repeating the protocol. In principle, the two orders of operation can be distinguished for all (ϕ, θ) where there is a measurable difference between the probabilities of the two orders of operation. We focus on the regions around the optimal situation $(\phi = 0, \theta = \pi/4)$ and begin by considering the first protocol in Fig. 5.3. Here, we see that the relevant yellow center region in panels c) and d) is narrow along the first axis and wide along the second axis. The same is true for the black center region in panels a) and b). This implies that the corresponding range of ϕ, where there is a large difference between the sequences, is small. Conversely, the range of θ is large. In the second protocol presented in the bottom four panels, we have an entirely different picture. Due to the cancellation of the relative dynamical phase resulting from the ϕ-flip, the errors associated with ϕ are suppressed. In panels e) and f), the central yellow region is wide along the first axis, meaning that a wide range of ϕ can be used. Especially in panels g) and h), we see the benefit of canceling the dynamical phase compared to panels a) and b), being virtually independent of the parameters. We have thus demonstrated the two proposed protocols and the advantages of the ϕ-flip numerically. To perform the ϕ-flip protocol, knowledge of the change in magnetic fields that winds ϕ by 2π is required. In experiment, this can for example be deduced through the process $\gamma_2 U_\downarrow(\phi, \theta) U_\uparrow(\phi, \theta)$, see panels a) and b). By fixing a value θ and varying ϕ, a horizontal line cut is made in the color map. By repeating the process for different values of ϕ the probability of measuring $|10\rangle$ is determined along this line. Due to the 2π periodicity of the peaks, the corresponding change in the magnetic field is derived. This chapter concludes the main narrative of the thesis. We proceed in the next two chapters with two smaller, supplementing projects before concluding with our final remarks.

Chapter 6

Two-qubit gates and scalability

The experimental path to show the non-Abelian properties of Majorana bound states has been challenging but shows great promise. The future of the long term ambition of a Majorana-based universal quantum computer is on the other hand difficult to foresee. In this chapter, we try to shed light on the possibilities in constructing charge-transfer devices which can perform multi-qubit gates. Specifically, we focus on the 4-Majorana rotation necessary for simulating interacting quantum systems evolved by quartic Hamiltonians. We begin this chapter by studying the general mathematical characteristics of 4-Majorana rotations before we discuss how to implement the 4-Majorana rotation on the level of the Hamiltonian. In the final section of this chapter, we explore higher-order Majorana rotations and their scalability.

6.1 A notation for Majorana operations

A fermionic quantum system with quartic interactions of the general form $c^\dagger c^\dagger cc$ can be written in terms of Majorana operators as,

$$H_{\text{quartic}} = \sum_{i,j,k,l} A_{ijkl}\gamma_i\gamma_j\gamma_k\gamma_l, \tag{6.1}$$

where $A^*_{ijkl} = A_{ijkl}$. The time evolution operator consequently is,

$$U_{\text{quartic}}(t) = \exp(-itH_{\text{quartic}}) = \exp\left(-it\sum_{i,j,k,l} A_{ijkl}\gamma_i\gamma_j\gamma_k\gamma_l\right). \tag{6.2}$$

To simulate such a quantum system, it is required to perform the 4-Majorana rotation,

$$e^{i\theta\gamma_1\gamma_2\gamma_3\gamma_4} = \cos\theta + i\sin\theta\gamma_1\gamma_2\gamma_3\gamma_4. \tag{6.3}$$

Inspired by Sec. 3.1, we aim to construct the 4-Majorana rotation from simpler unitaries. Here, the 2-Majorana rotation $e^{\theta\gamma_1\gamma_2}$ was the product of $a\gamma_1 + b\gamma_2$. We will first consider the mathematical restrictions present when trying to construct these 4-Majorana rotations from simpler unitary operations. Later, we will be concerned with how these can be physically realized. A first idea to effectively produce the 4-Majorana rotation is to try to make products of Hermitian, unitary operators of the form

$$a\gamma_1 + b\gamma_2 + c\gamma_3 + d\gamma_4. \tag{6.4}$$

The structure of the Majorana operators here is $1+1+1+1$. In the same notation, the 4-Majorana rotation can be expressed as $0+4$. The question whether products of the above operator results in a general 4-Majorana rotation, can now be framed as

$$(1+1+1+1)^n \stackrel{?}{=} 0+4. \tag{6.5}$$

In the same way, the 2-Majorana rotation can be expressed as $1(1+1) = (1+1)^2 = 0+2$. However, the above equality does not hold. For the $1+1+1+1$ operator to be unitary, all of the coefficients must be real due to the algebraic properties of the Majoranas. However, the coefficient to the 4 in the $0+4$ operator is imaginary. Thus, no product of $1+1+1+1$ operators can give a 4-Majorana rotation. Similar to the $1+1$ operation, the $1+1+1+1$ operation is due to a quadratic Hamiltonian. For this reason, the result $(1+1+1+1)^n \neq 0+4$ is not surprising as it would otherwise imply that quartic Hamiltonians can be simulated by quadratic ones. We can also understand this result differently: The $0+4$ operation depends on the parity of $i\gamma_1\gamma_2 = \pm$ and $i\gamma_3\gamma_4 = \pm$, amounting to four different combinations. The quadratic Hamiltonians resulting in $1+1$ or $1+1+1+1$ can only distinguish between the overall even and odd parity sectors which is not sufficient for the $0+4$ operation. Having concluded that we cannot perform the 4-Majorana rotation by a simple extension of the $1+1$ operation, we must reconsider our strategy. We begin by making our notation for the Majorana operations precise:

Rules	*Examples*
1. Majorana blocks are products of Majorana operators. A number represents the length of the Majorana block. Majorana blocks of length $4n+1$ have real coefficients and blocks of length $4n+3$ have imaginary coefficients such that both are Hermitian. Individual Majorana operators in a block of odd length are numbered in consecutive order.	$1 \to \gamma_1$, $3 \to i\gamma_1\gamma_2\gamma_3$
2. Operators of the first kind are Hermitian and unitary, and are build from Majorana blocks of odd length. Addition (+) adds blocks and does not reset the numbering of the Majorana operators.	$1+3 \to a\gamma_1 + ib\gamma_2\gamma_3\gamma_4$, $3+1 \to ia\gamma_1\gamma_2\gamma_3 + b\gamma_4$.
3. Operators of the second kind are products of an even number of operators of the first kind. Whether the coefficients of even numbers are real or imaginary and the numbering of individual Majoranas can be deduced by its relation to operators of the first kind.	$0+4 = 1(1+3) = a + ib\gamma_1\gamma_2\gamma_3\gamma_4$, $2+2 = 1(3+1) = ia\gamma_2\gamma_3 + b\gamma_1\gamma_4$.

These rules are formulated on the following considerations. We are interested in two classes of operators: 1) Operators that we hope to be directly physically executable by emptying or filling of a quantum dot once. 2) Those which are products of the first kind and thus rely on emptying and filling the dot multiple times, specifically the $2n$-Majorana rotation. The first kind are both Hermitian and unitary whereas the second kind are in general only unitary. To obtain Hermiticity, the

coefficients of $0, 1, 4, 5, \ldots$ must be real and for $2, 3, 6, 7, \ldots$, the coefficients must be imaginary due to the algebraic properties of the Majoranas. Unitarity is then ensured by the anticommutation of the different Majorana blocks. It is only Majorana blocks (products of Majorana operators) of odd length that anticommute. This implies that blocks of even length can only be constructed as products of an even number of operators of the first kind. Unitarity of the second kind of operators restricts the coefficients of the Majorana blocks of even length but these are not necessarily general. In all situations, they can be deduced with the existing rules by multiplying the first kind of operators.

With the notation, we are now positioned to construct the 4-Majorana rotation. To do this, we partition four into odd numbers to get the allowed operators of the first kind. This can be done in two ways, $1+1+1+1$ and $1+3$. In no way can $1+1+1+1$ be used to achieve $0+4$ due to the restrictions of the coefficients. Instead, we must use $1(1+3) = 0+4$. Likewise, for a 6-Majorana rotation $0+6$, we can partition six as $1+1+1+1+1+1$, $1+1+1+3$, $3+3$, $1+5$ and straightforwardly get $3(3+3) = 0+6$ or $1(1+5) = 0+6$. As with $(1+1+1+1)^n \neq 0+4$, we do in general not expect sums of more than two blocks to be able to produce the $2n$-Majorana rotations. This can again be understood as the Hamiltonians leading to $1+1+1+1+1+1$ or $1+1+1+3$ not being capable of distinguishing between the parities of $i\gamma_1\gamma_2$, $i\gamma_3\gamma_4$ and $i\gamma_5\gamma_6$. For an operator of the first kind, say $3+3$, there is overall parity conservation while the first 3 depends on $i\gamma_1\gamma_2$ and the second 3 depends on $i\gamma_5\gamma_6$. This example also generalizes to higher-order rotations and show that only operators of the first kind consisting of two blocks, can be used to build the $2n$-Majorana rotations. Interestingly, since the 3's correspond to a quartic Hamiltonian and $3(3+3) = 0+6$, sextic Hamiltonians can be simulated using quartic ones. In general, we have the relation $n+n = 0+2n$ implying that Hamiltonians with interactions of order $2n$ can be simulated by interactions of order $n+1$. In the final section of this chapter, we show how a quartic Hamiltonian effectively reduces to the relevant $n+1$ order Hamiltonian. As an intermediate step, we continue in the next section with theorizing the corresponding Hamiltonians capable of performing these operations, having understood the fundamentals of these higher-order rotations.

6.2 Hamiltonians and physical realizations

In this section, we study how the operators of the first kind can be implemented in physical Majorana systems. We begin with the $1+3$ operator and later see how all other operators of the first kind generalize from this. Extending the ideas from Sec. 3.1, our first guess is that the Hamiltonian

$$H = \varepsilon c_1^\dagger c_1 + (v_1^* c_1^\dagger - v_1 c_1)\gamma_1 + (v_2^* c_1^\dagger - v_2 c_1) i\gamma_2\gamma_3\gamma_4, \tag{6.6}$$

can be written in the form

$$H = \varepsilon \tilde{c}^\dagger \tilde{c} + v(\tilde{c}^\dagger - \tilde{c}) \left[\frac{|v_1|}{v}\gamma_1 + \frac{|v_2|}{v} i\gamma_2\gamma_3\gamma_4 \right], \tag{6.7}$$

such that empty or filling of the dot corresponds to performing a $1+3$ operations on the Majorana system. To see that this is indeed the case, we consider the Hamiltonian matrices in the basis $\{|000\rangle, |110\rangle\}$, $\{|011\rangle, |101\rangle\}$, $\{|001\rangle, |111\rangle\}$, $\{|010\rangle, |100\rangle\}$ with $|111\rangle = c^\dagger d_1^\dagger d_2^\dagger |000\rangle$ and $|000\rangle$ being short hand for $|0\rangle_{\mathrm{D}} |0\rangle_{\mathrm{M12}} |0\rangle_{\mathrm{M34}}$,

$$H^\sigma = \begin{pmatrix} 0 & v^\kappa \\ (v^\kappa)^* & \varepsilon \end{pmatrix}, \tag{6.8}$$

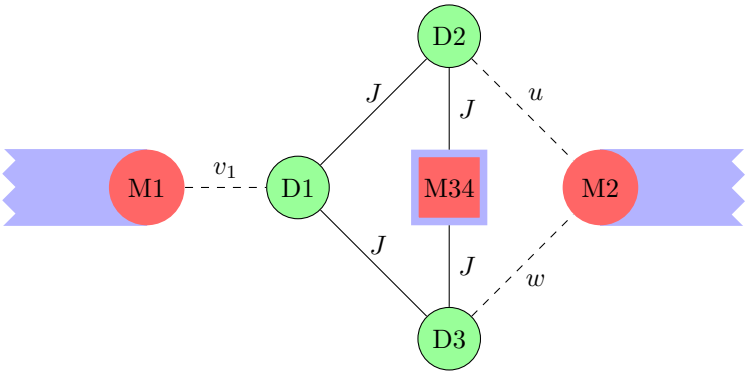

Figure 6.1: Model of the Hamiltonian in eq. (6.10). Light blue denotes the topological superconductor which houses the Majorana states. The Majorana state M1 is coupled to the quantum dot D1. Dots D2 and D3 are either inert or have the opposite occupation of D1, depending on the occupation of M34. The Majorana state M2 is coupled to D2 and D3 with couplings $-v_2^*, v_2^*$ respectively. This setup can perform a general 4-Majorana rotation on the Majorana system by adiabatically filling and emptying D1.

with $v^\kappa = v_1 + \kappa v_2$ and $\kappa = \pm$ labeling whether the parity of the dot is the same (+) or different (-) compared to the parity of the Majorana system. The Hamiltonian matrix decomposes into four 2-by-2-blocks as the overall parity and the parity of the M34-fermion is conserved. The ground state energies are identical to those of the two-Majorana system in Fig. 3.2,

$$H^\kappa = \varepsilon/2 - \sqrt{(\varepsilon/2)^2 + v^2 + \kappa \sin(2\theta)\sin(\phi/2)}, \tag{6.9}$$

where again $v^2 = |v_1|^2 + |v_2|^2$ and $\phi = 2\mathrm{Arg}(v_1/v_2)$. Following the reasoning from Sec. 3.1, v_1/v_2 can be tuned real such that the ground state is fourfold degenerate. Using this while rewriting in terms of $\tilde{c} = c_1 \exp(i \arg v_1)$ we reach eq. (6.7) as expected. This is a step towards designing a physically realizable setup in which the $1+3$ operation can be executed. However, the Hamiltonian discussed here does not have a direct physical representation due to the $(v_2^* c_1^\dagger - v_2 c_1) i\gamma_2\gamma_3\gamma_4$ term. This term can be interpreted as coupling the quantum dot to γ_2 with the sign of the coupling depending on the occupation of the M34 Fermion, $i\gamma_3\gamma_4 = d_2^\dagger d_2 - d_2 d_2^\dagger$. We seek to describe a device whose Hamiltonian effectively reduces to eq. (6.6). To achieve this, consider the setup illustrated in Fig. 6.1. Here, the occupation of the quantum dot D1 is controllable with the level energy ε as previously. It is coupled to a Majorana bound state M1 with tunable coupling v_1 while being strongly coupled to two other dots D2 and D3. The two dots are each coupled to a Majorana operator M2 with couplings u and w. There is also another pair of Majorana bound states M34 which is strongly coupled to the dots D2 and D3. The idea is to have the occupancy of D2 and D3 anti-mirrored to that of D1 while also being correlated with the occupancy of the Majorana fermion M34. A process where D1 is emptied would then fill either D2 or D3 depending on the occupation of M34. Having the couplings between D2/D3 and M2 to differ by a sign, will effectively implement the occupation dependent coupling between D1 and M2. The setup in Fig. 6.1 corresponds to the Hamiltonian,

$$\begin{aligned} H = H_0 &+ J_1 n_1 n_2 + J_2 n_1 n_3 \\ &+ J_3(1-n_1)(1-n_2) + J_4(1-n_1)(1-n_3) \\ &+ J_5 n_2(1+i\gamma_3\gamma_4) + J_6 n_3(1-i\gamma_3\gamma_4), \end{aligned} \tag{6.10}$$

with,

$$H_0 = \varepsilon n_1 + (v_1^* c_1^\dagger - v_1 c_1)\gamma_1 + (u^* c_2^\dagger - u c_2)\gamma_2 + (w^* c_3^\dagger - w c_3)\gamma_2. \tag{6.11}$$

For simplicity, the level energy of D2 and D3 is tuned to zero. The three dots each have fermionic annihilation operators c_1, c_2, c_3 and corresponding number operators $n_i = c_i^\dagger c_i$. The first term in H_0 describes the tunable dot level energy of D1 while the three remaining terms describe the couplings between the three dots and M1 and M2. The J_i's are similar in magnitude, fixed and large compared to the couplings v_1, u, w. The first four J-terms energetically favours dots D2 and D3 to have the opposite occupancy of D1. The last two J-terms penalizes having D2 and D3 occupied at the same time, while the occupancy of M34 determines whether D2 or D3 is occupied. The J-terms thus favors some states over others. An overview of the energies associated with different occupancies are given in Table 6.1. Imagine now the following process; initialise the dots in the ground state for $\varepsilon \to -\infty$, $|1\rangle_{D1}|0\rangle_{D2}|0\rangle_{D3} = |100\rangle$, and M34 in a superposition state, see the bottom panels in Tab. 6.1. The ground state energy is ε regardless of the occupation of M34. Empty D1 by changing ε adiabatically to $\varepsilon \to \infty$ (or at least $\varepsilon \gtrsim 2J_i$). For M34 unoccupied, the ground state is now $|010\rangle$ with energy J_4 from the J-terms, see the top panels of Tab. 6.1. Likewise, for M34 occupied, the ground state is $|001\rangle$ with energy J_3. The ground states are degenerate for $J_3 = J_4$ which implies that no relative dynamical phase will be developed between states with different occupancy of M34. If M34 is initialized in some state $\alpha|0\rangle_{M34} + \beta|1\rangle_{M34}$, then the process of emptying the dot results in

$$|100\rangle(\alpha|0\rangle_{M34} + \beta|1\rangle_{M34}) \to \alpha|010\rangle|0\rangle_{M34} + \beta|001\rangle|1\rangle_{M34} \tag{6.12}$$

The dots D2 and D3 are thus either inert in this process or continue to have opposite occupancy of D1, depending on the occupancy of M34. At the level of the Hamiltonian, the ground states of eq. (6.10) can be projected out by replacing,

$$c_2 \to c_1^\dagger \frac{1}{2}(1 - i\gamma_3\gamma_4), \qquad c_3 \to c_1^\dagger \frac{1}{2}(1 + i\gamma_3\gamma_4), \tag{6.13}$$

$\|0\rangle_{D1}\|0\rangle_{M34}$	$\|0\rangle_{D2}$	$\|1\rangle_{D2}$
$\|0\rangle_{D3}$	$J_3 + J_4$	J_4
$\|1\rangle_{D3}$	$J_3 + 2J_6$	$2J_6$

$\|0\rangle_{D1}\|1\rangle_{M34}$	$\|0\rangle_{D2}$	$\|1\rangle_{D2}$
$\|0\rangle_{D3}$	$J_3 + J_4$	$J_4 + 2J_5$
$\|1\rangle_{D3}$	J_3	$2J_5$

$\|1\rangle_{D1}\|0\rangle_{M34}$	$\|0\rangle_{D2}$	$\|1\rangle_{D2}$
$\|0\rangle_{D3}$	0	J_2
$\|1\rangle_{D3}$	$J_1 + 2J_6$	J_1+J_2+$2J_6$

$\|1\rangle_{D1}\|1\rangle_{M34}$	$\|0\rangle_{D2}$	$\|1\rangle_{D2}$
$\|0\rangle_{D3}$	0	$J_2 + 2J_5$
$\|1\rangle_{D3}$	J_1	J_1+J_2+$2J_5$

Table 6.1: The energies coming from the J-terms of all the sixteen states. The ground states are highlighted for each configuration of the occupancies of D1 and M34.

and thereby arriving at the effective Hamiltonian,

$$H_{\text{eff}} = \varepsilon c_1^\dagger c_1 + (v_1^* c_1^\dagger - v_1 c_1)\gamma_1 + \left(-\frac{u+w}{2}c_1^\dagger + \frac{u^*+w^*}{2}c_1\right)\gamma_2 + \left(\frac{u-w}{2}c_1^\dagger - \frac{u^*-w^*}{2}c_1\right) i\gamma_2\gamma_3\gamma_4. \tag{6.14}$$

Tuning $u = -w = v_2^*$, brings the effective Hamiltonian to the form of eq. (6.6). We have thus showed that the Hamiltonian in eq. (6.10) effectively reduces to the desired form in eq. (6.10) needed for the $1+3$ operation to be executed in the charge-transfer process. In the following section, we consider systems for higher-order Majorana rotations.

6.3 Scalability of Majorana rotations

The two-Majorana system depicted in Fig. 3.2 can execute the 2-Majorana rotation. It is a fundamentally simpler setup than Fig. 6.1 which is capable of performing the 4-Majorana rotation. This device proposal is still early in its conception and it is difficult to say if or when it is experimentally feasible to manufacture. However, it is still natural to ask whether it is always the case that the device complexity and structure increases also for higher-order Majorana rotations. We start by considering the 6-Majorana rotation $0+6$. To execute this operation, we must either be able to perform the $3+3$ operation or the $1+5$ operation. In the previous section, we saw how a 3-operation can be accomplished. To perform the $3+3$ operation, we can simply introduce additional dots and Majoranas and couple M1 to D1 in the same manner as M2 is coupled to D1 in Fig. 6.1. This addition does not change the fundamental complexity of the setup but rather introduces more of the same. This does not appear to be true for the $1+5$ operation. Note that being able to execute a 5-operation is more powerful than a 3-operation as the $5+5$ operation can produce the 10-Majorana rotation by applying it twice. The 5-operation requires a coupling dependent on the parity of two Majorana Fermions. In Fig. 6.2, the setup capable of executing the $1+3$ operation has been extended to enable the $1+5$ operation. Here, six additional quantum dots are introduced alongside a third pair of Majorana bound

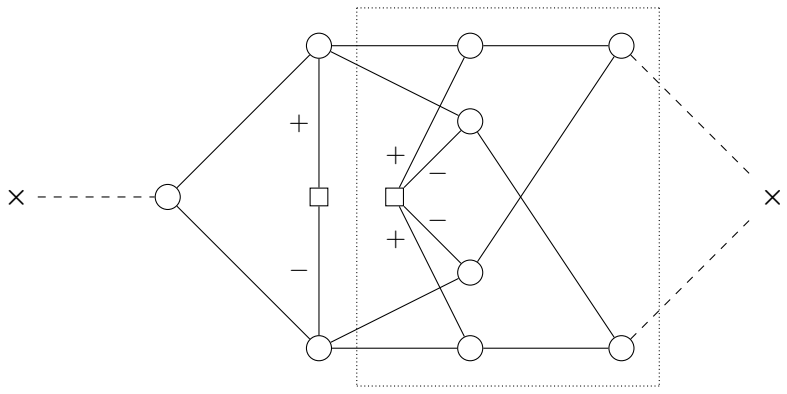

Figure 6.2: Sketch of a setup in which the $1+5$ operation can be executed. Crosses represent single Majorana bound state while squares represent Majorana pairs. Quantum dots are denoted by circles. Dashed lines are used for couplings between dots and Majorana bound states. Solid lines between dots represent anti-mirrored occupancy while the solid lines between dots and Majorana pairs denote the occupancy dependent coupling that appeared previously. The signs indicate whether the dots couple to the occupied or unoccupied Majorana Fermion. The box can be coupled to a copy of itself and in this way can any number of Majorana Fermions be coupled to the system in a scalable manner.

states. The occupancy of connected dots are anti-mirrored as was previously the case with D1, D2 and D3. The third pair of Majorana bound states are connected with the four middle layer dots in the same occupancy dependent fashion as was the case with M34 and D2 and D3. The four middle layer dots has knowledge of the occupancy of the two middle Majorana Fermions. This information is condensed in the two dots in the rightmost layer such that occupancy of these dots depends on the combined parity of the two middle Majorana Fermions. Coupling these dots to the rightmost Majorana bound state now gives the sought after parity dependent coupling between the leftmost dot and the rightmost Majorana bound state. The device complexity has again increased. The idea is that what is contained in the box of dotted lines in Fig. 6.2 is a building block which appends an additional pair of Majorana bound states. By replicating the box and inserting it between the existing box and the rightmost Majorana bound state, a system capable of performing a $1 + 7$ operation has now been achieved. Repeating this procedure will in principle allow us to design setups in which any operator of the first kind can be performed.

Chapter 7

A tunnel-braiding protocol for Majoranas

We have previously seen how to execute braiding-like operations on Majoranas using charge-transfer processes. A different method for performing operations on the Majoranas is through tunnel braiding. Like the charge-transfer process, the tunnel braiding is a braiding in a parameter-space; in this case, the space of tunnel couplings between a number of Majoranas and quantum dot. In this chapter, we use ideas from [22] to develop a protocol for demonstrating the non-Abelian nature of Majorana bound states. This is very similar to the charge-transfer protocols discussed previously. Instead of the charge-transfer process, it is replaced by the tunnel-braiding. This proposal has advantages and disadvantages compared to the charge-transfer protocols as we will see.

7.1 Basics of tunnel braiding

We begin this study by considering the system consisting of a quantum dot (with annihilation operator $c = 1/2(\gamma_a + i\gamma_b)$) coupled to four Majorana bound states γ_1, γ_2, γ_3 and γ_4,

$$H_{1234} = \varepsilon c^\dagger c + \sum_{i=1}^{4} (v_i^* c^\dagger - v_i c)\gamma_i, \tag{7.1}$$

with ε being the dot level energy and v_i are the tunnel couplings between the Majoranas and the dot. It is relevant to express the dot in terms of its Majorana operators,

$$H_{1234} = \frac{\varepsilon}{2} + \frac{i}{2}\varepsilon\gamma_a\gamma_b + \frac{i}{2}\sum_i^4 a_i\gamma_a\gamma_i + \frac{i}{2}\sum_i^4 b_i\gamma_b\gamma_i, \tag{7.2}$$

where $a_i = 2\,\mathrm{Re}(v_i)$ and $a_i = 2\,\mathrm{Im}(v_i)$. In the basis $\phi^\dagger = (\gamma_a, \gamma_b, \gamma_1, \gamma_2, \gamma_3, \gamma_4)$, we can rewrite the Hamiltonian as

$$H_{1234} - \frac{\varepsilon}{2} = \phi^\dagger \mathcal{H}_{1234}\phi, \quad \mathcal{H}_{1234} = \frac{i}{2}\begin{pmatrix} 0 & \varepsilon_1 & a_1 & a_2 & a_3 & a_4 \\ -\varepsilon_1 & 0 & b_1 & b_2 & b_3 & b_4 \\ -a_1 & -b_1 & 0 & 0 & 0 & 0 \\ -a_2 & -b_2 & 0 & 0 & 0 & 0 \\ -a_3 & -b_3 & 0 & 0 & 0 & 0 \\ -a_4 & -b_4 & 0 & 0 & 0 & 0 \end{pmatrix}. \tag{7.3}$$

In the special case where the coupling vectors $\mathbf{a} = (a_1, a_2, a_3, a_4)$ and $\mathbf{b} = (b_1, b_2, b_3, b_4)$ are zero, there are four Majorana zero-modes corresponding to the four Majorana bound states. When the coupling vectors are non-zero, this degeneracy splits, however, two Majorana zero-modes remain. These are spread over the four Majorana bound states. To see this, we look for zero energy solutions,

$$\mathcal{H}_{1234}\mathbf{q} = 0, \quad \mathbf{q} = (q_1, q_2, \mathbf{c})^T, \quad \mathbf{c} = (c_1, c_2, c_3, c_4)^T. \tag{7.4}$$

This leads to the equations,

$$\varepsilon q_2 + \mathbf{a}\cdot\mathbf{c} = 0, \tag{7.5}$$
$$-\varepsilon q_1 + \mathbf{b}\cdot\mathbf{c} = 0, \tag{7.6}$$
$$q_1\mathbf{a} + q_2\mathbf{b} = 0. \tag{7.7}$$

In general, we do not expect $\mathbf{a}$ and $\mathbf{b}$ to be parallel. Consequently, the third of the above equations imply that $q_1 = q_2 = 0$ and we have $\mathbf{a}\cdot\mathbf{c} = 0$ and $\mathbf{b}\cdot\mathbf{c} = 0$. Since the coupling vectors $\mathbf{a}$ and $\mathbf{b}$ and the vector $\mathbf{c}$ are 4-dimensional, there are two normalized, linearly independent solutions $\mathbf{c}^\alpha$ and $\mathbf{c}^\beta$ which are perpendicular to both $\mathbf{a}$ and $\mathbf{b}$. These two solutions correspond to two Majorana zero-modes spread over the Majorana bound states,

$$\gamma^\alpha = c_1^\alpha\gamma_1 + c_2^\alpha\gamma_2 + c_3^\alpha\gamma_3 + c_4^\alpha\gamma_4, \tag{7.8}$$
$$\gamma^\beta = c_1^\beta\gamma_1 + c_2^\beta\gamma_2 + c_3^\beta\gamma_3 + c_4^\beta\gamma_4. \tag{7.9}$$

We can braid these two Majorana zero-modes by adiabatically controlling the coupling vectors $\mathbf{a}$ and $\mathbf{b}$. To see this graphically, consider $\mathbf{b}$, $\mathbf{c}^\alpha$ and $\mathbf{c}^\beta$ in the 3-dimensional subspace perpendicular to $\mathbf{a}$:

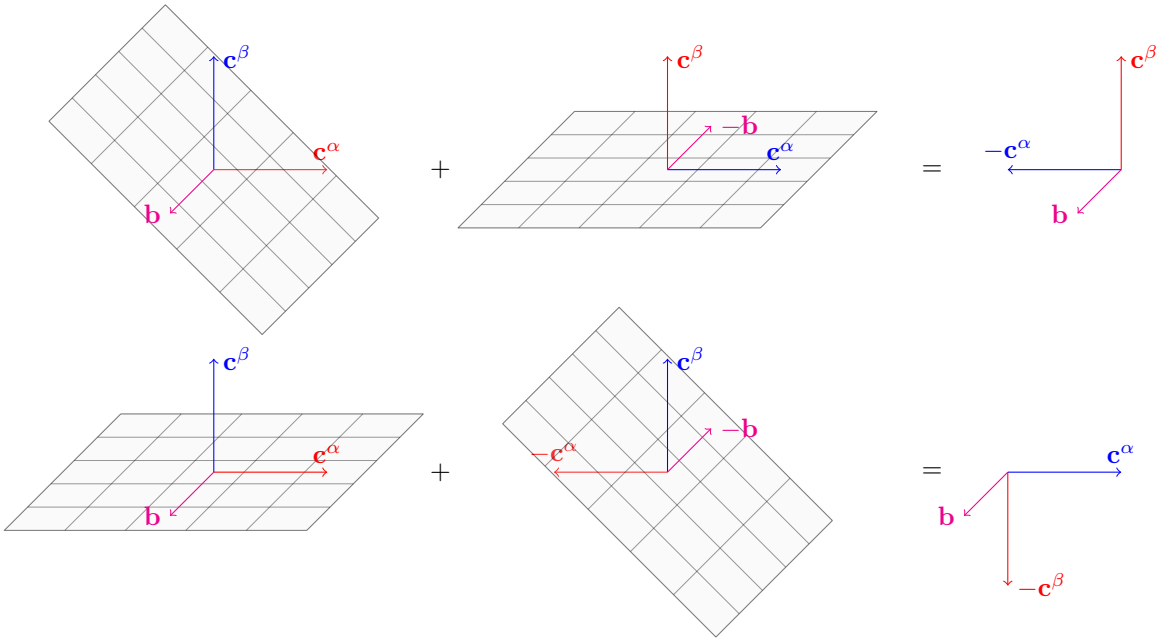

Figure 7.1: Illustration of the tunnel braidings $\mathbf{c}^\alpha \to \mathbf{c}^\beta$, $\mathbf{c}^\beta \to -\mathbf{c}^\alpha$ and $\mathbf{c}^\alpha \to -\mathbf{c}^\beta$, $\mathbf{c}^\beta \to \mathbf{c}^\alpha$ depending on the order of operations. The gray planes represent the rotation plane of the $\mathbf{b}$-vector.

Here, we imagine the three vectors to be fixed with respect to each other while their common endpoint is fixed to the origin. Then, we can rotate $\mathbf{b} \to -\mathbf{b}$ in the $\mathbf{b}$-$(\mathbf{c}^\alpha - \mathbf{c}^\beta)$-plane such that $\mathbf{c}^\alpha \to \mathbf{c}^\beta$ and

$\mathbf{c}^\beta \to \mathbf{c}^\alpha$. We can then rotate $-\mathbf{b} \to \mathbf{b}$ in the $\mathbf{b}$-$\mathbf{c}^\alpha$-plane which brings back $\mathbf{b}$ to its original position and takes $\mathbf{c}^\alpha \to -\mathbf{c}^\alpha$. In total, the operation corresponds to $\mathbf{c}^\alpha \to \mathbf{c}^\beta$, $\mathbf{c}^\beta \to -\mathbf{c}^\alpha$ and similarly for the associated Majorana zero-mode operators. If we instead reverse the order of operations, the resulting operation is $\mathbf{c}^\alpha \to -\mathbf{c}^\beta$, and $\mathbf{c}^\beta \to \mathbf{c}^\alpha$ which corresponds to braiding the other way around. Having demonstrated the braiding in tunnel-space, we have the sufficient ingredients for demonstrating the non-Abelian behavior of Majoranas. A benefit of the tunnel-braiding compared to the charge-transfer process is its inherent degeneracy which does not rely on the tuning of a parameter in the Hamiltonian. A downside is that the operation on the Majorana system depends on the path in parameter-space as opposed to the charge-transfer process. In practice, it might be difficult to control the coupling vectors to the precision in the example in Fig. 7.1. Instead, we can imagine the tip of $\mathbf{b}$ to follow any closed loop such that it returns to its original position. In this situation, the Majorana vectors and operators generally transform as

$$\gamma^\alpha \to \cos(\theta)\gamma^\alpha + \sin(\theta)\gamma^\beta, \tag{7.10}$$

$$\gamma^\beta \to \cos(\theta)\gamma^\beta - \sin(\theta)\gamma^\alpha. \tag{7.11}$$

By performing multiple loops, the rotation angles θ accumulate. In this way, braiding can be built from a large number of small loops in tunnel-space. Notice that reversing the orders of operations in the example in Fig. 7.1, corresponds to going the other way around the loop traced by the tip of $\mathbf{b}$. In conclusion, there is only a difference in the direction of the loop and not in which order different loops are performed. This is similar to the way the relative angle between the even and the odd ground states accumulate in Sec. 3.3. To also include the non-commutativity of successive loops, additional Majoranas should be included. By also coupling Majoranas γ_5 and γ_6 to the dot, the coupling vectors $\mathbf{a}$ and $\mathbf{b}$ are now 6-dimensional, leaving four linearly independent Majorana vectors perpendicular to $\mathbf{a}$ and $\mathbf{b}$. Braids between these four Majorana zero-modes can be accomplished by perform loops in the tunnel-space in the same manner as in Fig. 7.1. Being able to braid different pairs of Majoranas results in the loops being non-commuting. In the next section, we propose a protocol to demonstrate the non-Abelian nature of Majoranas using the simpler 4-Majorana setup rather then the 6-Majorana setup. We use the 4-Majorana setup as an example while its role may also be played by the 6-Majorana setup.

7.2 The tunnel-braiding protocol

This protocol will follow the same overall recipe as the charge-transfer protocols: 1) Initialize in the measurement-basis, 2) perform the braiding-like processes in the operation-basis and 3) measure the change in the Majorana system in the measurement-basis. In the previous section, we considered the main idea of step 2) and we continue in this section by adding steps 1) and 3). Coupling the quantum dot to the four Majoranas partly breaks the degeneracy, leaving two effective Majorana zero-modes. It is these zero-modes, we braid in the operation-basis. Consequently, we need two additional Majoranas to construct the measurement-basis. The total is now four Majorana zero-modes. To initialize the Majoranas, we need at least one additional quantum dot to break half of the degeneracy. For these reasons, we consider the geometry in Fig. 7.2 consisting of six Majorana bound states and two quantum dots. The two dots D1 and D2 have level energies ε_1 and ε_2 respectively. We can now state our proposed protocol.

The tunnel-braiding protocol

1. *Initialization:* The Majorana system is initialized by turning on the couplings u_1, u_2, v_3, v_4, v_5 and turning off the couplings v_2 and v_6. As default, we will keep $v_6 = 0$ throughout. The even and odd ground state energies in the D1/M12-system will in general be split and the system settles in its overall ground state. We take the parity of the D1/M12-system to be even in this case. In the D2/M3456-system, the even and odd ground states are degenerate. By waiting a long time, also this system will settle in a definite parity ground state through its coupling to the environment. We also take the parity of this system to be even. We have now initialized the system. Before continuing with the operations, we need to decouple D1 from M1 and M2 by letting $v_1 = v_2 = 0$. The next steps in the protocol become conceptually simpler if we first imagine tuning its level energy $\varepsilon_1 \to \infty$ such that the dot is emptied and the M12-system is left in a state of definite occupancy. After the dot has been decoupled, its level energy can be turned back to its original value, while it remains empty in its ground state.

2. *Braiding:* The operation on the Majorana system begins by coupling M2 to D2 by adiabatically turning on v_2. Then, we can perform arbitrary loops in the tunnel coupling-space by cyclically controlling the coupling parameters. By repeating the loops, we can accumulate the braiding-like operation. If also M6 is coupled to D2 through v_6, different loops in the parameter-space do not commute as three Majorana zero-modes are being braided. When the tunnel-braiding is complete, the tunnel couplings should be restored to their original value, in particular $v_2 = 0$. This procedure braids M2 with the other Majorana zero-mode distributed across M345 changing the occupancy of the M12-fermion.

3. *Measurement:* We can now measure the joint parity of the D1/M12-system by first restoring the tunnel couplings v_1 and v_2 and then measure the charge on D1. Ideally, the tunnel couplings should be turned on instantly. The continuous charge-measurement collapses the subsystem to a state with definite parity. Thus, the measurement can detect the change in occupancy of the M12-fermion as the dot has remained empty in its ground state.

We continue this section by providing a few mathematical details of the protocol. Having initialized the Majoranas in the even sectors, the M12-system is in the state $|0\rangle_{\mathrm{M12}}$. We call the Majorana zero-mode spread over M234 for M0. The initial state of the M3456-system can thus be expressed as $|0\rangle_{\mathrm{M06}}$. Performing the tunnel braiding on M2 and M0 results in a final state $\alpha\,|0\rangle_{\mathrm{M12}}\,|0\rangle_{\mathrm{M06}} + \beta\,|1\rangle_{\mathrm{M12}}\,|1\rangle_{\mathrm{M06}}$ as the overall parity of the system is conserved. We are interested in the occupancy of the M12-fermion which can be determined by measuring the charge of D1 when it is coupled to M1 and M2 [21]. In terms of the states in this subsystem, the tunnel-braiding has the effect

$$|0\rangle_{\mathrm{D1}}\,|0\rangle_{\mathrm{M12}} \to |0\rangle_{\mathrm{D1}}\,(\alpha\,|0\rangle_{\mathrm{M12}} + \beta\,|1\rangle)\,, \tag{7.12}$$

assuming that the sudden approximation can be used when the dot is coupled to the Majoranas. This state is not a ground state due to the energy splitting between the even and odd sectors. Since the charge-measurement is assumed to be a weak measurement in continuous time, the time evolution of

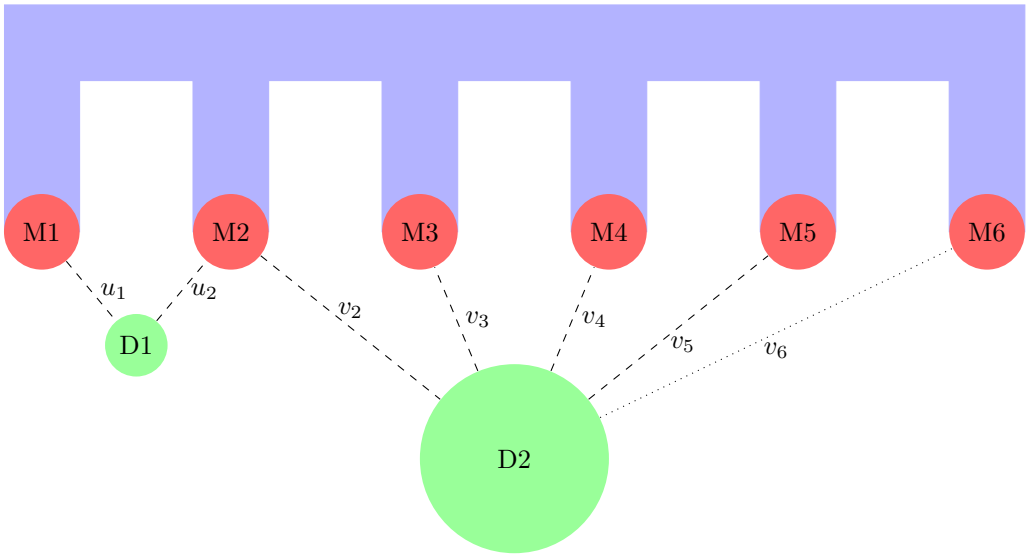

Figure 7.2: Device proposal for demonstrating the non-Abelian exchange statistics through tunnel-braiding. The single-level quantum dot D2 mediates a coupling between the Majorana bound states M2, M3, M4 and M5. By also coupling M6 to D2 enables the non-commuting braids of three Majorana zero-modes.

these states are relevant. We begin by reminding ourselves of the familiar Hamiltonian, eigenenergies and eigenstates of the D1/M12-system,

$$H^\rho = \begin{pmatrix} 0 & v^\rho \\ (v^\rho)^* & \varepsilon_1 \end{pmatrix}, \quad E^\rho_\pm = \frac{\varepsilon_1}{2} \pm \sqrt{\left(\frac{\varepsilon_1}{2}\right) + |v^\rho|^2}, \quad |\Psi^\rho_\pm\rangle = \frac{1}{\sqrt{(E^\rho_\pm)^2 + |v^\rho|^2}} \begin{pmatrix} v^\rho \\ E^\rho_\pm \end{pmatrix}, \tag{7.13}$$

with $v^\rho = v_1 + \rho i v_2$ and $|v^\rho|^2 = v^2 + \rho \sin(2\theta)\sin(\phi/2)$ in the parameterization $v_1 = v\cos(\theta)e^{i\phi/2}$, $v_2 = v\sin(\theta)$. In this basis, the states $|0\rangle_{\mathrm{D1}}|0\rangle_{\mathrm{M12}}$ and $|0\rangle_{\mathrm{D1}}|0\rangle_{\mathrm{M12}}$ both correspond to $(1,0)^T$. To include the time evolution we express this state in terms of the eigenstates,

$$|0\rangle_{\mathrm{D1}}|0(1)\rangle_{\mathrm{M12}} = \begin{pmatrix} 1 \\ 0 \end{pmatrix} = \frac{1}{v^\rho(E^\rho_+ - E^\rho_-)} \left[E^\rho_+ \begin{pmatrix} v^\rho \\ E^\rho_- \end{pmatrix} - E^\rho_- \begin{pmatrix} v^\rho \\ E^\rho_+ \end{pmatrix} \right], \tag{7.14}$$

for both the even and odd parities. We may now simply append the time evolution factor to each state to get the time evolved states,

$$|\psi^\rho(t)\rangle_{\mathrm{D1,M12}} = \frac{1}{v^\rho(E^\rho_+ - E^\rho_-)} \left[E^\rho_+ e^{-iE^\rho_- t} \begin{pmatrix} v^\rho \\ E^\rho_- \end{pmatrix} - E^\rho_- e^{-iE^\rho_+ t} \begin{pmatrix} v^\rho \\ E^\rho_+ \end{pmatrix} \right]. \tag{7.15}$$

The probability of measuring full occupancy of the dot as a function of time for a given parity sector is

$$|\langle 1|_{\mathrm{D1}}\langle 0(1)|_{\mathrm{M12}}|\psi^\rho(t)\rangle_{\mathrm{D1,M12}}|^2 = 4\left|\frac{E^\rho_+ E^\rho_-}{v^\rho(E^\rho_+ - E^\rho_-)}\right|^2 \sin^2\left(\frac{E^\rho_+ - E^\rho_-}{2}t\right) \tag{7.16}$$

By taking the time average and rewriting in terms of $x = \varepsilon_1/(2v)$ and $\lambda^\rho = \rho\sin(2\theta)\sin(\phi/2)$, we get

$$O^\rho = \frac{1+\lambda^\rho}{2(x^2+1+\lambda^\rho)}, \tag{7.17}$$

for the occupancy which is related to he charge-measurement through $C^{\rho} = eO^{\rho}$ where e is the charge of the electron. In the ideal situation $x = 0$ and $\lambda = 1$, the charge-measurement yield $C^{-} = 0$ and $C^{+} = e/2$ for the even and odd cases, distinguishing the two possibilities maximally. In conclusion, the charge-measurement of the dot can determine the occupancy of the M12-fermion. When measuring $|0\rangle_{\mathrm{D1}} (\alpha |0\rangle_{\mathrm{M12}} + \beta |1\rangle)$, the state is collapsed to $|0\rangle_{\mathrm{D1}} |0(1)\rangle_{\mathrm{M12}}$ with probability $|\alpha|^2(|\beta|^2)$ yielding a measurement outcome $C^{-(+)}$.

Chapter 8

Conclusion and outlook

In this thesis, we have studied the charge-transfer process of [1] in detail. The aim is to demonstrate the non-Abelian statistics of Majorana bound state. To perform the the charge-transfer process a single level quantum dot is weakly coupled to a Majorana system. By controlling the dot level energy adiabatically, charge can be transferred to the Majorana system, changing its parity. Due to the non-Abelian characteristics of the Majorana bound states, the operations performed by consecutive charge-transfer processes does not commute. By measuring the parity of the combined Majorana/dot-system through a charge-measurement of the dot, the order of operations can be distinguished, demonstrating the non-Abelian nature of Majorana bound states. The work in this thesis takes into account the errors in the coupling parameters between the dot and the Majorana bound states. In experiment, these parameters need to be tuned to achieve visibility of the non-Abelian effects. The main source of visibility reduction comes from the relative dynamical phase gained between the even and odd parity sectors of the Majorana/dot-system due to the ground state degeneracy being split when the parameters are not ideally tuned. The non-Abelian effects are associated with the relative geometric phase acquired between the even and odd parity sectors during the charge-transfer process. By studying the dependence of the coupling parameters on the dynamical and geometric phases we are able to propose an efficient protocol for demonstrating the non-Abelian statistics of Majorana bound states. Our proposal has advantages compared to the protocol suggested in [1]: 1) We need to manipulate only one pair of Majorana bound states, requiring only three operations. 2) The dynamical phases between consecutive charge-transfer processes can be canceled, achieving maximal visibility of the non-Abelian effects. The cancellation of the dynamical phases rely on winding the superconducting phase in the system by π. This can be achieved in experiment by controlling the magnet field through the device. In a numerical simulation of the time-dependent Schrödinger equation, we test the proposed protocol and find good agreement with the theory. In future experiments, it will be interesting to see if these results translate well to the experimental scene and if they can be used to demonstrate the non-Abelian statistics of Majoranas.

Another important aspect of the charge-transfer process is the adiabatic control of the dot level energy. To investigate the effects of non-adiabatic corrections, we apply adiabatic perturbation theory [2]. The two primary modes of errors due to non-adiabaticity are transitions out of the ground state manifold and corrections to the relative phases between the even and odd parity sectors. Using adiabatic perturbation theory and numerical simulations of the charge-transfer process, we find that it is optimal to control the rate of change of the dot level energy proportional to the energy gap

separating the ground state and the excited state. Comparing to simply controlling the dot level energy linearly, we find improvements in the suppression of both the transition amplitude and the corrections to the relative phase at a much shorter time scale of the process. It is beneficial for the time scale to be short to reduce the effects of the coupling to the environment. While applying adiabatic perturbation theory, we discover a subtle detail due to the adiabatic expansion parameter being dimensionful. For the charge-transfer system, we define the relevant dimensionless expansion parameter in adiabatic perturbation theory. For future work, it will be relevant to generalize the dimensionless expansion parameter and recast adiabatic perturbation theory in entirely dimensionless quantities. This may bring insights into how adiabatic transport is optimally performed and give the rigorous conditions for the adiabatic approximation. These result will in general be useful when studying manipulations of Majorana systems as adiabatic control of the system is often assumed.

In the first of the two smaller projects, we consider simultaneous manipulation of more than two Majorana bound states using charge-transfer. We introduce a shorthand notation for different types of operations on Majorana systems and use it to determine how to perform operations on 4 Majorana bound states. We propose a device capable of performing this operation and study its Hamiltonian. We also consider how to perform all other operations on a Majorana system by extending the setup. This project is still early in its conception and much future work still remains, especially when it comes to concrete physical implementations.

In the second of the smaller projects, we consider braiding in a tunnel coupling-space as a path to demonstrating the non-Abelian statistics of Majorana bound states. Instead of the charge-transfer process, by coupling four Majorana bound states to a quantum dot, the two remaining Majorana zero-modes can be braided through adiabatic control of the coupling parameters. We show this at a proof-of-concept level. We propose an initialization and measurement protocol while leaving the details of the tunnel-braiding for future work.

Bibliography

[1] K. Flensberg, *"Non-Abelian Operations on Majorana Fermions via Single-Charge Control"*, Phys. Rev. Lett. **106**, 090503 (2011).

[2] G. Rigolin, G. Ortiz, V.H. Ponce, *"Beyond the Quantum Adiabatic Approximation: Adiabatic Perturbation Theory"*, Phys. Rev. A **78**, 052508 (2008).

[3] E. Majorana, *"Teoria Simmetrica dell'Elettrone e del Positrone"*, Nuovo Cimento **14**, 171–184 (1937). English translation: *"A Symmetric Theory of Electrons and Positrons"*, Soryushiron Kenkyu **63**, 149–162 (1981).

[4] A. Baha Balantekin, A. de Gouvêa, B. Kayser, *"Addressing the Majorana vs. Dirac Question With Neutrino Decays"*, Physics Letters B **789**, 488–495 (2019).

[5] M. Leijnse, K. Flensberg, *"Introduction to Topological Superconductivity and Majorana Fermions"*, Semiconductor Science and Technology **27**, 124003 (2012).

[6] C.W.J. Beenakker, *"Search for Majorana Fermions in Superconductors"*, Annual Review of Condensed Matter Physics **4**, 113–136 (2013).

[7] A.Y. Kitaev, *"Unpaired Majorana Fermions in Quantum Wires"*, Phys. Usp. **44**, 131 (2001).

[8] M.Z. Hasan, C.L. Kane, *"Colloquium: Topological insulators"*, Rev. Mod. Phys. **82**, 3045–3067 (2010).

[9] C.W.J. Beenakker, *"Search for Non-Abelian Majorana Braiding Statistics in Superconductors"*, Lecture notes for the Les Houches summer school (July 2019), arXiv:1907.06497.

[10] C. Nayak, S. H. Simon, A. Stern et al. *"Non-Abelian Anyons and Topological Quantum Computation"*, Rev. Mod. Phys. **80**, 1083 (2008).

[11] A.Y. Kitaev, *"Fault Tolerant Quantum Computation by Anyons"*, Ann. Phys. **303**, 2–30 (2003).

[12] D. Gottesman, *"The Heisenberg Representation of Quantum Computers"*, 22nd International Colloquium on Group Theoretical Methods in Physics, 32–43 (1998).

[13] L. Fu, C.L. Kane, *"Superconducting Proximity Effect and Majorana Fermions at the Surface of a Topological Insulator"*, Phys. Rev. Lett. **105**, 096407 (2008).

[14] Y. Oreg, G. Refael, F. von Oppen, *"Helical Liquids and Majorana Bound States in Quantum Wires"*, Phys. Rev. Lett. **105**, 177002 (2010).

[15] R. Lutchyn, J. Sau, S. Das Sarma, *"Majorana Fermions and a Topological Phase Transition in Semiconductor-Superconductor Heterostructures"*, Phys. Rev. Lett. **105**, 077001 (2010).

[16] V. Mourik, K. Zuo, S.M. Frolov et al. *"Signatures of Majorana Fermions in Hybrid Superconductor-Semiconductor Nanowire Devices"*, Science **336**, 1003–1007 (2012).

[17] R. Lutchyn, E.P.A.M. Bakkers, L.P. Kouwenhoven, et al. *"Majorana Zero Modes in Superconductor–Semiconductor Heterostructures"*, Nat. Rev. Mater. **3**, 52–68 (2018).

[18] D.A. Ivanov, *"Non-Abelian Statistics of Half-Quantum Vortices in p-Wave Superconductors"*, Phys. Rev. Lett. **86**, 268–271 (2001)

[19] T. Karzig, W.S. Cole, D.I. Pikulin, *"Quasiparticle Poisoning of Majorana Qubits"*, arXiv:2004.01264, (2020)

[20] J. Alicea, Y. Oreg, G. Refael et al. *"Non-Abelian Statistics and Topological Quantum Information Processing in 1D Wire Networks"*, Nature Phys. **7**, 412 (2011).

[21] M.I.K. Munk, J. Schulenborg, R. Egger, K. Flensberg, *"Parity-to-charge conversion in Majorana qubit readout"*, arXiv:2004.02123, (2020)

[22] P. Brouwer, K. Flensberg, F. von Oppen, *Private Communication*, Feb. 2020.